U.PORTO
FACULDADE DE CIÊNCIAS
UNIVERSIDADE DO PORTO

MSc

2.º CICLO

FCUP
ICBAS
2020

U.PORTO

Biochemical and structural characterization of a potassium transporter from *Bacillus subtilis*

Marta Maria Noutel Lorga Gomes

FC

U.PORTO
FACULDADE DE CIÊNCIAS
UNIVERSIDADE DO PORTO

U.PORTO
INSTITUTO DE CIÊNCIAS
BIOMÉDICAS ABEL SALAZAR
UNIVERSIDADE DO PORTO

Biochemical and structural characterization of a potassium transporter from *Bacillus subtilis*

Marta Maria Noutel Lorga Gomes

Dissertação de Mestrado apresentada à
Faculdade de Ciências da Universidade do Porto e Instituto de Ciências Biomédicas Abel Salazar
Bioquímica

2020

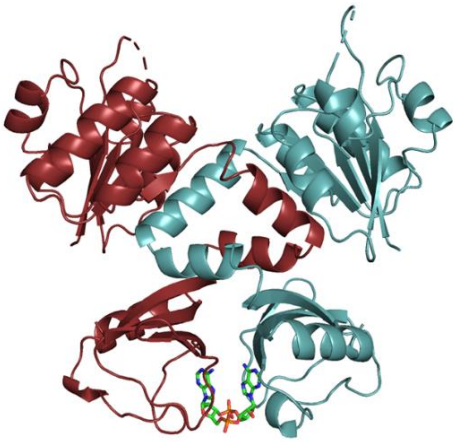

Biochemical and structural characterization of a potassium transporter from *Bacillus subtilis*

Marta Maria Noutel Lorga Gomes

Mestrado em Bioquímica

Departamento de Química e Bioquímica

2020

Orientador
João Morais Cabral, Investigador Principal, i3s

Coorientador:
Luís Gales, Professor Associado, ICBAS

INSTITUTO DE INVESTIGAÇÃO E INOVAÇÃO EM SAÚDE
UNIVERSIDADE DO PORTO

U.PORTO
INSTITUTO DE CIÊNCIAS BIOMÉDICAS ABEL SALAZAR
UNIVERSIDADE DO PORTO

U.PORTO
FACULDADE DE CIÊNCIAS
UNIVERSIDADE DO PORTO

Todas as correções determinadas pelo júri, e só essas, foram efetuadas.

O Presidente do Júri,

Porto, _____/_____/_____

Agradecimentos

Em primeiro lugar gostaria de expressar a minha gratidão ao meu orientador, Dr. João Morais Cabral por me ter acolhido no seu grupo de investigação, por todos os ensinamentos e disponibilidade para ajudar sempre que precisava. Muito obrigada por esta oportunidade.

De seguida, gostaria de agradecer à Dra. Carol Harley pela prontidão em me ajudar durante todo este processo e por tudo que me ensinou.

A todos os restantes membros do grupo: Celso Duarte, Omar Santin, Andreia Fernandes, Rita Rocha, João Jorge, Katharina Weinhaeupl e em especial, à Tatiana Cereija pelas horas que dedicou a ajudar-me.

Aos melhores colegas e amigos que tive o prazer de conhecer ao longo destes cinco anos: Rafaela Silva, André Carvalho, Gabriel Oliveira e Pedro Mesquita. Ao Flávio Dionísio, sem ti não teria tantas razões para agradecer.

Á Bárbara Silva e Inês Ferreira, por me continuarem a mostrar a verdadeira definição de amizade após tantos anos.

Ao Tomé Albuquerque, que nunca deixou o meu lado.

E por último, mas não menos importante, aos meus pais pelo apoio incondicional, sempre. Á minha irmã Rita, o meu exemplo a seguir.

Resumo

Iões metálicos, como Potássio (K^+) e Sódio (Na^+), são conhecidos por intervirem em vários processos biológicos fundamentais. O ião K^+ é o catião intracelular mais abundante em organismos vivos devido às suas funções bioquímicas e fisiológicas cruciais. *Bacillus subtilis*, uma das bactérias Gram-positivas mais bem caracterizadas, adaptam-se ao stress osmótico com uma reação baseada no influxo e efluxo de iões K^+. Os domínios de regulação da condutância de K^+ (RCK) comumente controlam a atividade de sistemas procarióticos de transporte de K^+ e ligandos biológicos, como o segundo mensageiro bacteriano di-adenosina monofosfato cíclico (c-di-AMP), ligam-se aos domínios RCK e induzem uma mudança conformacional que é propagada para o sistema de transporte. Recentemente, um domínio RCK foi identificado na proteína YjbQ de *Bacillus subtilis*, um antiportador de catião/protão putativo descrito como capaz de ligar c-di-AMP. Os principais objetivos deste trabalho são determinar a estrutura tridimensional do domínio RCK da proteína YjbQ e caracterizá-la em termos da sua função bioquímica.

Ao longo do curso deste trabalho foram estabelecidos protocolos de expressão a grande escala e purificação do domínio RCK da proteína YjbQ e o c-di-AMP foi identificado como um ligando deste domínio. A estrutura do domínio RCK co-cristalizado com c-di-AMP foi determinada a uma resolução de 1.85 Å a partir de cristais pertencentes ao grupo espacial $P2_12_12_1$ e demonstrou duas moléculas idênticas na unidade assimétrica. Uma segunda estrutura deste domínio na ausência de c-di-AMP foi obtida, o que permitiu a comparação das duas estruturas existentes. Por outro lado, vários testes funcionais foram realizados, no entanto nenhum resultado conclusivo foi obtido.

Palavras-chave: Potássio, antiportador de catião/protão, YjbQ, domínio RCK, c-di-AMP, cristalografia de raio-X.

Abstract

Metal ions, such as Potassium (K^+) and Sodium (Na^+), are known for intervening in a series of fundamental biological processes. K^+ is the most abundant intracellular cation in living organisms due to its crucial physiological and biochemical functions. *Bacillus subtilis*, one of the best characterized bacteria among Gram-positives, adapts to osmotic stress with a reaction based on the influx and efflux of K^+ ions. Regulators of K^+ conductance (RCK) domains commonly control the activity of prokaryotic K^+ transport systems. Biological ligands, such as the bacterial second messenger cyclic di-adenosine monophosphate (c-di-AMP), bind to the RCK domain inducing a conformational change that is propagated to the transport system. Recently, an RCK domain was identified in the protein YjbQ from *Bacillus subtilis*, a putative cation/proton antiporter and proposed to likely bind c-di-AMP. The major aim of this work was to determine the three-dimensional structure of the RCK domain of YjbQ and to characterize YjbQ in terms of biochemical function.

This work comprised the large-scale expression and purification for the RCK domain of YjbQ and c-di-AMP was identified as a ligand for this domain. The structure of the RCK domain co-crystallized with c-di-AMP was determined at a resolution of 1.85 Å from crystals belonging to space group $P2_12_12_1$ and containing two identical molecules in the asymmetric unit. A second structure of this domain in the absence of c-di-AMP was obtained, which allowed the comparison between the two structures. Various functional assays were performed yet no conclusive results were achieved.

Keywords: Potassium, cation/proton antiporter, YjbQ, RCK domain, c-di-AMP, X-ray crystallography.

Table of Contents

List of Tables

List of Figures

List of Abbreviations

ACMA	9-Amino-6-Chloro-2-Methoxyacridine
ADP	Adenosine diphosphate
AMP	Adenosine monophosphate
ATP	Adenosine triphosphate
BSA	Bovine Serum Albumin
cAMP	Cyclic adenosine monophosphate
c-di-AMP	Cyclic di-adenosine monophosphate
c-di-GMP	Cyclic di-guanosine monophosphate
cGMP	Cyclic guanosine monophosphate
CPA	Cation/proton antiporter
CPA1	Cation/proton Antiporter 1 subfamily
CPA2	Cation/proton Antiporter 2 subfamily
Da	Dalton
DAC	Diadenylate cyclase
dATP	Deoxyadenosine triphosphate
dCTP	Deoxycytidine triphosphate
DFNDB	1,5-difluoro-2,4-dinitrobenzene
dGTP	Deoxyguanosine triphosphate
DisA	DNA integrity scanning protein A
DMSO	Dimethyl sulfoxide
DNA	Deoxyribonucleic acid
DRaCALA	Differential Radial Capillary action of Ligand Assay
DSF	Differential Scanning Fluorimetry
DSP	Dithiobis(succinimidyl propionate)
DTSSP	3,3′-dithiobis(sulfosuccinimidylpropionate)
DTT	Dithiothreitol
dTTP	Deoxythymidine triphosphate
ECL	Enhanced chemiluminescence
EGS	Ethyleneglycol bis(succinimidylsuccinate)
GSH	Glutathione
GSX	Electrophilic conjugates of glutathione

HEPES	4-(2-hydroxyethyl)-1-piperazineethanesulfonic acid
His_6	Hexahistidine tag
IMAC	Immobilized Metal Affinity Chromatography
IPTG	Isopropyl-β-D-1-thiogalactopyranoside
ITC	Isothermal Titration Calorimetry
LB	Lysogeny Broth
LBK	Lysogeny broth with potassium
NAD^+	Nicotinamide adenine dinucleotide, oxidized
NADH	Nicotinamide adenine dinucleotide, reduced
OD	Optical density
pApA	Phosphoadenyl Adenosine
PCR	Polymerase Chain Reaction
PDB	Protein Data Bank
PEG	Polyethylene Glycol
PMSF	Phenylmethane sulfonyl fluoride
RCK	Regulator of conductance of K^+
RCK_C	C-terminal subdomain of an RCK domain
RCK_N	N-terminal subdomain of an RCK domain
RFU	Relative fluorescence units
RNA	Ribonucleic acid
rpm	Revolutions per minute
SD	Standard Deviation
SDS	Sodium dodecyl sulfate
SDS-PAGE	Sodium dodecyl sulfate polyacrylamide gel electrophoresis
SEC	Size exclusion chromatography
SPT	Supernatant
TBE	Tris-borate-EDTA
TCEP	Tris(2-carboxyethyl)phosphine
TE	Total Extract
Thr	Thrombin
T_m	Melting Temperature
Tris	Tris(hydroxymethyl)aminomethane

1. Introduction

1.1. The importance of metal ions

Metal ions are participants in a series of fundamental biological processes. Alkali and alkali earth metals, such as Sodium (Na^+), Potassium (K^+), Magnesium (Mg^{2+}), Calcium (Ca^{2+}) are vital for the stability, proper folding and normal functioning of RNA and proteins. K^+ is the most abundant intracellular cation in living organisms[1] and not only acts as a buffer for the negative charge in nucleic acids and helps in establishing the membrane potential, but also is important for proper enzyme activity[2]. K^+ and Mg^{2+}, have pronounced synergistic effects despite differences in chemical properties. In fact, Mg^{2+} is significantly smaller (ionic radius 0.72 Å) when compared to K^+ (ionic radius 1.51 Å) and exhibits a strong preference for octahedral coordination[3]. On the other hand, K^+ is less charged and leans towards higher coordination numbers, usually between 8 and 12[4]. This disparity precludes the possibility of their competition but rather expands the variety of environments and possible interactions for these cations, which is particularly favourable for macromolecular machineries. In fact, ribosomes, the largest and most abundant RNA-containing macromolecular complexes in all cell types, require both K^+ and Mg^{2+} to preserve their integrity and correct function[4].

In a normal healthy person, K^+ appears predominantly in the intracellular fluid (≈ 150 mM)[5] whereas its concentration in the extracellular fluid is maintained within a narrow range, usually between 3.5 and 5 mM[6]. This ionic distribution is a critical determinant for the resting membrane potential of cells and is highly influenced by the activity of the sodium and potassium pump (Na^+-K^+-ATPase), which transports Na^+ and K^+ across the cell membrane by active transport. For each molecule of ATP hydrolysed, two K^+ ions are transported inside while three Na^+ ions are driven out of the cell, leading to an unequal dispersal of Na^+ and K^+ that can be seen in nearly all vertebrate cells[7].

1.2. Osmoregulation in *Bacillus subtilis*

Potassium and glutamate are the ions that exist in larger quantities inside each living cell but, despite nearly all bacteria possessing pathways for glutamate biosynthesis, potassium can only be acquired by transport. For example, Gram-negative bacterium

Escherichia coli accumulates these two ions in concentration ranges between 200 and 400 mM for potassium and about 100 mM for glutamate[8]. Since the concentration of potassium in typical bacterial habitats is usually around 100 µM to 10 mM, there is a visible need for highly effective uptake systems to be able to accumulate and enrich the intracellular milieu[9]. On the other hand, the intracellular concentration of Na^+ is kept at a much lower concentration (between 2-20 mM) when compared to the external medium, as bacteria are known to actively extrude Na^+ ions[10]. As a consequence, bacteria maintain an inwardly directed Na^+ gradient that can be used to drive multiple processes, such as accumulation of nutrients[11] or motility[12].

As all microorganisms lack the ability to actively transport water, their water content is determined by fluctuations in the conditions of the external environment. For example, changes in external salinity or osmolality contribute greatly to the hydration status of the cytoplasm and the turgor of the microorganism. To keep hydration and turgor within physiologically acceptable limits, bacteria control their intracellular solute pools[13]. One of the strategies that bacteria use to surpass a possible sudden osmotic increase is the accumulation of ions and organic osmolytes in conditions of high osmolality and their expulsion through mechanosensitive channels when external osmolality decreases[14]. The process of adaptation to external increased osmolality is usually characterized by a two-phase adaptation reaction: the first stage begins with the fast uptake of K^+ ions to compensate for the water efflux that accompanies the increase in external salinity[15]. The second stage of this reaction is necessary to equilibrate the concentration of K^+ inside and outside of the cells, frequently involving the synthesis or uptake of compatible osmolytes and efflux of K^+[16].

Bacillus subtilis, one of the best characterized bacteria among Gram-positives, is a spore-forming bacterium commonly found in soils and widely used as a model for the study of Gram-positive bacteria. *B. subtilis* constitutes an example of microorganism that uses the two-phase adaptation reaction mentioned above, meaning that its viability is closely dependent to K^+ [17]. An experiment conducted by Whatmore et al[18], demonstrated that in exponentially growing cells subjected to an osmotic shock with 0.4 M NaCl, the levels of intracellular K^+ rose from a basal level of 350 mM to 650 mM within 1 hour.

Curiously, *B. subtilis* can stand salinities higher than 0.4 M NaCl [19], which indicates that K^+ intracellular concentrations can reach values higher than 650 mM in severely osmotically challenged cells. In addition, *B. subtilis*, under high salinity conditions, synthetizes the amino acid L-proline, an osmoprotectant compatible with cellular

metabolism[20]. Proline has the ability to act as a chemical chaperone, assisting in protein folding and preventing aggregation in osmotically challenged cells[21].

However, the processes described so far only constitute the first step of the adaptative response and, as it was mentioned above, the increased uptake of potassium and proline biosynthesis are insufficient to ensure the growth of *B. subtilis* in harsh high osmolarity environments. The accumulation of large amounts of other osmoprotectants is vital to assure the well-functioning of the cell and glycine betaine stands out for being one of the most important. Glycine betaine has the particularity to be metabolically inert in *B. subtilis* under both high and low-osmolarity growth conditions, and its accumulation can be achieved either through synthesis or by direct uptake from the environment[19]. Synthesis can be achieved either by *de novo* synthesis or by an enzymatically driven two-step oxidation process of precursor choline[22]. *De novo* synthesis of glycine betaine is characterized by a stepwise methylation of the amino acid glycine, a process that demands high energy[23]. Due to this fact, glycine betaine is most frequently produced through oxidation of choline, a compound typically imported by bacteria as they cannot synthetize choline[24]. For this purpose, in *Bacillus subtilis*, there are two ABC transporters with high affinity to choline: OpuB and OpuC[25]. The OpuB system only imports choline and the intermediate in glycine betaine synthesis, whereas OpuC imports a broad range of substrates[24]. In addition, there are other two ABC transporters (OpuA and OpuD) that transport glycine betaine from the exterior, as glycine betaine is also synthesized by plants[22,26].

In *B. subtilis*, the systems responsible for the uptake of osmoprotectans and biosynthesis of glycine betaine have been characterized with considerable detail. On the other hand, there is still a lack of understanding about K^+ transporters and K^+ homeostasis in *Bacillus subtilis*. Both these topics are going to be addressed in the following chapter.

1.3. Potassium homeostasis in *Bacillus Subtilis*

To fulfil the necessity to acquire potassium from the external media, *Bacillus subtilis*, like many other bacteria, possess multiple high and low-affinity K^+ uptake systems that allow efficient transport under all environmental conditions[8]. In *B. subtilis*, there are three potassium importers that have been identified, where KtrAB and KtrCD are the most studied.

KtrAB and KtrCD are hetero-oligomeric transporters that consist on a membrane-embedded subunit (KtrB and KtrD) and a peripheral regulatory subunit (KtrA and KtrC), which regulate KtrAB and KtrCD through a ligand-mediated conformational switch mechanism[17,27]. Experiments conducted by Holtmann et al[17], show that both components of an individual Ktr system in *B. subtilis* are required for K^+ uptake activity. Moreover, KtrA and KtrC regulatory subunits are part of the family of regulators of K^+ conductance (RCK) domains[28]. RCK domains are ubiquitous among the major K^+ selective transport systems and can be found either within a cytoplasmic subunit (like KtrA and KtrC) or covalently linked to the C terminus of pore-forming transmembrane domain[29,30]. Many RCK domain structures have been determined and all of them revealed RCK dimers with a domain that adopts the Rossman fold[31], composed by six alternating beta strands and alpha helices, where the sixth alpha helix is swapped between adjoining domains[32] and serves as a dimerization motif (**Figure 1.1**).

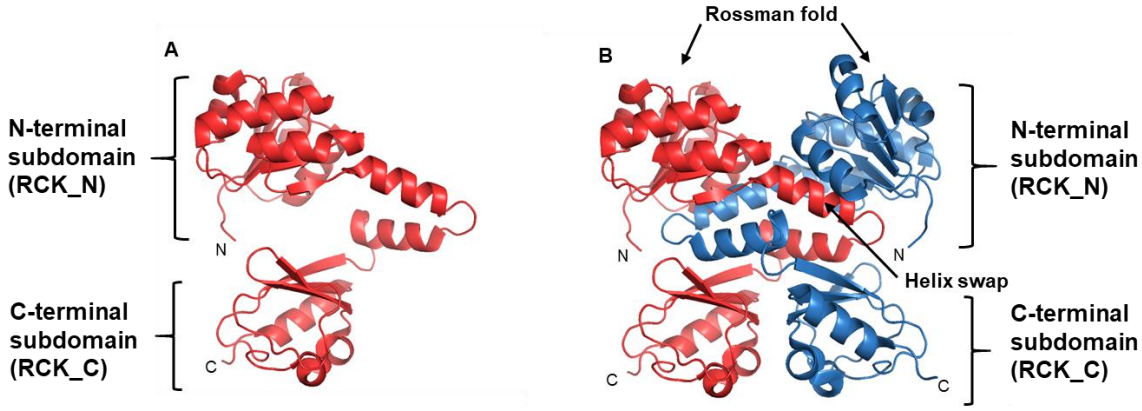

Figure 1.1 - Representation of an RCK domain from a prokaryotic potassium channel. **A)** a single subunit of the RCK domain in the MthK, a K^+ channel from *Methanothermobacter thermoautotrophicus*. **B)** homodimer of the MthK RCK domain (PDB accession code: 2AEM). Monomers are colored in either red or blue. This figure was generated by PyMOL.

Besides the Rossman-fold domain, many RCK domains also contain a smaller domain and therefore can be subdivided into two subdomains: the N-terminal subdomain (termed RCK_N) and the C-terminal subdomain (termed RCK_C). The RCK_N, exhibiting the well conserved Rossman fold, is linked to the less well-conserved RCK_C subdomain through a linker[33]. RCK domains are known to bind a diverse range of biological ligands, such as NAD^+/NADH, ATP, cyclic nucleotides, metal ions like Ca^{2+} and to modulate channel activity[34,35,36]. Briefly, when the ligand binds to the RCK domain, a conformational change is triggered, leading to an activation of the RCK domain and subsequent opening of the channel[33,37]. RCK domains have been also identified in

eukaryotic K^+ channels and are present across phyla and kingdoms, which highlights the importance of these domains in physiological regulation of K^+[33].

Potassium homeostasis is controlled not only by import proteins but also by exporters. In *E. coli,* the K^+ efflux system Kef has been characterized with a high level of detail. Kef proteins in *E. coli*, comprising KefFC and KefGB, are K^+/ H^+ antiporters activated by glutathione (GSH) and its electrophilic conjugates (GSX)[38,39]. GSH acts as an inhibitor of Kef, holding the transporter in an inactive state. However, in the presence of electrophiles, GSH chemically reacts with these species forming GSX, which activate the Kef system resulting in K^+ efflux and concomitant H^+ influx[38]. In Gram-positive bacteria, GSH is absent[40], instead they produce other low-molecular-weight thiols like bacillithiol, which may serve as a substitute for GSH[41]. Potassium efflux systems in *Bacillus subtilis* are far from being completely understood, with three putative exporters proposed: the YugO K^+ channel[42], the K^+/H^+ antiporter KhtTU[43] and the cation exporter YjbQ[44].

1.4. Cyclic-di-AMP: an essential second messenger in bacteria

In their natural environments, living organisms are constantly exposed to different external stimuli. In order to cope with these changes, cells receive and process those stimuli through signal transduction pathways and respond accordingly. Many cyclic nucleotides act as second messengers, having fundamental roles in signalling pathways capable of sensing environmental changes[45]. This ability of cyclic nucleotides to act as second messengers is not exclusive of eukaryotes, as prokaryotes equally exhibit these molecules and, since the discovery of the original second messenger, cyclic adenosine monophosphate (cAMP), many additional cyclic nucleotides that act as second messengers have been discovered. This growing list includes cyclic guanosine monophosphate (cGMP), cyclic di-guanosine monophosphate (c-di-GMP) and cyclic di-adenosine monophosphate (c-di-AMP). c-di-AMP (**Figure 1.2**) has been subject of intense research since its discovery in Gram-positive bacteria. Interestingly, low-GC Gram-positive bacteria, such as *Bacillus subtilis*, *Staphylococcus aureus*, *Listeria monocytogenes* and many others (the Firmicutes), are unable to live in the absence of c-di-AMP[46]. This second messenger has been shown to be implicated in many essential cellular processes including cell wall and membrane homeostasis, DNA damage repair, sporulation and importantly, regulation of potassium homeostasis [47]. Thus, c-di-AMP is so far the only known second messenger that is as essential for the bacteria that produce

it[48]. Bacteria, such as *Bacillus subtilis* or *Listeria monocytogenes*, produce both c-di-AMP and c-di-GMP but the signalling pathways for these two cyclic nucleotides rarely co-exist in the same organism. For example, bacterial species like *Staphylococcus* and *Streptococcus* do not have functional c-di-GMP synthesizing enzymes[49].

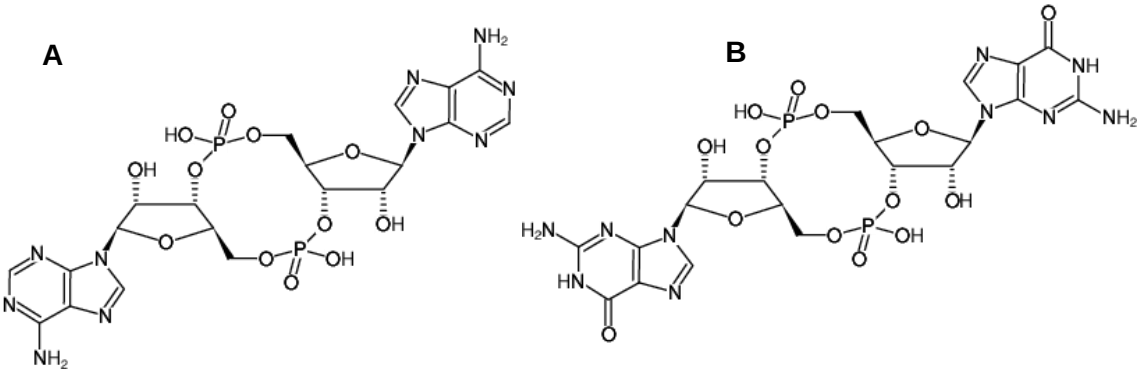

Figure 1.2 - Structural formula of two cyclic nucleotides. A) cyclic-di-AMP molecule, **B)** cyclic-di-GMP molecule.

c-di-AMP is synthetized by cyclase domain-containing enzymes known as diadenylate cyclases (DACs), either from two molecules of ATP or ADP[48]. The first DAC domain to be identified was in the DNA integrity scanning protein A (DisA), which functions as a DNA check point protein[50]. Later, other DAC domain-containing proteins were found, which led to the classification of DACs into four classes: DisA, CdaA, CdaS and CdaM. Commonly, organisms only contain one type of DACs, however *Bacillus subtilis* constitutes an exception as it contains three: DisA, CdaA, and CdaS[51]. Between these three proteins, the diadenylate cyclase CdaA seems to be the most important one as it is present is all low-GC Gram-positive bacteria, including *Staphylococcus aureus* and *Listeria monocytogenes*[52]. However, logically, bacteria need to possess both synthesis and degradation enzymes in order to balance the cellular level of second messenger molecules. In *Bacillus subtilis* c-di-AMP is degraded by two phosphodiesterases named GdpP and PgpH, converting it into phosphoadenyl adenosine (pApA) which can be further degraded into two molecules of AMP[47] (**Figure 1.3**).

Several targets of c-di-AMP are involved in the transport of osmolytes such as carnitine, potassium and maybe other ionic species[49]. It is known that c-di-AMP binds to multiple K^+ transporters, specifically to the RCK domains of proteins. Bearing in mind that RCK domains are widely distributed, this suggests that c-di-AMP is a major regulator of K^+ in bacterial species. It was previously shown that c-di-AMP binds to *Staphylococcus aureus* KtrC with an inhibitory effect in the K^+ flux[53]. As Ktr channels from *Bacillus subtilis* share a high degree of similarity with their orthologs in *S.aureus*, it is likely that c-di-AMP will

also inactivate the Ktr channels from *B. subtilis*. In addition, c-di-AMP is predicted to bind to the RCK domain of YjbQ stimulating its efflux activity[54].

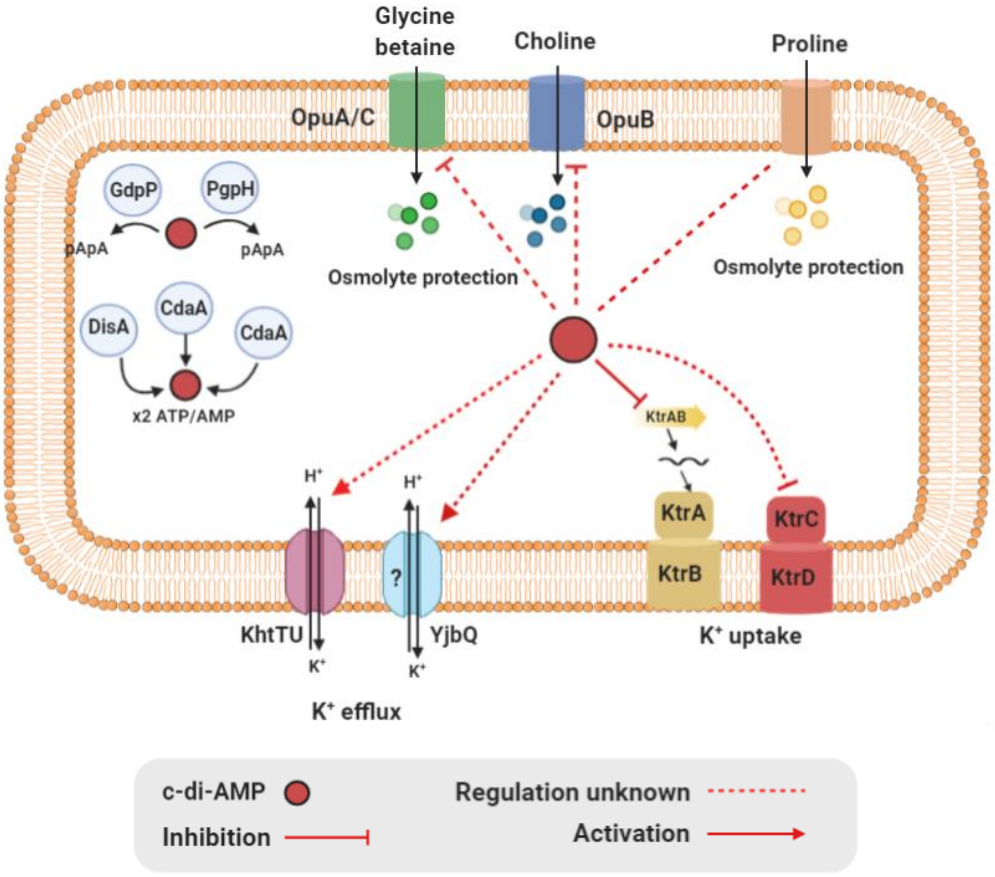

Figure 1.3 - Overview of the cellular targets that are presumed and known to be regulated by c-di-AMP in *Bacillus subtilis*. Synthesis and degradation of c-di-AMP and targets that are presumed and known to be regulated by this nucleotide. KtrC inhibition by c-di-AMP is known in *S.aureus* and presumed in *Bacillus subtilis*. The transport activity of the Opu osmolyte uptake system is inhibited by c-di-AMP in *S. aureus* and *L. monocytogenes* and presumed in *Bacillus subtilis*.

1.5. Cation/proton antiporters in bacteria

Many biological processes depend on transporters that regulate the pH, volume and cation homeostasis in both eukaryotic cells and in prokaryotes. Cation/proton antiporters (CPAs) play a crucial part in all living species, as CPAs typically function as exchangers of monovalent cations, mainly K^+ and Na^+, accompanied with an inward movement of one or two protons[55]. In bacteria, this antiport motion is energized by a proton-motive force across the membrane, that is created by proton pumping during respiration or ATP hydrolysis[56]. Whereas some CPAs are electroneutral, meaning that during exchange there is no net charge build-up, others are classified as electrogenic, exchanging an

unequal number of protons and monovalent cations[55]. Phylogenetic studies have divided CPAs into two distinct families: CPA1 and CPA2, based on their individual electrogenicity and ion selectivity profile. However, this classification is still questionable as there is still much debate when it comes to the mechanism behind electrogenicity.

The proposed CPA2 family contains both prokaryotic and eukaryotic transporters, such as the above-mentioned *E. coli* K^+ efflux proteins KefFC and KefGB, *Bacillus pseudofirmus* NH_4^+ and K^+ transporter AmhT and *Bacillus subtilis* K^+/H^+ antiporter KhtTU[43]. The latter is characterized for being a part of an operon composed by three different open reading frames: *khtU*, *khtT* and *khtS*[57]. This apparent operon encodes potassium-transport-related proteins that exhibit sequence similarity to CPA2 family members stated above[43]. In early 2006, studies conducted by Fujisawa et al[57] proposed that KhtU, a transmembrane protein, catalysed K^+ transport. In the K^+ uptake deficient mutant TK2420 from *E. coli,* expression of KhtU exacerbates the K^+-dependent phenotype of this strain, revealing its capacity to export K^+ ions. In 2007, the same group demonstrated that KhtT and KhtU, when expressed together, exhibit K^+/H^+ antiport activity, leading to the conclusion that KhtU requires its ancillary protein KhtT to exhibit antiport activity[43].

1.6. The YjbQ protein: a putative cation exporter

The other putative K^+ exporter in *B. subtilis*, YjbQ, remains uncharacterized. This protein is also presented as a CPA2 transporter and in the *Subtiwiki* database, a resource gathering information about *Bacillus subtilis*[58], YjbQ is presented as a K^+/H^+ antiporter, functioning as an exporter for K^+ ions. However, no publications support the proposed function of this protein. Instead, this proposal results from the 52% amino acid sequence similarity with CpaA, a putative potassium exporter from *Staphylococcus aureus* (SaCpaA)[59]. Studies conducted by Chin et al.[59] suggested that *Sa*CpaA acts as a cation−proton antiporter, with no obvious specificity for Na^+ or K^+. Furthermore, it was proved that SaCpaA C-terminal RCK domain, demonstrated to elute as a dimer in size exclusion chromatography, showed strong affinity for c-di-AMP in Isothermal titration calorimetry (ITC). As the main focus of their studies was the structural properties of SaCpaA, its functional characterization lacks some detail. They managed to co-crystallize the complete SaCpaA RCK domain with c-di-AMP. However, after calculating the electronic density map of the SaCpaA_RCK dimer at 3.5 Å, it was concluded that the density was of bad quality and it was not possible to build a high-quality molecular

structure into the density (**Figure 1.4 A**). As a consequence, the authors decided to crystallize a truncated version of SaCpaA, which included only the RCK_C sub-domain together with c-di-AMP. This N-terminal truncation did not seem to affect the structure of the CTD as the SaCpaA_RCK_CTD_c-di-AMP complex structure appeared to superimpose well with the full-length SaCpaA_RCK−c-di-AMP complex. With this, the truncated structure of *Sa*CpaA was determined at a much-improved resolution of 1.82 Å and constitutes the only version of this protein deposited on Protein Data Bank (PDB accession code: 5F29) (**Figure 1.4 B**).

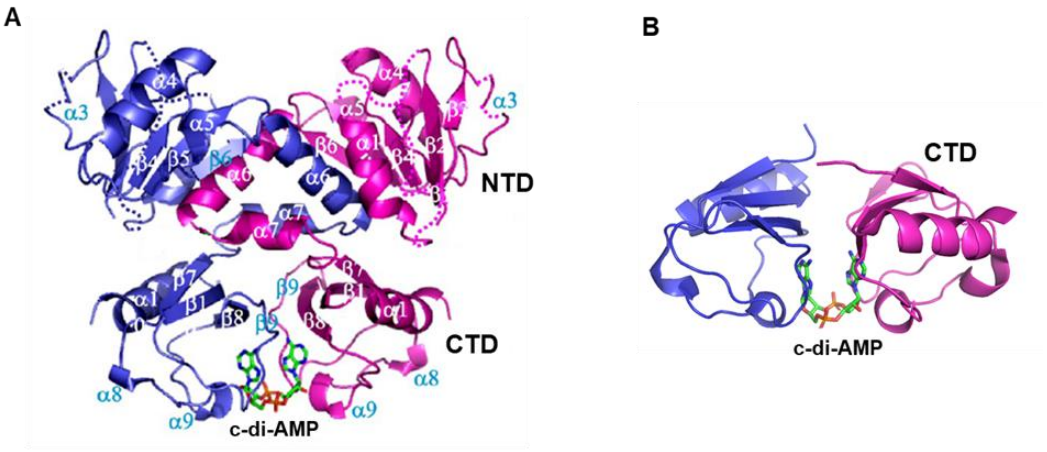

Figure 1.4 - Structure of the SaCpaA_RCK−c-di-AMP and SaCpaA_RCK_CTD_c-di-AMP. A) Incomplete structure of the RCK domain of SaCpaA. Invisible regions in the more dynamic N-terminal domain (NTD) region are connected by dotted lines. Adapted from 59. **B)** Structure of the C-terminal subdomain of the RCK domain, deposited on PDB (accession code: 5F29). Image generated by PyMOL.

Similarly, YjbQ contains a C-terminal RCK domain but, unlike SaCpaA, its binding and affinity to c-di-AMP are not clearly characterized. Recently, Gundlach et al[44] using a differential radial capillary action of ligand assay (DRaCALA), suggested that YjbQ binds to c-di-AMP [44]. DRaCALA is a method to quickly measure protein-ligand interactions, shown to be useful in a first analysis on protein interactions, as it does not require a purified protein sample. Altogether, it is safe to conclude that it is necessary to investigate deeper into YjbQ biochemical and structural properties in order to characterize its functional and molecular properties.

2. Objectives

The main goal for this work was to characterize the structural and functional properties of the YjbQ protein from *Bacillus subtilis.* We were interested in answering questions such as: is YjbQ a K^+/H^+ antiporter? Is the activity of YjbQ regulated by c-di-AMP? What is the structure of the RCK domain of YjbQ? What are the residues that define the c-di-AMP binding site? What is the molecular mechanism of YjbQ regulation by c-di-AMP?

To tackle these questions, the optimal conditions for the RCK domain of YjbQ expression and purification conditions were determined, the regulatory domain was crystallized, with and without ligand, the three-dimensional structures by X-ray crystallography were determined.

To investigate the so-far unknown function of YjbQ the structural characterization was complemented with functional assays using *in vivo* phenotype complementation assays and *in vitro* fluorescence-based assays.

3. Materials and Methods

3.1. Reagents, Growth media and Bacterial strains

Bacterial growth media were prepared according to **Table 3.1**; sterilization was realised by autoclaving for 20 minutes at 121ºC. Information about the *E. coli* competent cell strains used during this work is displayed in **Table 3.2**.

Table 3.1- Composition of growth media used in cell cultures used throughout this work.

Lysogeny Broth (LB)	10 g/L Tryptone, 5 g/L Yeast Extract, 10 g/L NaCl
LB with K^+ (LBK)	10 g/L Tryptone, 5 g/L Yeast Extract, 10 g/L KCl

Table 3.2 - Genotype information of the *E. coli* strains used throughout this work.

NEB 5-alpha	fhuA2 Δ(argF-lacZ) U169 phoA glnV44 Φ80 Δ(lacZ)M15 gyrA96 recA1 relA1 endA1 thi-1 hsdR17
BL21(DE3)	F- ompT lon hsdSB (rB-mB-) gal dcm (DE3)
KNabc	Derivative of TG1 cells (ΔnhaA, ΔnhaB, ΔchaA)
TK2420	ΔKdp, ΔKup, ΔTrk

3.2. Molecular cloning

3.2.1. Cloning using restriction enzyme digestion

Insert amplification was performed using 25-30 cycles of polymerase chain reaction (PCR) with *Bacillus subtilis* genomic DNA or with plasmid containing the gene fragment of interest and respective oligomers (**Table 3.3**). PCR reactions were executed with either Pfu or Phusion DNA polymerases (Thermo Scientific) and confirmed by agarose gel electrophoresis (1% (w/v) agarose in TBE buffer). DNA fragments were purified with QIAquick Gel Extraction Kit (QIAGEN). The resulting PCR products and respective cloning vectors were digested for 2 hours at 37ºC with the appropriate restriction enzymes. Digestion was followed by gel purification and ligation reaction by incubating T4 DNA Ligase (Thermo Scientific) with digested PCR product and vector at 4ºC

overnight. Ligation products were transformed into NEB 5-alpha cells and plated onto LB-agar plates supplemented with the appropriated antibiotic.

A minimum of six colonies were selected from each plate and inoculated in 5-10 mL of liquid LB with antibiotic and grown at 37ºC, 225 rpm overnight. A second PCR reaction was performed on lysed cells from each culture and the PCR products were analysed by an agarose gel electrophoresis (1% (w/v) agarose in TBE buffer) to assess if the DNA fragment of interest had been successfully inserted in the vector. DNA from 2 positive clone cultures was extracted using NZYTech's MiniPrep Kit, DNA sequence of insert was determined (Eurofins Genomics, Germany) and analysed for the presence of potential mutations.

3.2.2. Gibson Assembly

The DNA construct created by Gibson assembly (**Table 3.4**) was obtained by PCR with Phusion DNA polymerase (Thermo Scientific) and respective oligomers. Two different PCR reactions were performed in order to produce DNA segments with overlapping regions: one reaction for the amplification of the vector and another for the insert. The success of each reaction was confirmed by agarose gel electrophoresis (1% (w/v) agarose in TBE buffer) followed by gel purification. 20-30 ng of insert and vector were mixed into a final volume of 5 µL. The amount of insert and vector added was calculated considering the length and concentration of each fragment. 5 µL solution containing the DNA molecules of interest was mixed with 15 µL solution of Gibson mix, containing 1.33x of Isothermal Master Mix (500 mM Tris-HCl pH 7.5; 50 mM $MgCl_2$; 1 mM dGTP, dCTP, dTTP and dATP; 50 mM DTT; 25% PEG-8000; 5 mM of NAD) and 0.005 U/µL T5 exonuclease, 0.04 U/µL Phusion polymerase (Thermo Scientific), 5.4 U/µL Taq DNA ligase. The resulting solution was incubated at 50ºC for 1 hour. The assembly mix was transformed into NEB 5-alpha cells and plated onto LB-agar plates supplemented with the appropriated antibiotic. Identification of positive clones followed the protocol described in the previous section.

3.2.3. Site-directed mutagenesis

Mutant complementary DNA strands (**Table 3.5**) were synthetized by PCR using complementary oligonucleotides containing the desired mutation according to the

QuikChange Manual[60]. The PCR product was incubated with 1 µL of DpnI restriction enzyme (10 U/µL, Thermo Scientific) for 1 hour at 37ºC to remove the methylated wild-type DNA strands.

The final reaction product was transformed into NEB 5-alpha cells and plated onto LB-agar plates supplemented with the appropriate antibiotic. One or two clones were sent for sequencing according to protocol described above.

Table 3.3 – Primers used to prepare the vectors used in the studies on YjbQ.

Construct name	Vector	Insert	Tags	Oligomers
pBAD_yjbQ	$pBAD_{His\ b}$ (Ampicillin)	YjbQ	None	Forward (XhoI): 5'-ACCGCTCGAGAGCGCATACATCTGTCGC-3' Reverse (EcoRI): 3'- AAGCGAATTCTTATCCTTCCAATGTTTTC-5'
pET15b_RCK_1*	pET-15b (Ampicillin)	RCK domain of YjbQ	N-terminal: His_6-Thr**	Forward (NdeI): 5'-CTAGACATATGCGGGAAGAGCAGCCGGAGGAG-3' Reverse (BamHI): 3'-CTAGAGGATCCTTATCCTTCCAATGTTTTCTTAAG-5'
pET15b_RCK_2*	pET-15b (Ampicillin)	RCK domain of YjbQ	N-terminal: His_6-Thr**	Forward (NdeI): 5'-CTAGACATATGAAAAAGACGATTACGTTCATTG-3' Reverse (BamHI): 3'-CTAGAGGATCCTTATCCTTCCAATGTTTTCTTAAG-5'
pBAD33_DAC	pBAD33 (Chloramphenicol)	DAC domain of CdaA	None	Forward (XbaI): 5'-GCTCTAGAATCATTATTCGCTTTTGCCTC-3' Reverse (KpnI): 3'-CAGGGGTACCTGTTTAACTTTAATAAGGAGATAT-5'

(*) RCK_1 and RCK_2 both correspond to the RCK domain of yjbQ. The only difference between them is the length of the insert itself, as RCK_2 lacks the first 21 base pairs of RCK_1.

(**) "Thr" symbolizes a thrombin cleavage site (nucleotide sequence CTGGTGCCGCGCGGCAGC, coding for the amino acid sequence LVPR↓GS, recognized by this protease. Arrow indicates cleavage point.) present in the vector pET-15b soon after the N-terminal His_6-tag sequence.

Table 3.4 – Primers used to prepare the His-tagged YjbQ.

Construct name	Vector	Insert	Tags	Oligomers
pBAD_yjbQ +TAG	$pBAD_{His\ b}$ (Ampicillin)	YjbQ	N-terminal: His_6-Thr	**Vector amplification** Forward: 5'-TCCACCAGTCATGCTAGCCATACC-3' Reverse: 3'-GATCTGCAGCTGGTACCATATGGG-5' **Insert amplification** Forward: 5'-TATGGTACCAGCTGCAGATCTTATCCTTCCAATGTTTTCTTAAGATCCGTTACGTAC-3' Reverse: 5'-TGGCTAGCATGACTGGTGGAATGGCGCATACATCTGTCGC-3'

Table 3.5 – Primers used to prepare mutant YjbQ strains.

Construct name	Vector	Insert	Tags	Oligomers
pBAD_yjbQmut1*	$pBAD_{His\ b}$ (Ampicillin)	Mutant YjbQ	None	Forward*: 5'- AAATTATACAAACGG**TAA**GAGCAGCCGGAGGAGAAAAAG -3' Reverse: 3'- CTTTTTCTCCTCCGGCTGCTCTTACCGTTTGTATAATTT-5'
pBAD_yjbQmut2*	$pBAD_{His\ b}$ (Ampicillin)	Mutant YjbQ	None	Forward*: 5'- GAGCAGCCGGAGGAGAAA**TAA**ACGATTACGTTCATTGGC-3' Reverse: 3'- GCCAATGAACGTAATCGTTTATTTCTCCTCCGGCTGCTC -5'

(*) Both YjbQ mutant constructs lack the cytoplasmatic RCK domain of the protein. The only difference between them is that the stop codon in pBAD_yjbQmut2 appears 18 base pairs after the one in pBAD_yjbQmut1.

(**) Both forward oligomers used in site-directed mutagenesis possess the stop codon "**TAA**" in the middle of the sequence.

3.3. Small-scale Protein Expression Tests

Protein expression with the constructs pET15b_RCK$_1$ and pET15b_RCK$_2$ was tested using *E. coli* strain BL21(DE3) and LB growth media (see media composition in section x). Induction time and temperature were tested: 3 hours at 37ºC or overnight at 18ºC (~17 hours). The latter included induction of heat and cold-shock chaperones by 1% ethanol and ice-bath treatment, respectively, prior to addition of inducer. Protein expression was induced by adding 0.5 mM of isopropyl-β-D-1-thiogalactopyranoside (IPTG) when the optical density at 600 nm (OD_{600nm}) of the cell culture reached values between 0.6 to 0.8.

Small-scale expression tests were performed by inoculating 50 mL of liquid media plus antibiotic with a resuspension of transformed colonies followed by whatever set of conditions being tested. Cells were then pelleted, resuspended in Expression Test Lysis Buffer (20 mM Tris pH 7.5; 100 mM NaCl; 0.01 mg/mL lysozyme; 0.01 mg/mL DNAase; 1 mM TCEP) and lysed by sonication cycles (Branson sonifier 250; 3-4 cycles of 15 seconds each, power level 3, duty cycle of 30%). Total protein and soluble protein expression levels were assessed by SDS-PAGE (17% gel) from total extract (TE) fraction (just after sonication) and supernatant (SPT) fraction (after a 10 min, 12000 g centrifugation of lysates).

3.4. RCK domain Expression and Purification Protocol

The standard large-scale protocol for YjbQ RCK domain expression and purification developed in this work consists of the following steps: *E. coli* BL21(DE3) competent cells were transformed with pET15b_RCK1 or pET15b_RCK2 expression vectors and plated onto LB plates containing 100 µg/mL ampicillin. The next day, all colonies on the plate were resuspended in LB media and OD_{600nm} was determined. 4L culture flasks containing 1L LB media (with 100 µg/ml ampicillin) were inoculated with a fraction of resuspended cells corresponding to 6 OD_{600nm}. Cells were grown in an orbital shaker at 37ºC, 160 rpm until OD_{600nm} reached 0.8~0.9, at which point, cells were induced with 0.5 mM IPTG and incubated at 18ºC overnight (~17 hours). Induced cultures were then pelleted for 20 mins at 3500 rpm, 4ºC and stored at -20 ºC. Pellets were resuspended in 20 mL of Lysis Buffer (50 mM Tris-HCl pH 8.0; 150 mM NaCl) followed by cell lysis using a prechilled Emulsifex-C5 (Avestin).

Unwanted proteolytic digestion was inhibited by adding 1 mM PMSF, 1 µg/mL Leupeptin and 1µg/mL Pepstatin A prior to lysis. Lysate was centrifuged (45 minutes, 1700 rpm, 4ºC) and the supernatant was loaded into a pre-equilibrated nickel affinity purification column. Flow-through was reloaded at least two times into the column to increase the probability of binding. Beads were then washed with 5 column volumes (25 mL) of Lysis buffer and bound protein was eluted using solutions with 10 mM, 20 mM, 150 mM and 300 mM of Imidazole. To assess which fractions contained protein all eluted samples were submitted to SDS-PAGE analysis. Selected fractions were dialysed overnight (~16 hours) in the presence of 1 µL of thrombin. The following day, dialyzed protein was concentrated and injected (at 13 mg/mL) in a size-exclusion chromatography Superdex 200 10/300 GL column (GE Healthcare) pre-equilibrated with 1 column volume (20 mL) of Lysis buffer. Purified protein fractions were pooled together and concentrated. Protein concentration was determined by Bradford quantification assay.

3.5. Ligand Testing by Thermal Shift Assay

The Sypro Orange thermal shift assay was used to identify potential small molecule ligands of the RCK domain of YjbQ. Two protein concentrations were tested: 1.5 µM and 3.0 µM. Each sample consisted of the purified protein sample (in the corresponding buffer: 20 mM Tris pH 8.0; 150 mM NaCl), a 2.5 X diluted Sypro Orange Protein Gel Stain and the small molecule ligand at concentrations that varied between 0.1 mM and 1 mM. The final mixture for each sample was prepared by adding 40 µL of protein and Sypro Orange dye plus 10 µL of the potential ligand. The experiment was then setup in a 96-well PCR White Plate (Bio-Rad) and performed in a iQ5 real-time PCR system (Bio-Rad) using the Cy3 filter specific for Sypro Orange detection (λ_{ex} = 490 nm / 5λ_{em} = 575 nm), with the temperature varying from 25 ºC to 95 ºC in 0.5 ºC increments of 30 seconds each. Data were analysed using the CFX Manager Software (Bio-Rad).

3.6. Size-exclusion chromatography experiments

The influence of pH, protein concentration and presence of c-di-AMP in the oligomerization of the RCK domain of YjbQ were tested by size-exclusion chromatography.

For testing the effect of pH, 200 µL of previously dialysed RCK domain at 13 mg/mL were mixed with 50 µL of 1M Tris-HCl pH 8.0 and 9.0 or Bis-Tris pH 6.5 and the resulting mix (at 10.4 mg/mL) was injected in a size-exclusion chromatography Superdex 200 10/300 GL column (GE Healthcare) pre-equilibrated in a solution with 150 mM of NaCl and 20 mM of the corresponding buffer.

To test the impact of protein concentration, dialysed protein (in 20 mM of HEPES pH 6.5 and 150 mM of NaCl) was concentrated, and its concentration was determined by Bradford quantification assay. Thereafter, protein samples were injected at three different concentrations: 8 mg/mL, 18 mg/mL and 1.5 mg/mL and injected in a Superdex 200 10/300 GL column (GE Healthcare) pre-equilibrated in a solution with 20 mM HEPES pH 6.5 and 150 mM of NaCl.

For evaluation of the impact of c-di-AMP, RCK domain samples at 5.3 mg/mL with and without 1 mM c-di-AMP were injected in a Superdex 200 Increase 5/150 GL column (GE Healthcare) pre-equilibrated in a solution with 20 mM of HEPES pH 6.5, 150 mM of NaCl. In the injection of the protein in the presence of c-di-AMP, the column was pre-equilibrated in the same solution supplemented with 30 µM of c-di-AMP.

3.7. Membrane preparation and Cross-linking experiments

A cell pellet from a 100 mL of *E. coli* BL21(DE3) culture expressing full-length YjbQ with a C-terminal His tag (construct name: pBAD_yjbQ +TAG) was resuspended in buffer (20 mM HEPES pH 8.0; 50 mM NaCl; 100 mM KCl) and lysed by three passages through an Emulsiflex-C5 cell-cracker (Avestin). Membranes were prepared after a low speed 10-min spin at 10,000 rpm (rotor JA25-50), 4 °C followed by a high-speed spin at 50,000 rpm (rotor Ti-70) for 1.5 h at 4 °C. Pellets were resuspended in 1 mL of buffer, and total protein concentration was determined by Bradford quantification assay.

The protein suspension was diluted to 2 mg/ml total protein concentration and the amino group-reactive cross-linkers (3,3′-dithiobis(sulfosuccinimidylpropionate) (DTSSP) and ethyleneglycol bis(succinimidylsuccinate) (EGS)) , at four different concentrations: 31.25 µM, 62.5 µM, 125 µM and 500 µM (freshly made stock at 25 mM in DMSO), were added to membrane aliquots. The mixture was incubated at room temperature for 30 minutes and each reaction was stopped by addition of Tris buffer solution (pH 7.5) to a final concentration of 100 mM and incubated for 15 minutes.

Samples were run in a 8% SDS-PAGE, blotted onto polyvinylidene difluoride membrane, probed with an Mouse-α-His as primary antibody and a horseradish peroxidase conjugated Goat-α-Mouse as secondary antibody. The blot was developed using the enhanced chemiluminescence (ECL) reagent method.

3.8. Complementation studies in *E. coli* mutant strains

3.8.1. Complementation assays with the *E. coli* TK2420 strain

Complementation assays with the *E. coli* TK2420 strain were performed as previously described by Albright et al[61] with slight modifications. Wild-type and mutant YjbQ strains were cloned into a L-arabinose-inducible vector ($pBAD_{His\ b}$), and empty vector was used as negative control.

Minimal media consisted of a 69 mM sodium/potassium phosphate buffer, pH ~7.0, plus 8 mM $(NH_4)_2SO_4$, 400 µM $MgSO_4$, 6 µM $FeSO_4$, 1 mM sodium citrate, 1 mg/liter thiamine HCl, 2 g/liter glucose, 10 mg/liter $CaCl_2$, 6 µM ferric chloride. A fixed ratio of hydrogen phosphate to dihydrogen phosphate was used, keeping the pH and overall phosphate concentration and monovalent cation concentration constant even as the K^+: Na^+ ratios were varied. Different percentages of L-arabinose protein-expression inducer were tested to determine which was appropriate for the assay. Optical density of cultures was measured at 595 nm after 16 hours of shaking at 37ºC.

In the initial tests, transformed cells were plated on LBK agar plates and three individual colonies for each protein version were picked and grown separately in 5 mL of minimal media containing 30 mM K^+, overnight (~ 16 hours) at 37°C. A 5 µl aliquot of the overnight cultures was then used to inoculate 5 ml of minimal media prepared with different K^+ concentrations (10; 20; 30; 40; 50; 115 mM).

Complementation assays with co-expression of YjbQ and CdaA DAC domain were performed following a similar protocol proposed by Gundlach et al[44]. Initially, cells were cultivated overnight in 30 mL of minimal media with 30 mM K^+ at 37ºC, culture was harvested, washed two times and resuspended in a 10 mM K^+ solution.

Fresh minimal medium (with K^+ concentrations 10, 20, 30, 40, 50 and 115 mM) was inoculated with a fraction of resuspended cells corresponding to 0.2 OD_{600nm}, plus

0.002% of L-arabinose. Optical density at 595 nm was measured after 16 hours of shaking at 37ºC.

KtrAB and KtrBC co-expression with DAC domain was performed in a similar fashion to YjbQ co-expression. Cells were cultivated in 30 mL of minimal media supplemented with 30 mM of K^+ at 37ºC, harvested, washed two times and resuspended in a 10 mM K^+ solution. Fresh minimal medium supplemented with 0.3 and 1 mM of K^+ were inoculated with fractions of cells with four different starting OD_{600nm}, corresponding to 0.005, 0.01, 0.05 and 0.1 OD_{600nm}. Two different concentrations of L-arabinose were tested: 0.002 and 0.2%. Optical density at 595 nm was measured after 16 hours of shaking at 37ºC.

Complementation assays with the *E. coli* Knabc strain

Recombinant plasmids $pBAD_{His\ b}$, pBAD_yjbQ, and pBAD_yjbQ together with pBAD33_DAC were transformed into $Na^+(K^+)$ $(Ca^{2+})/H^+$ antiporter-deficient *E. coli* strain KNabc. Test and control transformants were cultured in 30 mL of fresh LBK media at 37ºC for 16 hours.

An aliquot of the overnight cultures (adjusted to 0.05 final OD_{595nm}) was then used to inoculate 5 ml of LBK media prepared with different Na^+ concentrations (0; 50; 100; 150; 200; 300; 400; 500; 800 mM). Optical density at 595 nm was measured after 16 hours of shaking at 37ºC.

3.9. YjbQ Everted Vesicles and Antiporter Activity Assay

Everted vesicles containing YjbQ putative antiporter were prepared by growing KNabc cells (a K^+/H^+, Na^+/H^+ and Ca^{2+}/H^+ antiporter-deficient *E. coli* strain)transformed with pBAD_yjbQ in liquid LBK media (supplemented with 100 µg/mL ampicillin) until OD_{600nm} reached 0.9-1.0. At this point cultures were induced with 0.2% of Arabinose, incubated at 37ºC for 3 hours and pelleted by a 30 minute, 3500 g centrifugation. The cell pellet was resuspended in a minimum volume of Vesicle Lysis Buffer (20 mM HEPES pH 7.0; 140 mM Choline Chloride, 0.5 mM DTT and 250 mM Sucrose), pelleted again and weighed. Cells were again resuspended in Vesicle Lysis Buffer and lysed by passage through a French Press at a pressure of 4000 psi. 10 µg/mL of DNAse and 5 mM $MgCl_2$ were added to the lysed cells sample and the mixture was incubated for 30 minutes at

room temperature. Unbroken cells were pelleted by two sequential centrifugations of 15 min at 5000 g.

Everted vesicles were extracted from the spin-cleared lysate by a 1 hour and 10-minute centrifugation at 100,000 g, with the resulting pellet being resuspended once, washed and pelleted again.

The vesicle pellet was resuspended in 1 mL Vesicle Lysis Buffer per gram of original wet cell weigh. Total protein concentration was estimated using Bradford reagent method using bovine serum albumin (BSA) as standard and vesicles were stored in small aliquots at -80ºC.

To perform the assay, vesicles were diluted in Vesicle Assay Buffer (20 mM Tris-HCl pH 7.5 or 8.5; 140 mM Choline Chloride; 5 mM $MgCl_2$) to a concentration of 133 µg/mL. 9-Amino-6-Chloro-2-Methoxyacridine (ACMA) was used as a fluorescence probe to quantify changes in transmembrane proton gradient; ACMA was added at a final concentration of 2 µM, seconds before running the assay. Fluorescence was measured using a HORIBA Fluoromax-4 cuvette spectrofluorometer with constant stirring and excitation and emission wavelengths of 410 nm and 480 nm, respectively. An integration rate of 0.2 seconds and 2-nm slits were selected. A respiration-generated pH gradient was generated by addition of 4 mM Sodium Lactate or Lactic acid, resulting in a quenching in ACMA fluorescence.

YjbQ antiporter activity was studied by addition of salt (KCl and NaCl in the presence or absence of $MgCl_2$) and measurement of H^+ flux resulting from antiport. The effect of c-di-AMP on the function of YjbQ was studied by addition of the ligand to the sample cuvette seconds before the salt was added. All assays were performed at room temperature.

3.10. X-ray crystallography

Crystallization screens for the RCK domain of YjbQ were performed using purified protein at 8 mg/mL, after clearing aggregates through centrifugation for 10 minutes at 12000 g at 4ºC in a table-top centrifuge. Initial screens were performed by mixing solutions of commercial crystallization screens (Morpheus (Molecular Dimensions), JBScreen Basic (Jena Bioscience), Wizard Classic 1 and 2 (Molecular Dimensions)) and

protein with and without c-diAMP (1 mM). c-di-AMP was obtained from Jena Bioscience in powder form and the solution was prepared by resuspension in 20 mM Tris-HCl pH 8.0. The same solution of c-di-AMP was used throughout this process, in order to reduce the number of variables in the crystallization assays.

Each initial screening drop consisted of 0.6 µL drops (0.3 µL protein plus c-di-AMP and 0.3 µL reservoir solution) and 40 µL of reservoir solution, incubated at 20ºC. Conditions that gave rise to crystals were optimized by varying precipitant concentrations, drop size, pH and temperature and using the macro-seeding technique; see Appendix. Drops were set up using the sitting drop method with a crystallization robot (Oryx 4 by Douglas Instruments).

Crystals suitable for collection of x-ray data were cryo-protected in mother liquor supplemented with 10-20% (v/v) glycerol, flash-cooled in liquid nitrogen and diffraction data were recorded in Proxima I beamline at the Soleil Synchrotron in Paris, France.

3.11. Sequence conservation analysis

Identification of conserved regions in the RCK domain of YjbQ and mapping onto the structure was performed using The Consurf Server[62,63,64], a web-based tool to estimate the evolutionary conservation of amino and nucleic acids. Based on the Uniprot repository[65], 150 sequences homologous to YjbQ were clustered and highly similar sequences were removed by the server.

Evolutionary conservation scores were automatically calculated and projected into the three-dimensional protein structure. The continuous conservation scores were divided into a discrete scale colours, from turquoise (variable region) to maroon (most conserved region).

3.12. YjbQ's CPA motif and phenotype analysis

A three-dimensional model of the transmembrane domain of YjbQ was obtained using Swiss-Model[66], a protein structure homology-modelling server and the structure of NapA, a sodium-proton antiporter from *Thermus thermophilus* (PDB accession code: 4BWZ), as a template. This model was compared to other cation/proton antiporters described in

the literature[55], in order to analyse the residues that determine functional properties of YjbQ . Functionally interesting residues was visualized in PyMOL. A pairwise sequence alignment between YjbQ and the other CPAs was also done via the Clustal Omega (EMBL-EBI) sequence alignment tool.

4. Results & Discussion

4.1. Protein Expression and Purification

The first step in characterizing the biochemical and biophysical properties of the RCK domain of YjbQ was to determine and optimize the conditions for large-scale expression and purification.

4.1.1. YjbQ RCK domain Expression and Purification

The best conditions for expression of the RCK domain of YjbQ were tested as described in section **3.3**. In short, the general strategy was inducing protein expression in *E. coli* BL21(DE3) transformed with pET15b_RCK1 and pET15b_RCK_2, at different temperatures and induction periods. Protein expression was assessed by SDS-PAGE analysis (**Figure 4.1**).

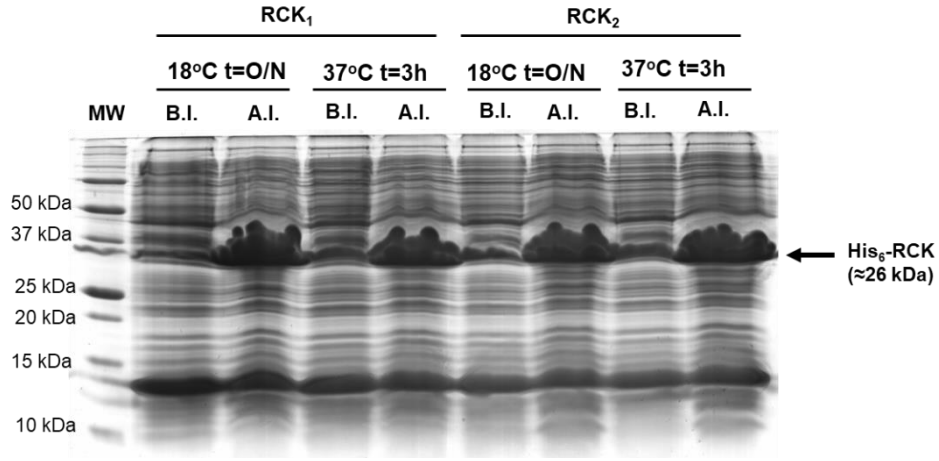

Figure 4.1 - SDS-PAGE gel of the RCK domain of YjbQ induction test in BL21(DE3) *E. coli* strain. Total cell lysates before induction (B.I) and after induction (A.I.) with 0.5 mM of IPTG were loaded in a 17% SDS-PAGE gel and stained with NZYTech's BlueSafe gel stain. Molecular weight protein markers are indicated on the left (Bio-Rad's Precision Plus Protein™ All Blue Prestained Protein Standards); the expected positions of His-tagged RCK domain is marked on the right. Legend for each lane is displayed above each lane.

The gel shows that both RCK_1 and RCK_2 are equally expressed well after induction with IPTG, regardless of temperature and time of induction. As such, the next step was to assess whether RCK_1 and RCK_2 were being produced as soluble proteins by SDS-PAGE analysis (**Figure 4.2**).

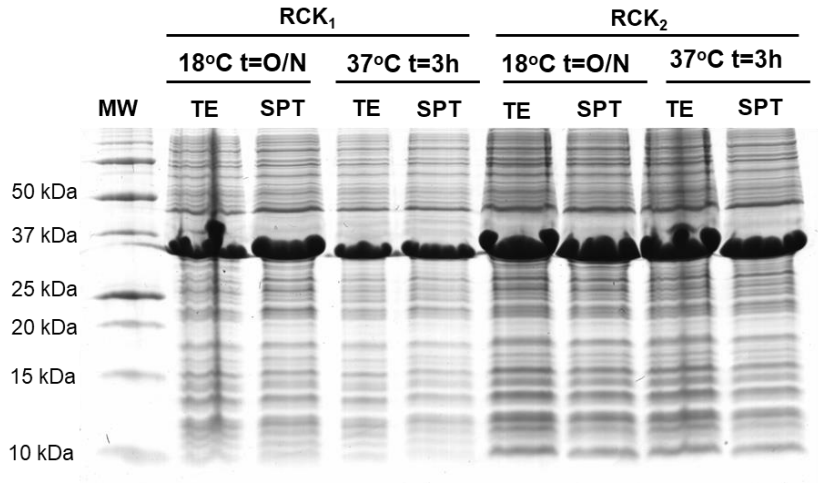

Figure 4.2 - SDS-PAGE gel of the RCK domain of YjbQ expression tests in BL21(DE3) *E. coli* strain. Cells were lysed by sonication and centrifuged. Pre-centrifugation Total Extract (TE) and post-centrifugation supernatant (SPT) samples were then loaded in a 17% SDS-PAGE gel and stained with NZYTech's BlueSafe gel stain. Molecular weight protein markers are indicated on the left (Bio-Rad's Precision Plus Protein™ All Blue Prestained Protein Standards).

The SDS-PAGE gel shows that the both RKC1 and RCK2 proteins are produced mainly as soluble protein, in apparently large quantities, in all conditions tested. With this, one of the conditions was selected to proceed: overnight induction at 18ºC. In addition, to simplify the experiment, only the RCK_1 construct was selected for large-scale expression since both RCK constructs share high similarities in sequence and behaviour. Large-scale expression and purification of the RCK domain of YjbQ was then optimized, ultimately being standardized as described in Materials and Methods, section **3.4**. The outcome of the first steps of the RCK domain purification protocol, consisting on immobilized metal affinity chromatography (IMAC) using nickel beads and thrombin digestion are shown in the figures below.

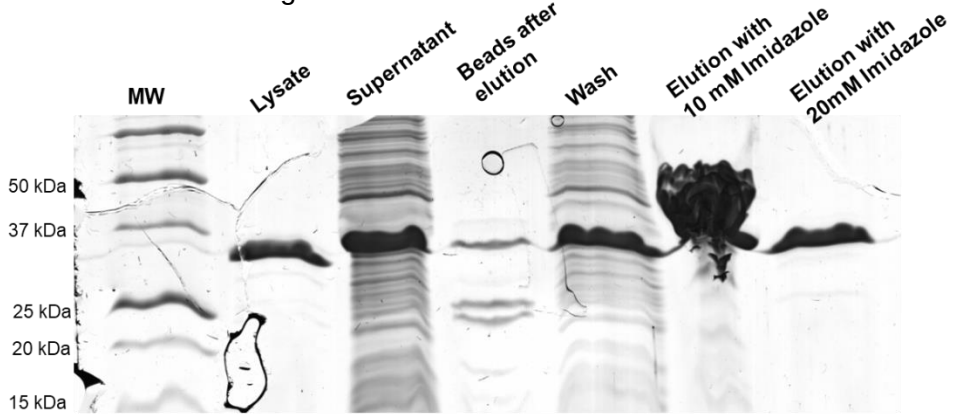

Figure 4.3 - SDS-PAGE gel of the overall IMAC purification protocol for the RCK domain of YjbQ. The cell extract supernatant was loaded in an IMAC column and the beads were washed with Lysis buffer. The first elution steps were made with 10 and 20 mM Imidazole solutions. Legend for each lane is displayed above the gel.

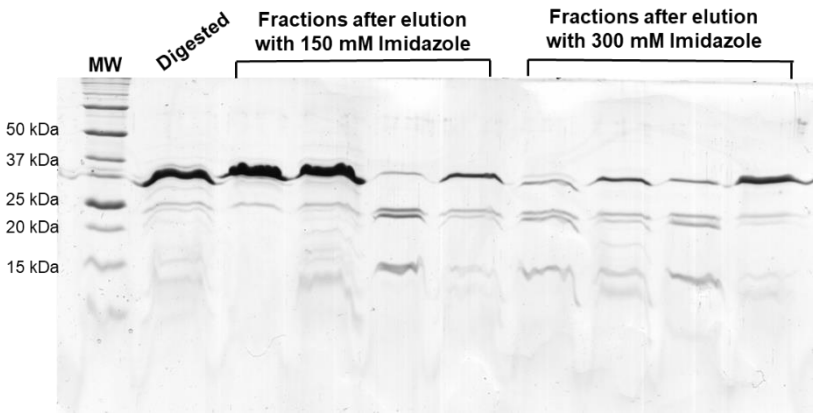

Figure 4.4 - SDS-PAGE gel of the overall IMAC purification protocol for the RCK domain of YjbQ. The cell extract supernatant was loaded in an IMAC column and the elution was performed using solutions with increasing concentrations of Imidazole. Overnight dialysis in the presence of thrombin yielded a fraction of tagless RCK domain. Legend for each lane is displayed above the gel.

After analysing the two SDS-PAGE gels, it is visible that large part of the protein was eluted in the first step of the elution process with 10 mM of Imidazole (**Figure 4.3**). Concordantly, the elution fractions with higher concentrations of Imidazole show very little protein when compared to the fraction eluted with 10 mM of Imidazole (**Figure 4.3**, **4.4**). Thrombin-digested RCK was then further purified using size exclusion chromatography; the chromatogram obtained is shown in **Figure 4.5**.

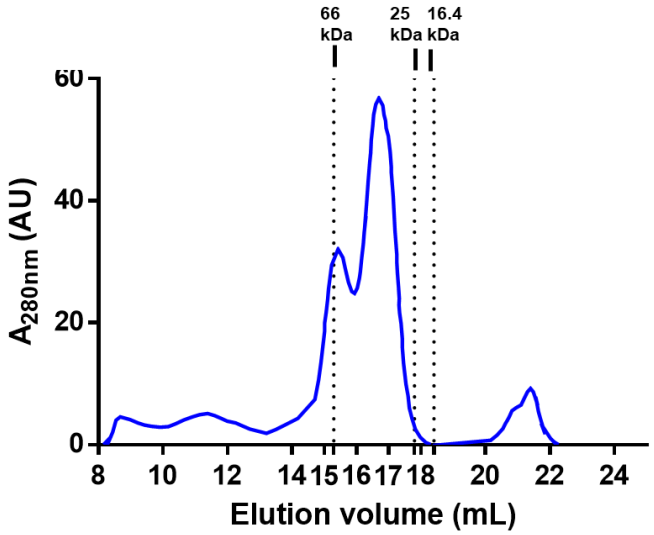

Figure 4.5 - Chromatogram of RCK domain purification by size-exclusion chromatography at pH 8.0. This protein exhibits two elution peaks at approximately 15 and 17 mL of elution volume in the Superdex 200 10/300 GL column. Molecular weights of the standards used for the calibration of the column are shown at the top of the figure.

The RCK domain of YjbQ size-exclusion chromatography profile shows two sharp peaks, suggesting that the protein exists in two different forms. The first peak appears is observed around 15 mL and the second around 17 mL. Comparing the peaks and correspondent elution volume with a previously determined calibration curve for Superdex 200 10/300 GL column, the apparent molecular weight of the protein eluted in the first and second peak correspond to approximately 60 kDa and 30 kDa, respectively (**Figure 4.5**). Since the molecular weight of the RCK domain of YjbQ is approximately 26 kDa, this suggests that the first peak corresponds to a RCK domain dimer and the second to a monomer.

The protocol for expression and purification of the RCK domain yields approximately 12 mg of pure protein per liter of culture.

4.2. Ligand Testing by Thermal Shift Assay

As mentioned above, it has been proposed that c-di-AMP binds to the RCK domain of YjbQ. As such, for both structural and functional purposes, an experiment was performed to confirm whether c-di-AMP is a ligand of the RCK domain of YjbQ as well as to find other potential ligands. The technique used for this goal was the Sypro Orange Thermal Shift Assay, also known as Differential Scanning Fluorimetry (DSF). The basic scheme of this technique involves the incubation of the natively folded protein with a fluorescent dye (SYPRO Orange), which binds to the hydrophobic regions of a protein and changes its fluorescence. As the temperature increases, the protein begins to unfold and expose its hydrophobic regions to the solvent, allowing the dye to bind to its hydrophobic regions and increase the fluorescence signal. Further increases in temperature lead to protein aggregation and fluorescence quenching. As such, there is a clear fluorescence transition due to temperature induced protein unfolding. The melting temperature (Tm) is defined as the mid-point of such transition, which can easily be determined by calculating the 1st derivative of experimental curve. When comparing the Tm of untreated and ligand supplemented protein samples, a ΔTm is generated, a parameter that is closely related to thermal stabilization or destabilization. When ΔTm takes a positive value bigger than 2ºC, usually this gives an indication that that the molecule tested stabilizes the protein and, as such, is a potential ligand[67].

In these experiments, I first determined the temperature of melting for the RCK domain of YjbQ without any ligand added. Having this value established, several ligands

(nucleotides, metal ions and cyclic nucleotides including c-di-AMP and c-di-GMP) were added at high concentrations (to force the bound state) in parallel samples (**Figure 4.6**).

The Tm of YjbQ's RCK domain was determined as 56.2± 0.4 ºC (n=6). This value was used as a point of comparison for the melting temperatures of the protein in the presence of the different ligands (**Table 4.1**).

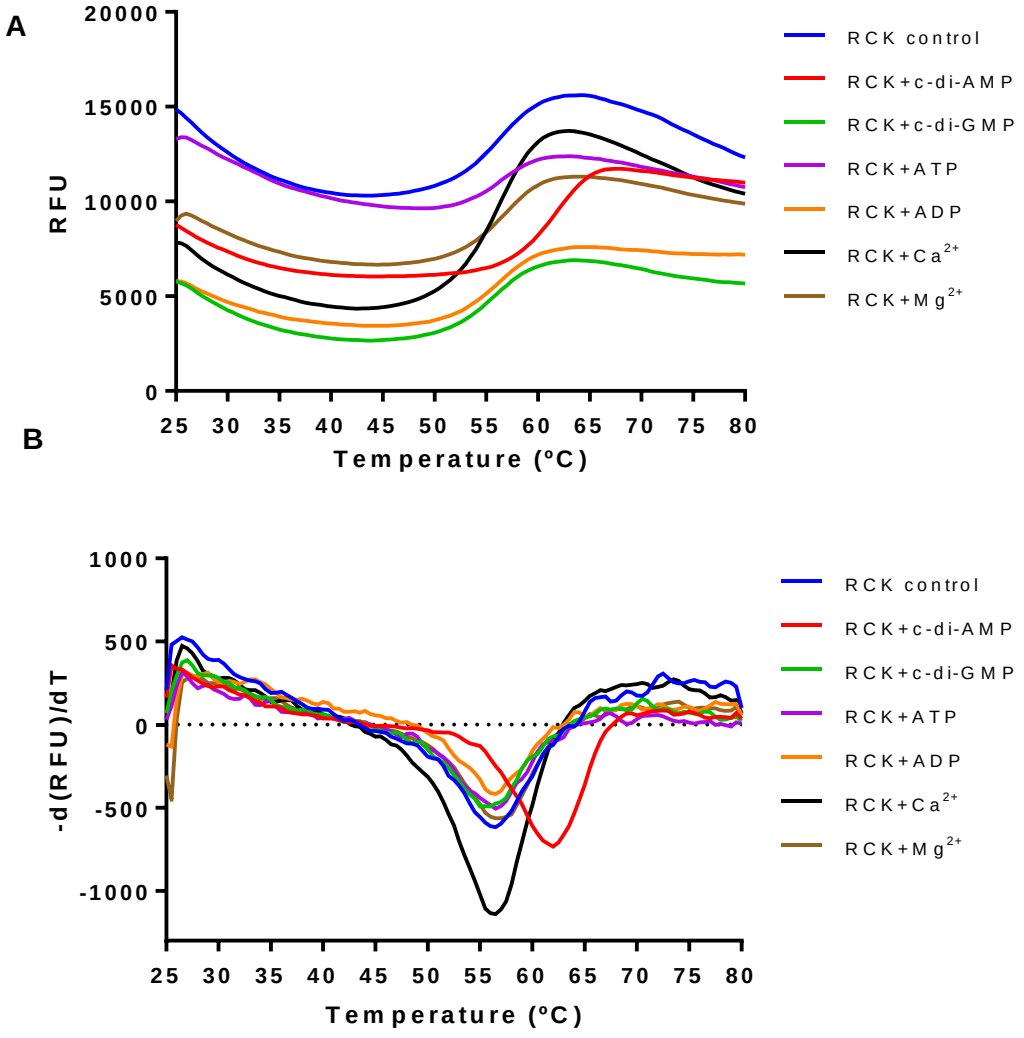

Figure 4.6 - Thermal shift assay results for the RCK domain of YjbQ, supplemented with several potential biological ligands. Representative **A)** melting curves and **B)** corresponding 1st derivative curves of the RCK domain in the absence (control) and presence of potential ligands:0.1 mM c-di-AMP, 0.1 mM c-di-GMP, 1 mM ATP, 1mM ADP, 1 mM Mg^{2+} and 1 mM Ca^{2+}.

Table 4.1 - Melting temperature [(Tm (ºC)] values obtained for the RCK domain in the presence of different ligands.
Legend: Number of repetitions (n), standard deviation (SD) and Tm shift for each ligand used.

Ligand	n	Tm (ºC)	SD	ΔTm
RCK domain control	6	56.2	0.4	-
c-di-AMP	6	62.0	0	+5.8
c-di-GMP	6	56.0	0.2	-0.2
ATP	6	56.5	0.3	+0.5
ADP	6	56.5	0.3	+0.3
Ca^{2+}	6	57.5	0.4	+1.3
Mg^{2+}	6	57.0	0.2	+0.8

Among the six tested potential ligands for the RCK domain of YjbQ, only c-di-AMP produced a ΔTm considered relevant in this type of assay (≥ 2ºC). The effect caused by c-di-AMP appears to be specific, as c-di-GMP does not show an apparent effect (**Table 4.1**, **Figure 4.6**). Thus, this data confirm that c-di-AMP is a potential ligand for YjbQ.

4.3. Size-exclusion chromatography experiments

Size exclusion chromatography (SEC) apart from being a good separation method for proteins, also gives a great deal of information about the protein that is being purified. The elution profile can be used to estimate the molecular weight and consequently, the oligomeric state of the injected protein. As previously shown, the size-exclusion purification chromatogram of the RCK domain of YjbQ exhibits two distinct elution peaks. However, there is not much information concerning the behaviour of the RCK domain in SEC. With this, multiple questions began to arise: does the RCK domain maintain the same elution profile under different pH? Does the elution profile change when the protein is injected at different concentrations? To address these questions, a series of experiments were designed to monitor the elution profile of the RCK domain under different variables.

To test the effect of pH on the RCK domain of YjbQ, three SEC runs were performed each at a different pH: pH 6.5 (Bis-Tris), pH 9.0 (Tris-HCl) and pH 8.0 (Tris-HCl); (the purification protocol for the RCK domain was at pH 8.0) (**Figure 4.7**).

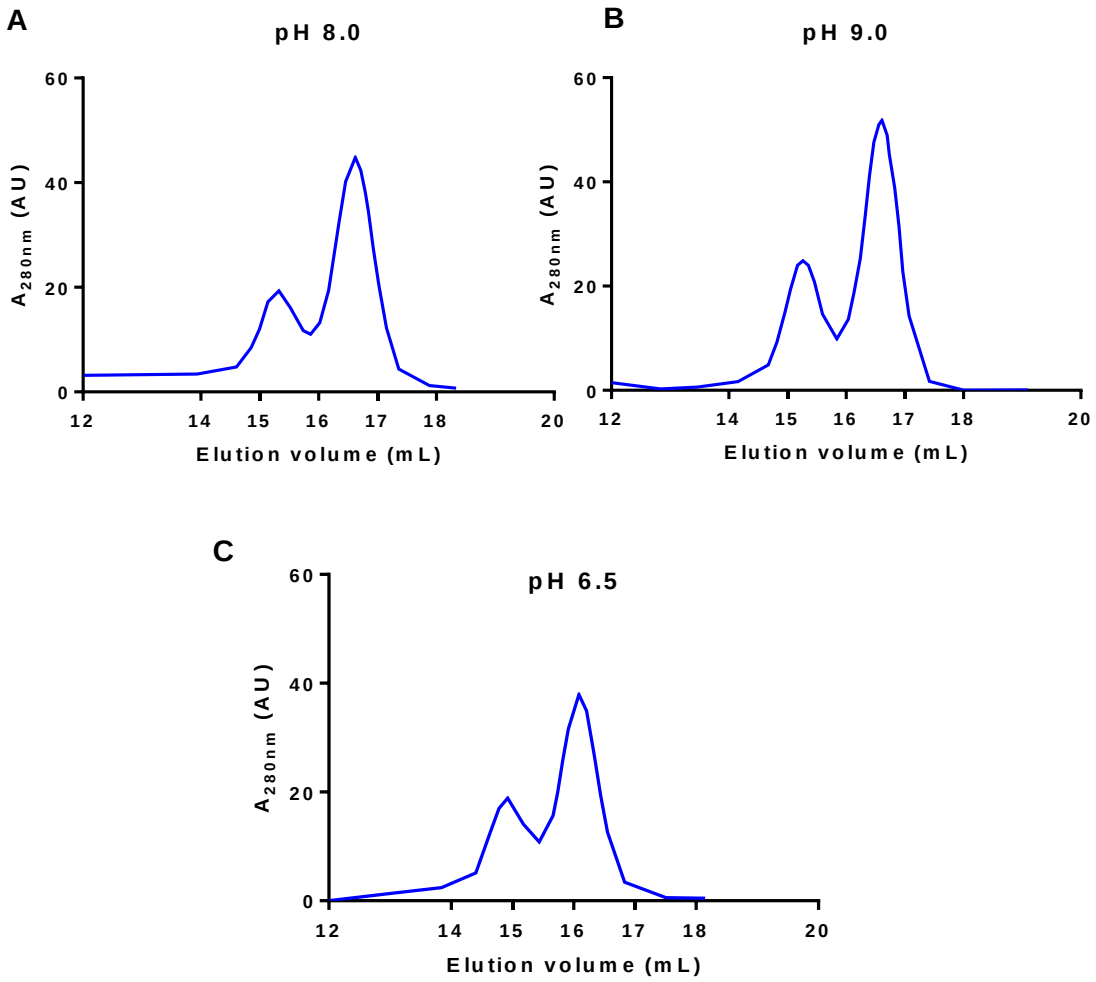

Figure 4.7 - Effect of pH on the RCK domain of YjbQ monitored by size exclusion chromatography. Elution profiles of the RCK domain of YjbQ at **A)** pH 8.0; **B)** pH 9.0 and **C)** pH 6.5 at 13 mg/mL in the Superdex 200 10/300 GL column.

From this data, it is clear that the initial SEC profile remains, as two elution peaks around 15 and 17 mL were registered in all conditions. However, at pH 6.5, the peaks suffered a slight shift to the left, which was not considered to be relevant. With this, it is safe to conclude that the elution profile in SEC and possibly the oligomeric behaviour of the RCK domain is not pH-dependent.

To evaluate if the elution profile is affected by protein concentration, RCK domain at three different concentrations (1.5 mg/mL, 8 mg/mL and 18 mg/mL) were submitted to SEC analysis (**Figure 4.8**).

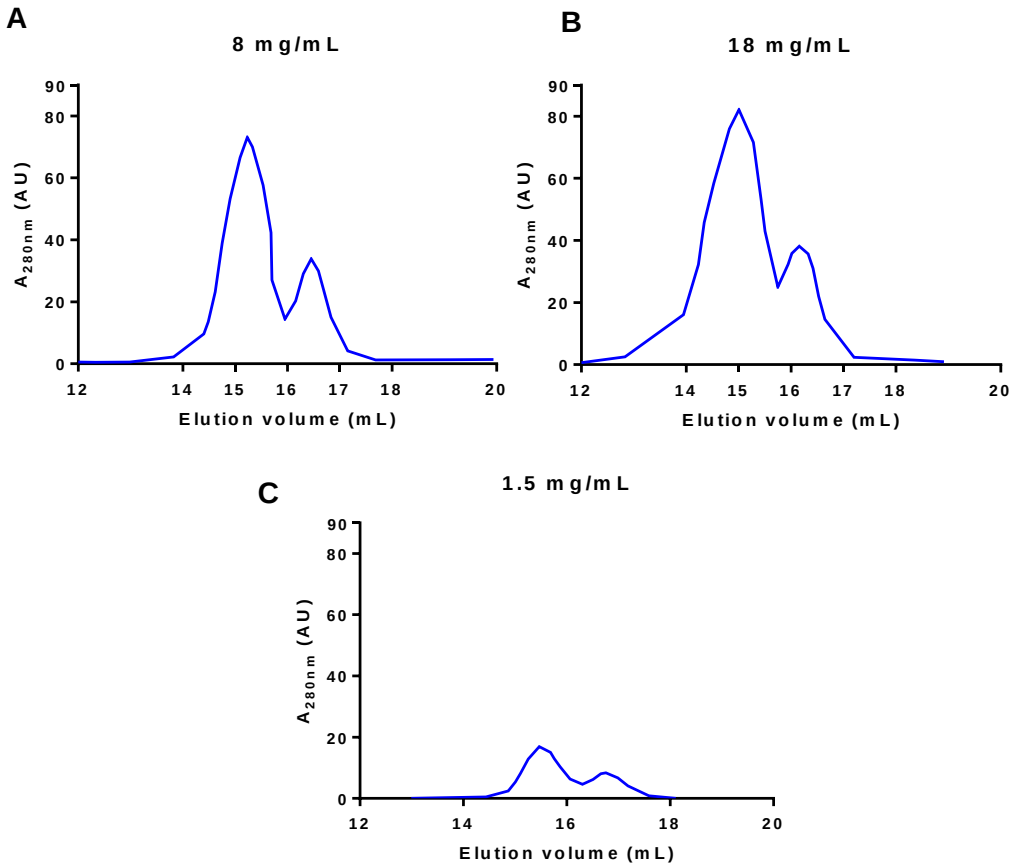

Figure 4.8 - Effect of concentration on the RCK domain of YjbQ monitored by size exclusion chromatography. Elution profiles with **A)** 8mg/mL; **B)** 18 mg/mL and **C)** 1.5 mg/mL of purified protein in 20 mM HEPES pH 6.5; 150 mM NaCl in the Superdex 200 10/300 GL column.

In this experiment, there was a sudden change of profile in the SEC chromatogram and, unlike the last set of experiments, the first peak appeared as the largest peak in the chromatogram. The protein preparation used in these experiments is exactly the same as that in **Figure 4.7**. The reasons underlying the change in the elution profile are unclear, it is possibly something related sample handling. Nevertheless, the elution volume of the two peaks remains the same across experiments. Importantly, when comparing the three resulting chromatograms of this experiment (**Figure 4.8 A, B, C**), the same profile is registered, which leads to the conclusion the behaviour of the RCK domain is not concentration-dependent.

Thermal shift assay results demonstrated that c-di-AMP is a potential ligand for YjbQ. Knowing this, c-di-AMP might play an important function in YjbQ oligomeric state and therefore, influence its SEC profile. Thus, another round of experiments was performed in order to compare the protein elution profile with and without c-di-AMP (**Figure 4.9**). The size-exclusion chromatography was performed with a small analytical column

(Superdex 200 Increase 5/150 GL column) and therefore the elution volumes are different from those observed before.

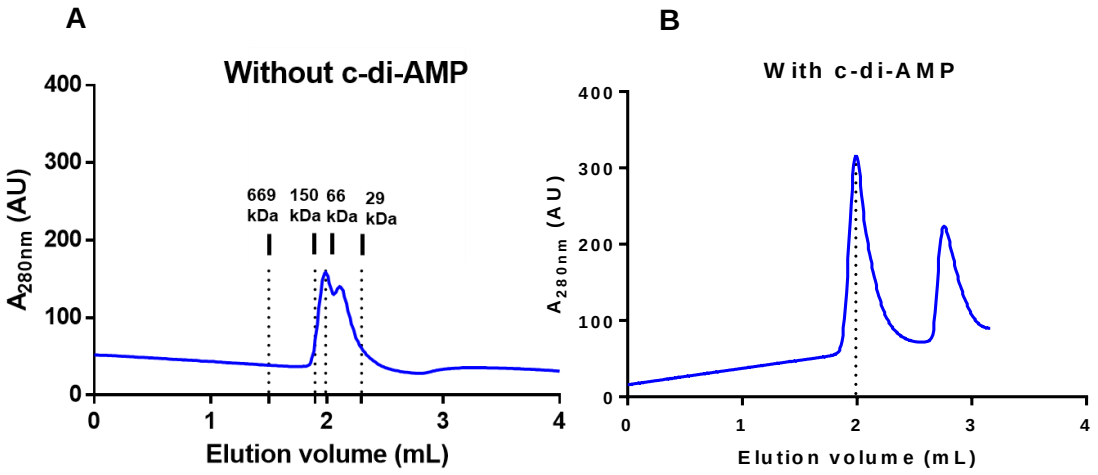

Figure 4.9 - Effect of c-di-AMP on the RCK domain of YjbQ monitored by size exclusion chromatography. A) Elution profile with protein sample at 5.3 mg/mL without c-di-AMP. Molecular weights of the standards used for the calibration of the column are shown at the top of the panel. **B)** Elution profile with protein at 5.3 mg/mL incubated with 1 mM of c-di-AMP. Experiments performed in a Superdex 200 Increase 5/150 GL column pre-equilibrated in a solution with 20 mM of HEPES pH 6.5, 150 mM of NaCl and 30 µM of c-di-AMP. Both experiments were only performed once.

From the two panels of **Figure 4.9**, which are represented in the same scale to simplify its comparison, it is clear that the presence of c-di-AMP changes the RCK domain elution profile. When adding 1 mM of c-di-AMP, the elution profile deviates towards the lower elution volume peak. This result shows that c-di-AMP stabilizes one of the conformations of the protein, possibly its dimeric form, as the elution volumes and correspondent molecular weights in this column match the ones registered in the Superdex 200 10/300 GL column. In the Superdex 200 Increase 5/150 GL column, the elution volume of 2 mL corresponds to a molecular weight of approximately 60 kDa, consistent with a RCK domain dimer. In other words, when c-di-AMP binds to the RCK domain of YjbQ, it triggers its dimerization and leads to a prevalence of this form over the monomeric state (second peak).

4.4. Crystallographic studies of the RCK domain of YjbQ

There is no structural information available on the YjbQ protein. Since obtaining a three-dimensional structure of a protein is an important step in achieving a better

understanding of its molecular and biochemical properties, crystallization of the RCK domain of YjbQ was attempted. At first, crystallization screenings with commercial solutions were performed using the vapor diffusion sitting-drop method and purified RCK domain concentrated up to 8 mg/mL and supplemented with 1 mM of c-di-AMP, as described in section 3.10. This approach proved successful as crystals appeared in several different conditions. Crystallization conditions were similar to each other and were comprised by PEG8000 or PEG400 as a precipitant, in a pH range between 6.5 and 8.5, and in the presence of divalent salts, such as Magnesium chloride and Calcium acetate (**Figure 4.10 A**). Morphology of resulting crystals was also similar, needles. Examples of these crystals are shown in **Figure 4.10**.

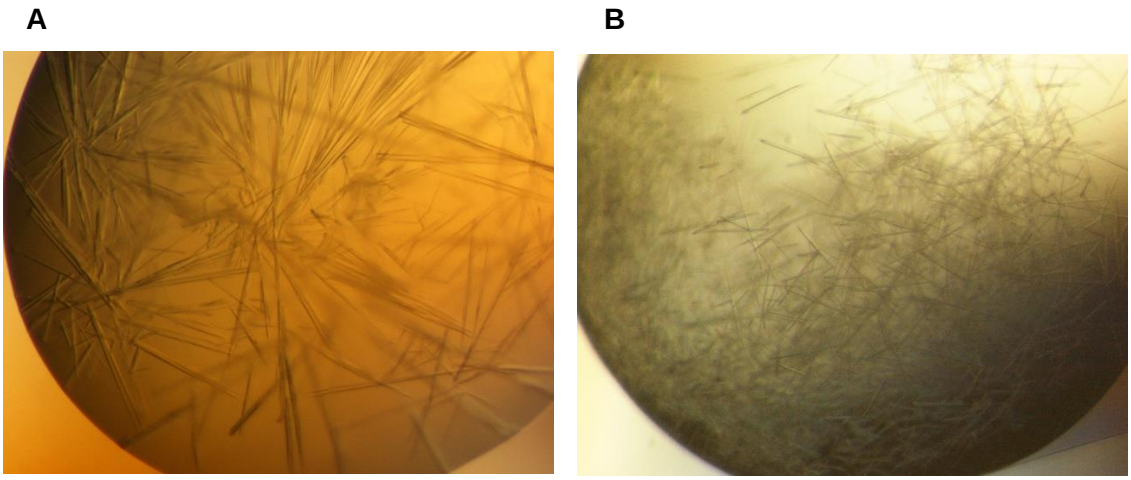

Figure 4.10 - Crystals obtained in the initial crystallization screening for the RCK domain incubated with c-di-AMP. The commercial kit used was Molecular Dimensions' Wizard I&II. **A)** Condition E3: 20% PEG8000, 100 mM Tris-HCl pH 8.5; 200 mM Magnesium chloride. **B)** Condition C1: 30% PEG400, 100 mM Tris-HCl pH 8.5, 200 mM Magnesium chloride. Both conditions were found using the following drop setup: 0.3 µL of reservoir solution + 0.3 µL of 8 mg/mL of purified RCK domain with 1 mM c-di-AMP, placed in a sitting-drop 96-well plate at 20ºC.

Handmade screens were developed in order to reproduce crystals and optimize nucleation and size (see **Appendix**). These screens consisted on fine-tuning around the initial condition using a range of the same (or similar) reagents as the commercial kit. In the end, crystal-forming conditions were successfully reproduced, however crystal size did not seem improve, as resulting crystals appeared once again in the form of very thin needles, difficult to use in X-ray diffraction experiments (**Figure 4.11**).

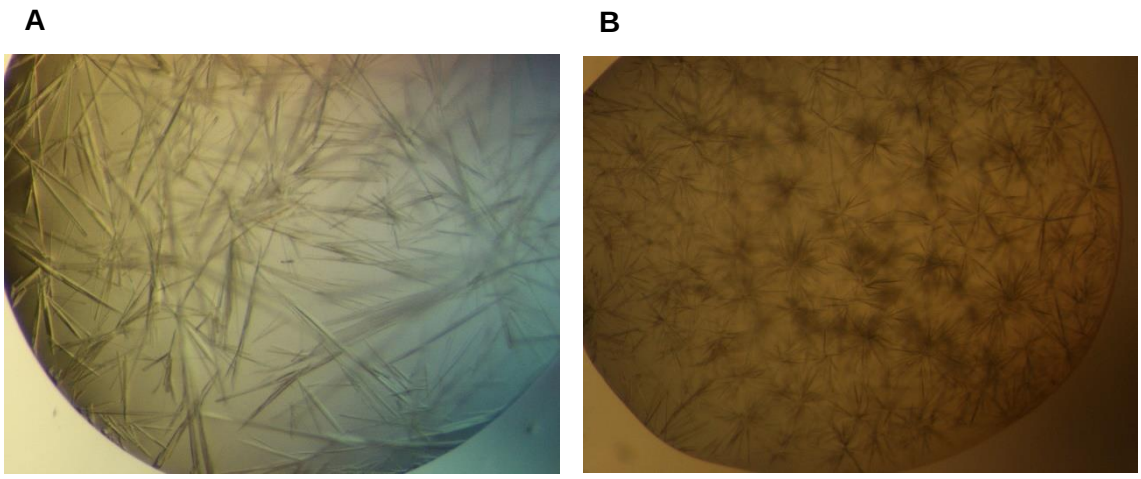

Figure 4.11 - Examples of crystals obtained from the handmade optimization assays. A) Crystals obtained in optimization screen around condition E3: 28% PEG400, 100 mM Tris-HCl pH 7.5; 200 mM Magnesium chloride. **B)** Crystals obtained in optimization screen around condition C1: 24% PEG8000, 100 mM Tris-HCl pH 8.0, 200 mM Magnesium chloride. Both conditions were found using the following drop setup: 0.3 µL of reservoir solution + 0.3 µL of 8 mg/mL of purified RCK domain with 1 mM c-di-AMP, placed in a sitting-drop 96-well plate at 20ºC.

In a second phase, crystallization assays were performed using bigger drop volumes (1µL total volume, volume of initial screening drops was 0.6 µL) and left at different temperatures, to assess the impact of these variables on crystal growth. In addition, the technique of Streak Seeding was performed. This technique allows crystals to grow in the Metastable Zone, where spontaneous nucleation cannot occur, but single crystals can continue to grow, reducing the number of crystals in the drop and increasing their size (**Figure 4.12**).

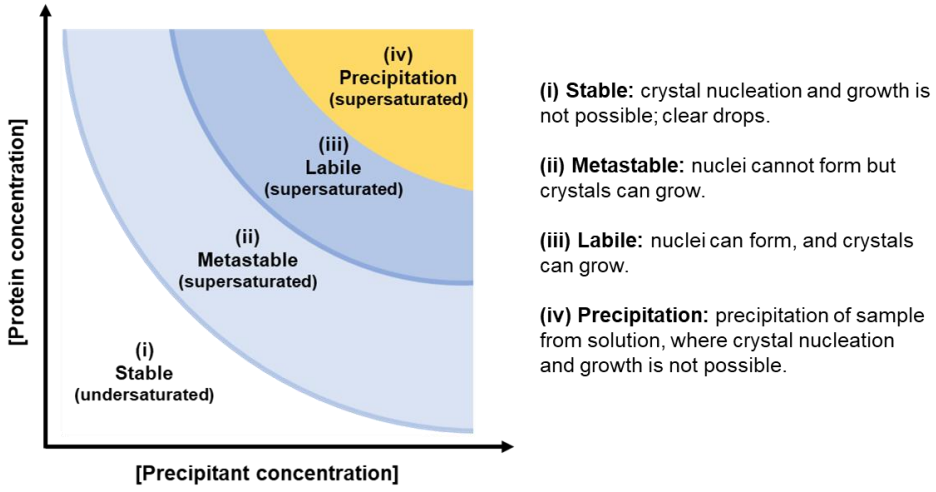

Figure 4.12 - Protein crystallization phase diagram. Different zones of phase diagram represent the conditions in which the protein solution exists over a period of time.

The technique involves placing a crystal seed (or solution of seeds) in a protein/precipitant condition that was found to not give rise to precipitate or crystals. Thus, seeds from thin needle-shaped crystals were collected with a wire loop and streaked into clear drops within the same crystallization plate. This technique proved to be useful, as large and good-looking needle-shaped crystals appeared on previously clear drops. Examples are shown in **Figure 4.13**.

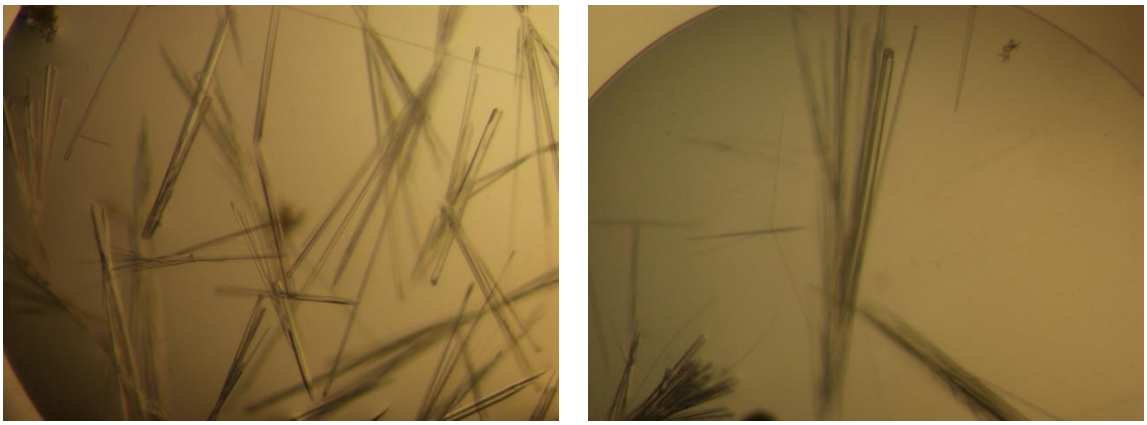

Figure 4.13 - Examples of crystals obtained with Streak Seeding technique. Seeds were collected from thin needle-shaped crystals which grew in a condition with 28% PEG8000; 100 mM Tris-HCl pH 7.5; 100 mM Magnesium chloride.

Crystallization of YjbQ RCK domain in the absence of c-di-AMP was also attempted using the same crystallization approach. The same commercial screens were used, yet there was not enough time to execute optimization screens. Strikingly, crystals grew around the same conditions as before and exhibited a sufficiently good size for X-ray diffraction. In the end, 45 crystals (with and without c-di-AMP) were collected and soaked in cryoprotected solutions (replicas of the reservoir solution supplemented with 10-20% final concentration of glycerol), with the exception of crystals from Morpheus screen (Molecular Dimensions) as its conditions are already cryoprotected. Afterwards, crystals were frozen in liquid nitrogen and sent for X-ray diffraction analysis and collection at the Proxima I beamline in the Soleil Synchrotron (Paris, France).

Crystals with and without c-di-AMP diffracted up to 1.85 and 2.19 Å, respectively. In both cases, several datasets were collected and, in the end, the two datasets with the best resolution were used to solve the structures (statistical analysis shown on **Table 4.2**).

Table 4.2 - Summary of the statistical analysis of the top two datasets collected using YjbQ crystals.

	Dataset with c-di-AMP	Dataset without c-di-AMP
Unit cell dimensions	a=110.64 b=120.10 c=36.10 (Å) α=90 β=90 γ=90 (º)	a=36.23 b=93.02 c=25.26 (Å) α=90 β=90 γ=90 (º)
Space group	P2 2_1 2_1	$P2_1$ 2_1 2_1
Resolution limit (Å)	40.69 -1.85 (1.89 -1.85) [a]	46.51-2.19 (2.26-2.19)
R_{merge}	0.086 (2.873)	0.113 (1.674)
R_{meas}	0.089 (3.013)	0.115 (1.707)
Number of observations	560130 (27208)	598292 (48862)
Number of unique observations	42129 (2504)	22502 (1889)
Mean I/(σI)	15.5 (0.8)	21.97 (2.58)
$CC_{1/2}$	1.00 (0.442)	1.00 (0.802)
Completeness (%)	99.8 (97.1)	99.6 (96.2)
Multiplicity	13.3 (10.9)	26.6 (25.9)

[a]Values in parenthesis are for high-resolution shell.

4.5. Protein structure determination

The best crystals in the presence and absence of c-di-AMP belonged to different space groups (P2 $2_1$$2_1$ and $P2_1$$2_1$$2_1$,respectively) and both structures were solved by Molecular Replacement. The structures of the C-terminal and N-terminal subdomains of YjbQ's RCK domain with c-di-AMP were determined using the coordinates of the C-terminal subdomain of the RCK domain of *Sa*CpaA (PDB accession code: 5F29) and the coordinates of the N-terminal subdomain of KtrA from *Bacillus subtilis* (PDB accession code: 4J91) as search models, respectively. The final structure was refined to 1.85 Å with an R_{work} and R_{free} of 20.25 and 24.22%, respectively.

Similarly, the structure of the RCK domain of YjbQ without c-di-AMP was solved using the structure of the RCK domain with c-di-AMP as model. The final structure was refined

to 2.19 Å with an R_{work} and R_{free} of 21.80 and 25.56%, respectively. Refinement statistics are summarized in **Table 4.3**.

Table 4.3 - YjbQ's RCK domain refinement statistics.

	Dataset with c-di-AMP	**Dataset without c-di-AMP**
Resolution range (Å)	40.69 - 1.85	46.51 - 2.19
R_{work} (%)	20.25	21.80
R_{free} (%)	24.22	25.56
Number of residues	416	416
Number of waters	70	23
Rmsd bond length (Å)	0.013	0.005
Rmsd angles (º)	1.55	0.88
Ramachandran favoured (%)	98	98
Ramanchandran outliers (%)	0	0

4.5.1. The conformations of RCK domains

The monomer of the RCK domain of YjbQ comprises three distinct regions: the N-terminal subdomain consisting of a central five-parallel strand β-sheet packed by α-helices on both sides, a C-terminal subdomain consisting on four antiparallel strand β-sheet packed by α-helices on one side and a linker with a Helix-turn-Helix (HTH) motif consisting on two α-helices (α6 and α7, Figure **4.14**). These two α-helices swap the dyad twice, causing the C-terminal domain to be located on the same side of the dimer as the N-terminal domain (**Figure 4.14**). The overall organization of the RCK domain of YjbQ was assessed using the structure without c-di-AMP.

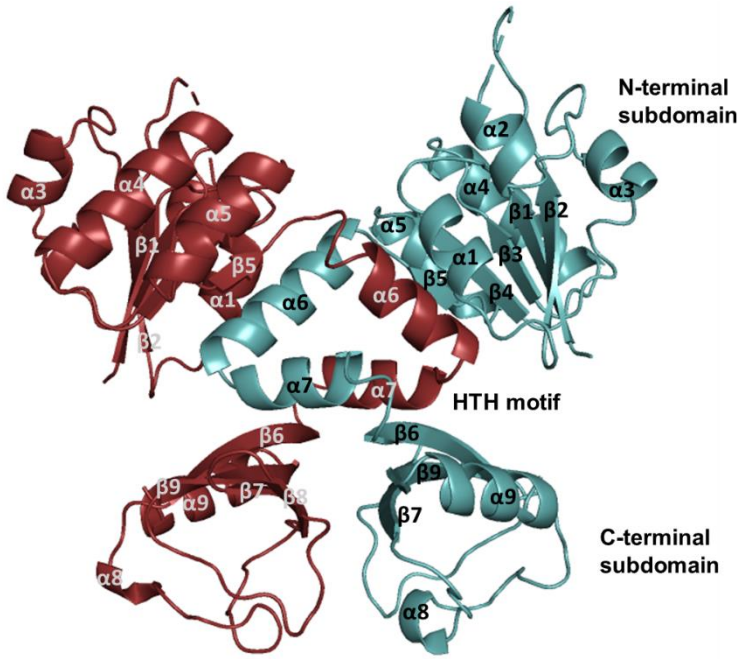

Figure 4.14- Overall characteristics of the RCK domain of YjbQ. The structure is drawn as a cartoon, with secondary elements labelled. The structure contains two protomers coloured in teal and red. Image generated by PyMOL.

RCK domains in prokaryotic K^+-transporters share similar structural features. In particular, in their dimeric organization, in the fold of the N-terminal subdomain (adopting the Rossman fold) and the C-terminal subdomain. A differentiating feature between RCK domains is the way that the two sub-domains are related to each other. **Figure 4.15** represents two well-characterized RCK domains from two ion channels: *Bacillus subtilis* KtrA (**Figure 4.15 A**) and *Methanothermobacter thermoautotrophicus* MthK (**Figure 4.15 B**) and the RCK domain from *Bacillus subtilis* YjbQ (**Figure 4.15 C**). The N-terminal subdomains are remarkably similar across all three, with the alternating βαβαβ structural arrangement that is extended into a final helix (α6, **Figure 4.15 A**) that is swapped between subunits and packed against the N-domain. As stated above, the C-terminal subdomains are also similar, however there are two solutions for the connection with the N-domain. In the KtrA structure, a β-strand (β7, **Figure 4.15 A**) establishes that connection and is the first structural element in the fold, while in the MthK, this element is substituted by an helix (α7, **Figure 4.15 B**) which stands slightly apart from the fold of the C-domain. This difference gives rise to a change in the overall organization of the RCK dimer. In KtrA, the N- and C-domains of one subunit stand in opposite sides of the two-fold axis of symmetry that organizes the dimer. In the MthK, the two subdomains are on the same side of the symmetry axis. The RCK domain of YjbQ is similar to the one present in MthK.

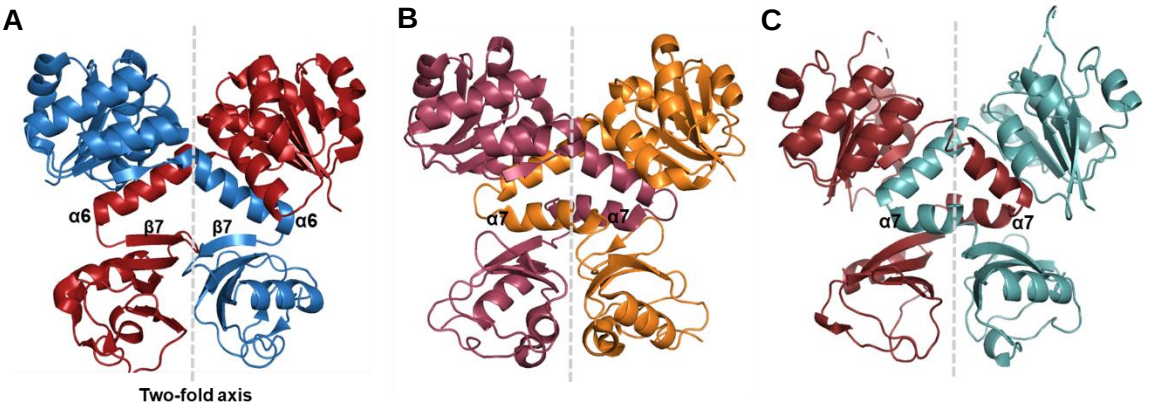

Figure 4.15- Structural representation of three RCK domains from prokaryotic transporters. RCK homodimers from **A)** KtrA from *Bacillus subtilis* (PDB accession code: 4J90); **B)** MthK from *Methanothermobacter thermoautotrophicus* (PDB accession code: 2AEM); and **C)** YjbQ from *Bacillus subtilis*. Subunits are shown in different colours. Images generated by PyMOL.

Curiously, the RCK domains from MthK and KtrA share the ability to form an octamer [28,68], a feature that YjbQ does not possess. The crystal lattice contacts in KtrA's RCK domain reveal an octameric ring organization with a quaternary arrangement (tetramer of dimers), similar to the one observed in the MthK structure (**Figure 4.16 A**,**B**). These dimer-to-dimer interfaces are located in the N-terminal subdomain of the RCK domain, more specifically in the helices α4 and α5 (**Figure 4.16 C**). These helices display apolar residues on its exposed surface that mediate the dimer-to-dimer interaction. For instance, in *Bacillus subtilis* KtrA, these two helices are enriched with Leucine, Isoleucine and Tyrosine (**Figure 4.16 D**).

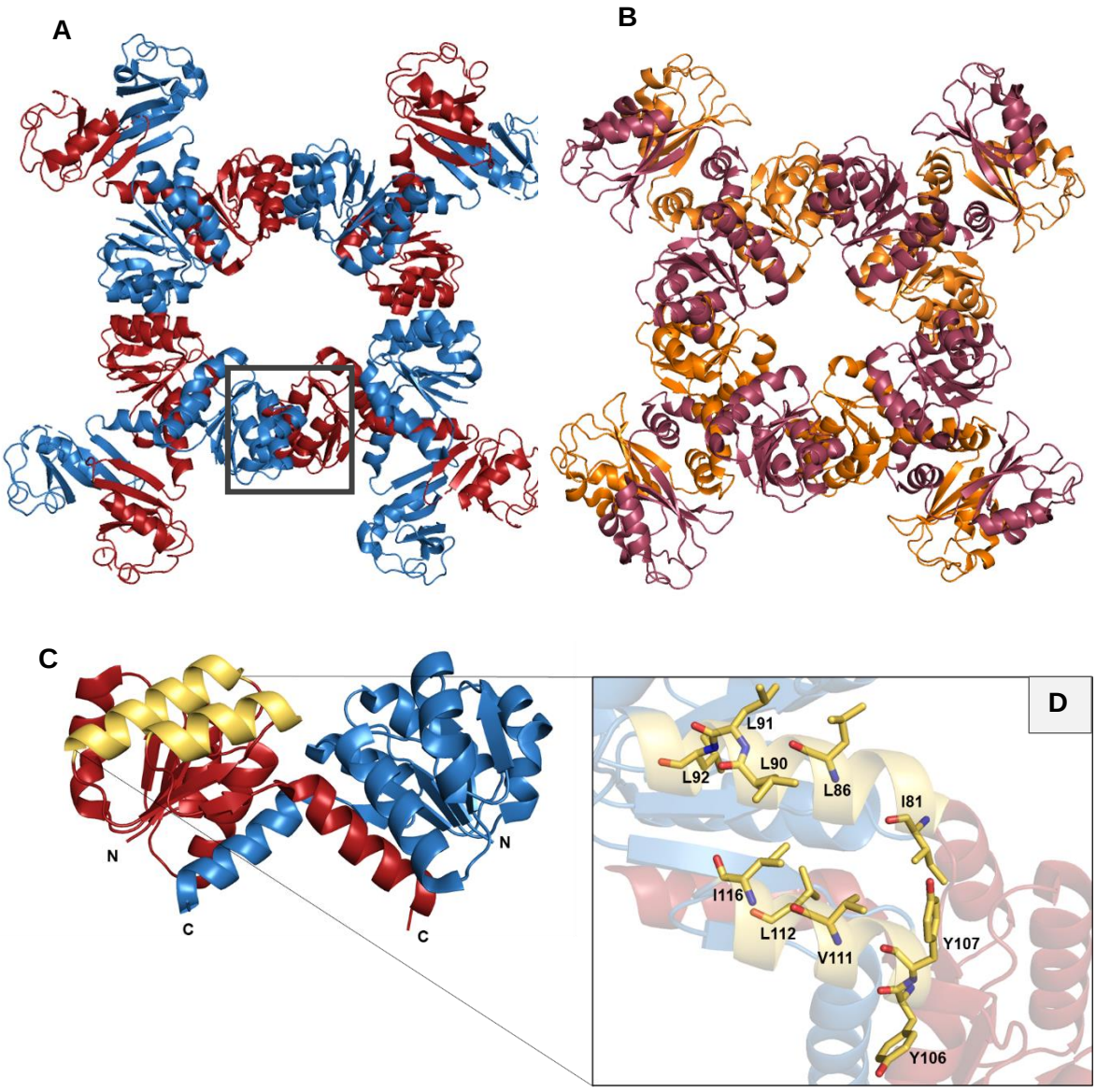

Figure 4.16 - The octameric conformation of the RCK domain of KtrA from Bacillus subtilis. A) View of the RCK-domain octameric ring from the KtrA channel (PDB accession code: 4J90); Black square delimits the dimer-to-dimer interface. **B)** View of the RCK-domain octameric ring from the MthK channel (PDB accession code: 2AEM). **C)** Cartoon representation of the N-terminal subdomain of the KtrA homodimer. Yellow shading on two of the helices represents the molecular surfaces involved in dimer-to-dimer interfaces in KtrA's RCK domain. **D)** Close-up of the apolar region involved in dimer-to-dimer interface of KtrA. Images generated by PyMOL.

The same region in YjbQ's RCK domain is not as strongly populated with apolar residues (**Figure 4.17**). This difference in the top two helices of the N-terminal might be the explanation for why YjbQ does not establish dimer-to-dimer contacts and therefore, does not form octameric rings.

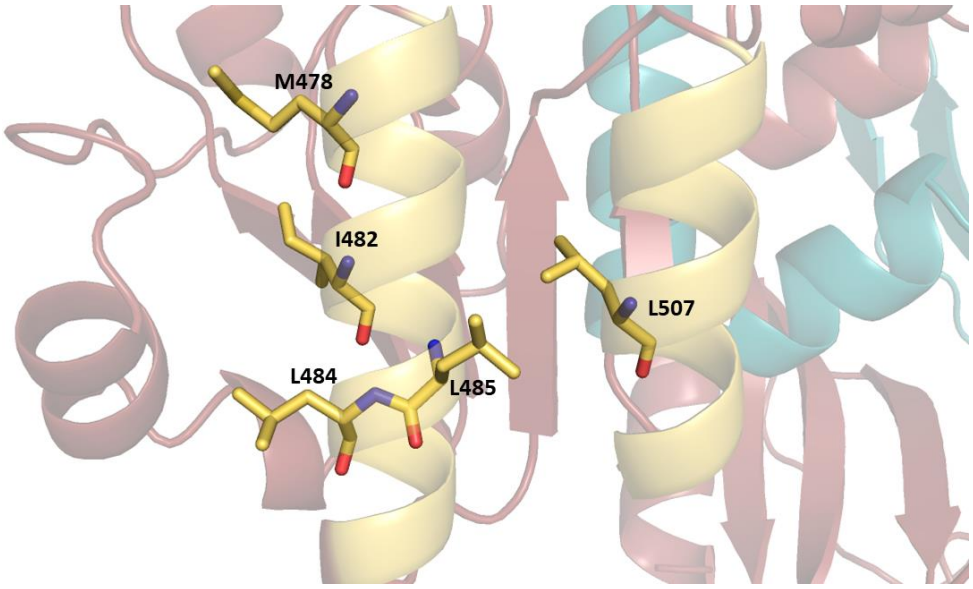

Figure 4.17 – Apolar residues present in the two helices located in the hypothetical dimer-to-dimer interface of YjbQ. Helices in the hypothetical dimer-to-dimer interface are shown in cartoon and coloured in yellow. Image generated by PyMOL.

4.5.2. Structural feature of the N-terminal subdomain of YjbQ

Many N-terminal RCK subdomains commonly possess a characteristic nucleotide-binding site, as KtrA does (**Figure 4.18**, ATP (shown as sticks coloured in green)).). This binding site is characterized by a fingerprint consensus sequence GxGxxG, in which the lack of side-chains in the glycines creates a pocket for binding of the phosphate groups. In addition, at the end of the second β strand of the sub-domain there is a conserved negatively charged residue (Glutamate or Aspartate)that forms hydrogen bonds with the ribose of the nucleotide[69]. KtrA binds ATP and ADP in this binding pocket and the sequence GLGRFG (Glycine-Leucine-Glycine-Arginine-Phenylalanine-Glycine) is visible and extremely close to the ATP molecule (**Figure 4.18 C**). The negatively charged residue Aspartate (D36) is also present, coordinating with the ribose 2' hydroxyl of the adenosine group (**Figure 4.18 C**). In contrast, YjbQ does not possess this nucleotide-binding motif. This being said, the N-terminal subdomain of YjbQ was submitted to a sequence conservation analysis with the program Consurf, in order to check the region corresponding to the nucleotide-binding domain of KtrA (**Figure 4.19**).

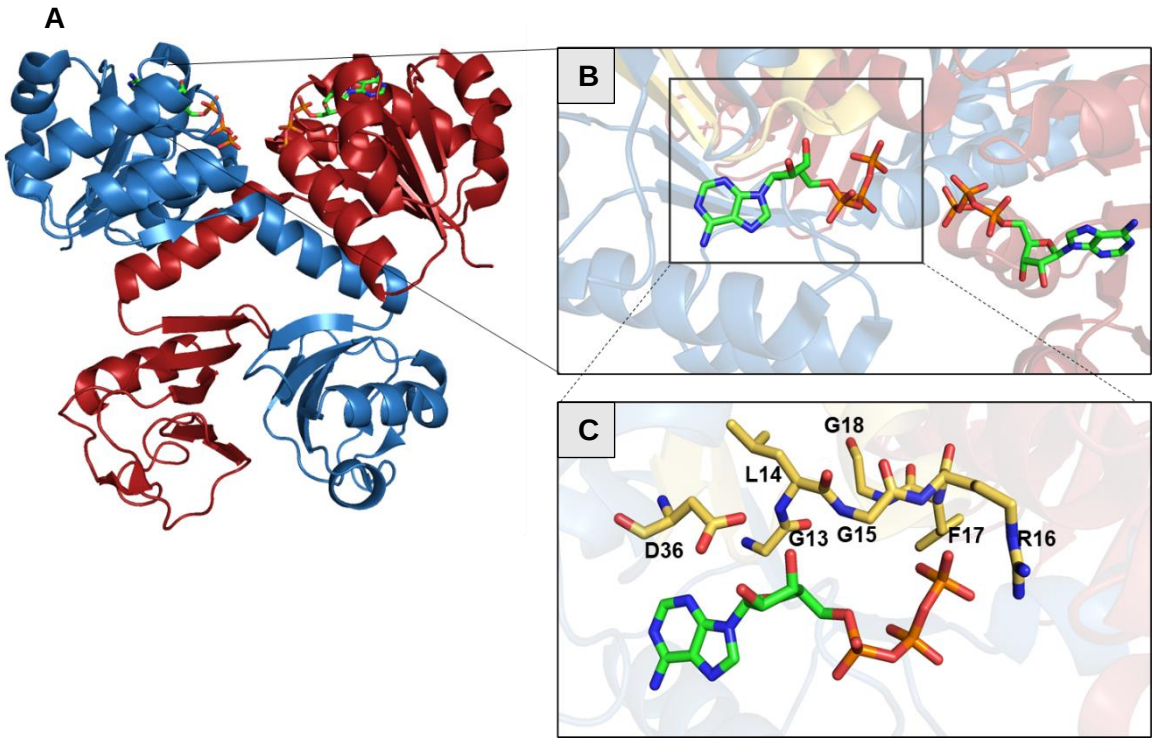

Figure 4.18 - Nucleotide binding site of KtrA from *Bacillus subtilis*. A) RCK domain of KtrA with two ATP molecules. ATP molecules are drawn as sticks with green carbon atoms (PDB accession code: 4J90). **B)** Overview of the ATP binding site. Black square delimits the zone where the nucleotide-binding motif is situated. **C)** Constituent residues of the nucleotide-binding motif. Image generated by PyMOL.

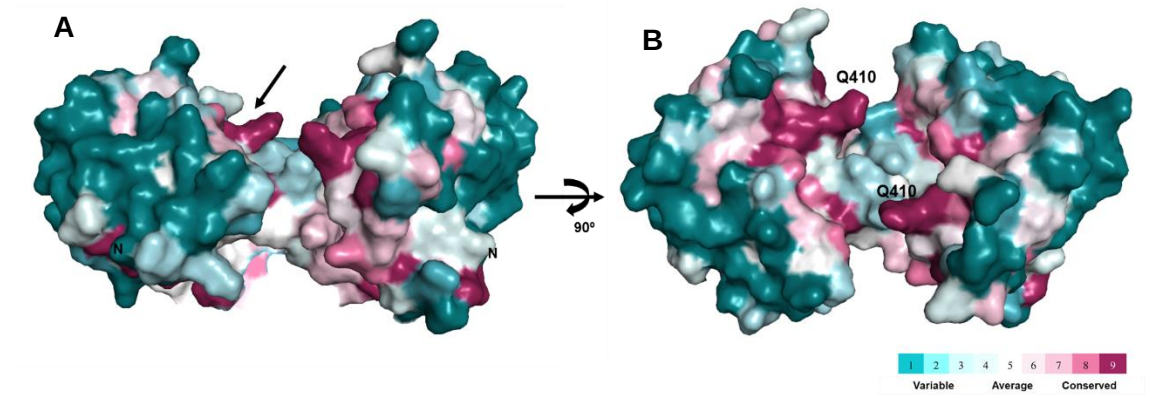

Figure 4.19 - Consurf conservation analysis on the N-terminal subdomain of YjbQ. A) Overview of the conservation score of the N-terminal subdomain. Arrow points to the region of the RCK domain of YjbQ where KtrA binds a nucleotide. **B)** 90º rotation on the N-terminal subdomain. Both surface structures are coloured by its conservation grades, using the nine grade colour-coding bar of Consurf Server. On the conservation scale, grade 1 was defined as the most highly variable amino acid positions (turquoise), and grade 9 was defined as the most highly conserved positions (maroon). Image generated by PyMOL.

Analysing **Figure 4.19**, it becomes clear that the N-terminal subdomain of YjbQ has regions with a low degree of conservation among homologous antiporters. The region in YjbQ, which corresponds to the nucleotide-binding region in KtrA, exhibits a low-to-medium conservation score with the exception of the region which comprises a highly-conserved glutamine (Q410) (**Figure 4.19 B**) located in the region between the two subunits. The reason for its high conservation is unknown. However, if YjbQ had the ability to bind nucleotides in the N-terminal subdomain, it would be expectable that this region displayed a stronger degree of conservation.

4.5.3. The effect of c-di-AMP on the structure of the RCK domain of YjbQ

As described above, c-di-AMP binds to the RCK domain of YjbQ. Analysis of the structure crystallized in the presence of c-di-AMP reveals that the nucleotide is bound in the C-terminal subdomain, in the interface between the two lobes of the RCK domain (**Figure 4.20**, c-di-AMP shown as sticks coloured in green). A simple visual comparison between the structure with and without c-di-AMP suggests that the presence of this ligand does not affect the overall structure of YjbQ's RCK domain (**Figure 4.20 A**,**B**).

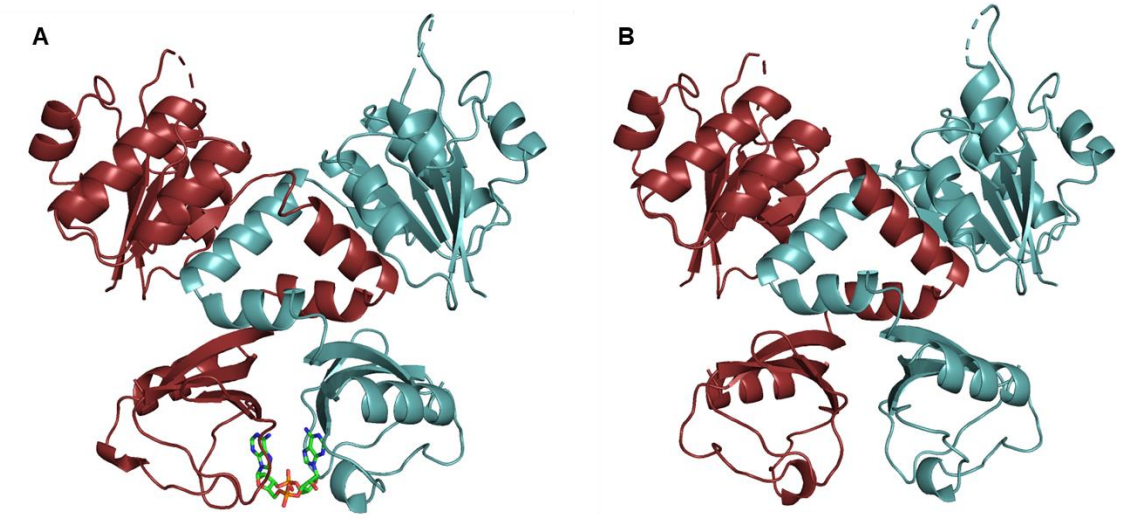

Figure 4.20 - The RCK domain of YjbQ in the presence and absence of c-di-AMP. Cartoon representation of the RCK domain **A)** in the presence of c-di-AMP (bound in C-terminal domain dime and drawn as sticks with green carbon atoms) and **B)** absence of c-di-AMP. Image generated by PyMOL.

To further investigate the possible differences in both structures, a superimposition of both structures was performed by aligning the first 50 residues of the N-terminus of the

red-coloured subunit (**Figure 4.21**). Apart from the flexible loops, the structure with c-di-AMP (coloured in teal and red) is not greatly changed when compared to the one without c-di-AMP (coloured in pink) both at the level of the subunit N-terminal domain and at the level of the spatial relationship between N-terminal domains in the dimer.

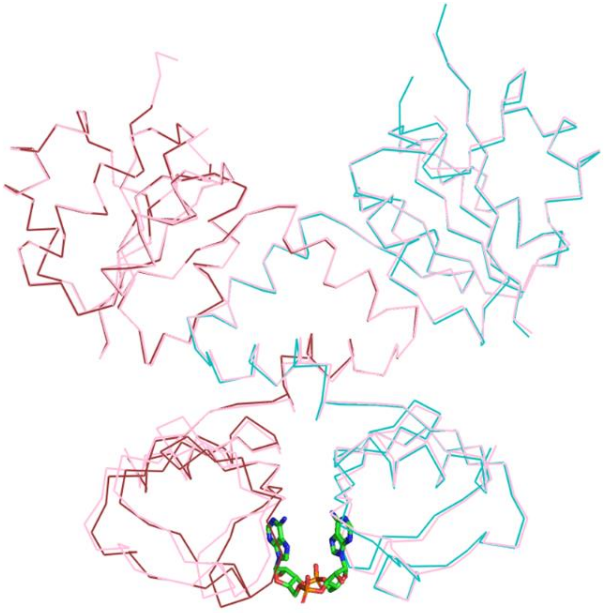

Figure 4.21 – Overall view of the superimposed RCK domain structures of YjbQ. Ribbon representation of the RCK domain of YjbQ in the presence (coloured in red and teal) and absence (coloured in pink) of c-di-AMP. c-di-AMP drawn as sticks with green carbon atoms. Image generated by PyMOL.

To analyse c-di-AMP's effect on the binding pocket of the RCK domain of YjbQ, a superimposition was performed with the residues 545 to 557 and 592 to 613 in the C-terminal subdomain, which appeared to be least changed region. The major, yet relatively small, differences are located in the region that surrounds the c-di-AMP molecule (**Figure 4.22 A**, **B**). Measuring the distance between the C-alpha carbon of the same residue (Arginine 562) in the two subunits of the RCK domain of both structures, reveals a widening of the separation across the dimer interface of around 2 Å (**Figure 4.22 C**). In the absence of c-di-AMP, the distance across c-di-AMP's binding site is 14.8 Å, while in the presence of ligand this distance shifts to 13.17 Å. This implies that the C-terminal subdomain of the RCK domain closes slightly upon binding of c-di-AMP. In contrast, the deviations of the flexible loops within each subunit of the C-terminal subdomain are not significant. For example, the C-alpha carbon of residues 562 and 569 shift by less than 1 Å (**Figure 4.22 D**).

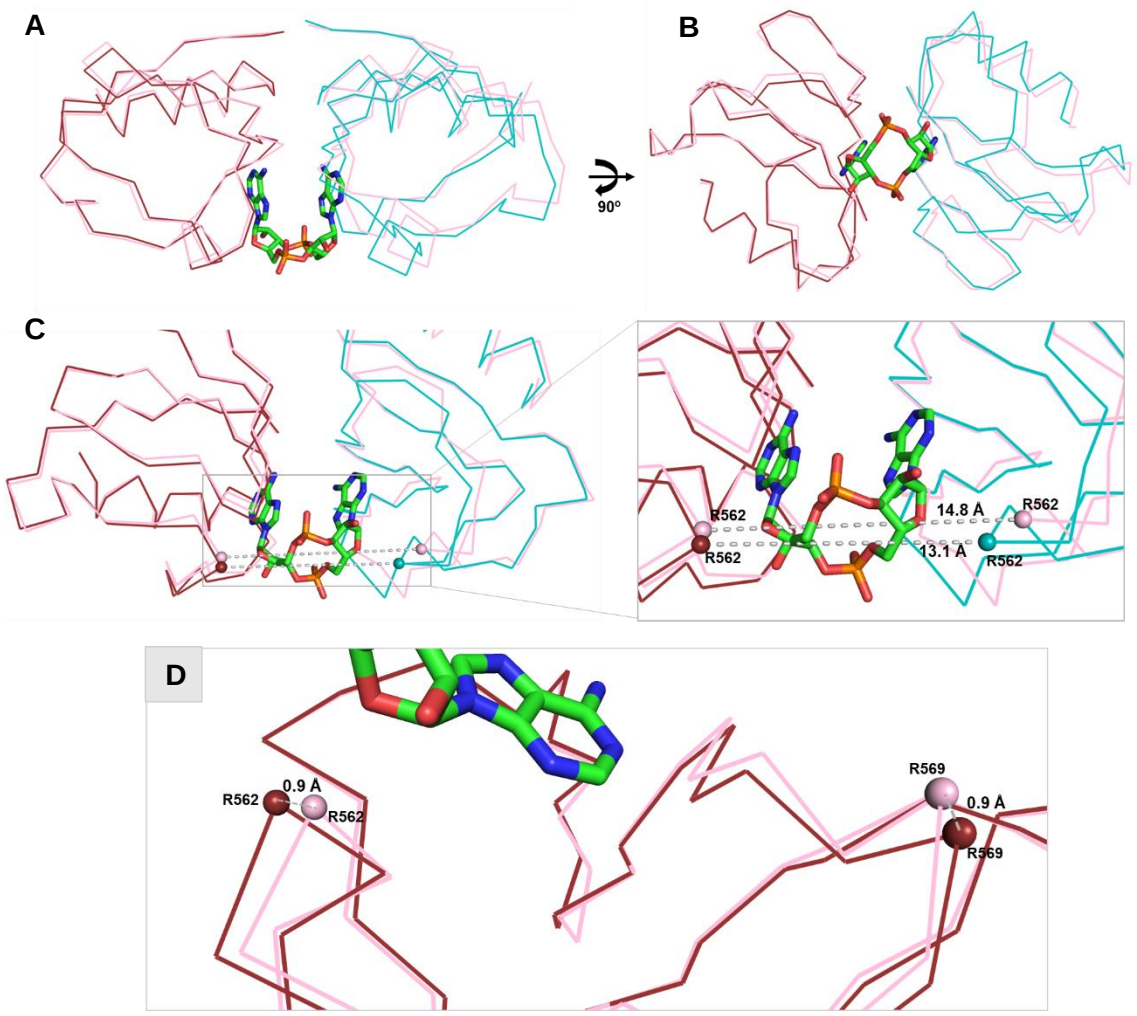

Figure 4.22 - C-terminal subdomain of the RCK domain of YjbQ in the presence and absence of c-di-AMP. Ribbon representations of the RCK domain of YjBQ in the presence (coloured in red and teal) and absence of c-di-AMP (coloured in pink). c-di-AMP is drawn as sticks with green carbon atoms. **A)** Overall view of the c-di-AMP binding pocket with the two superimposed structures. **B)** 90º degree rotation relative to A). **C)** Distance between the C-alpha carbon (represented as a sphere) of Arginine 562 in the two superimposed structures. **D)** Intra-subunit deviations between two loops in the structures. Images generated by PyMOL.

4.5.4. The binding site for c-di-AMP in RCK domains

In the C-terminal subdomain of the RCK domain of YjbQ, apolar residues surround the adenine bases of c-di-AMP. In contrast, polar residues at the mouth of the binding site participate in the interaction with the ribose and phosphate groups of the nucleotide (**Figure 4.23 B**). The hydrophobic interactions involve residues Phe565, Leu560, Phe561 and Ile570. In addition, two water molecules are clearly detectable in the ligand-

binding site of c-di-AMP and are found to mediate a network of hydrogen bonds between the protein and the ligand. Each water molecule forms three hydrogen bonds with the surrounding atoms, including the adenine ring, the phosphate oxygen of the lactone ring and the His584 Nδ atom (**Figure 4.23 C**).

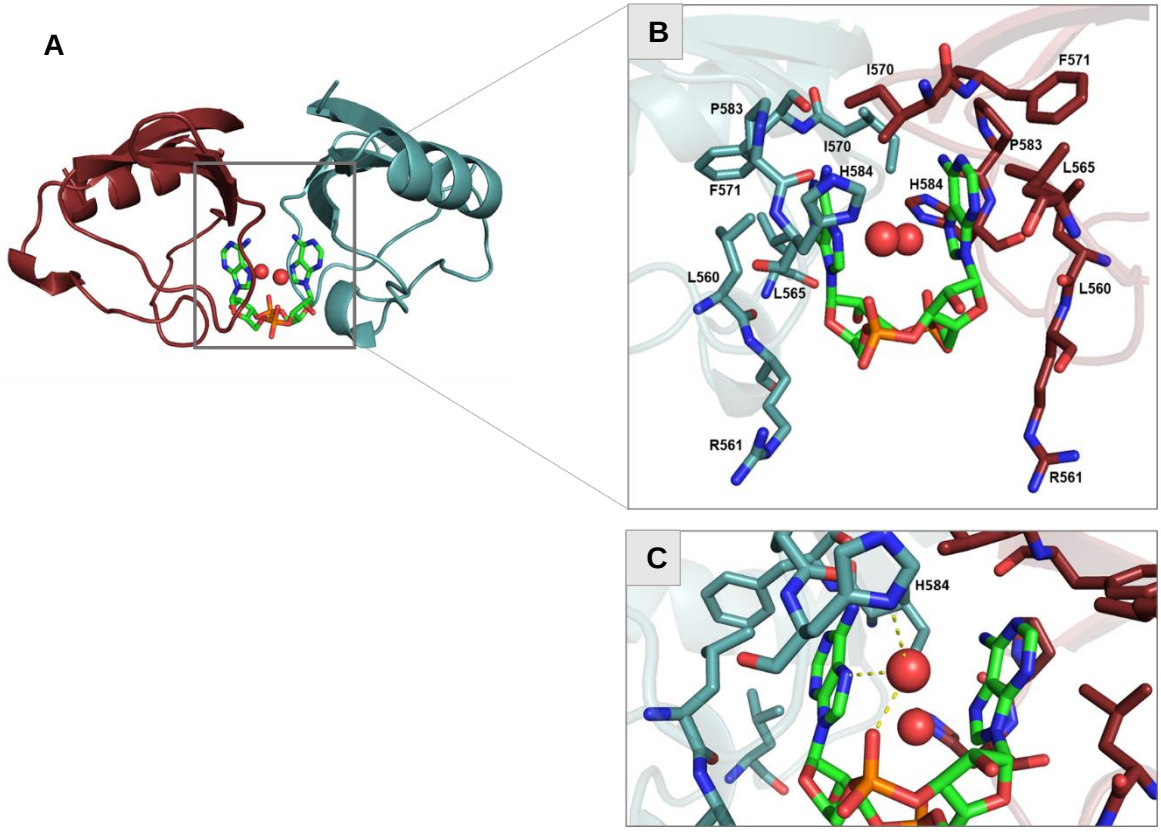

Figure 4.23 - Structural characteristics of the C-terminal subdomain of the RCK domain of YjbQ. A) The C-terminal subdomain in complex with c-di-AMP shown as cartoon, with the protomers coloured in teal and red. c-di-AMP is drawn as sticks with green carbon atoms. Two water molecules are shown as red-coloured spheres. **B)** Detailed interactions on the c-di-AMP binding pocket. **C)** Detailed view on the coordination of one water molecule in the binding pocket. Images generated by PyMOL.

Just as the N-terminal subdomain, the C-terminal subdomain was submitted to a conservation analysis with Consurf. The binding-site for c-di-AMP appears to be the most conserved region in the RCK domain of YjbQ exhibiting moderate-to-high conservation (**Figure 4.24 A**). Residues Arg561, Iso570, Pro583 and His584 have the highest degree of conservation within the binding-pocket of c-di-AMP (**Figure 4.24 B**).

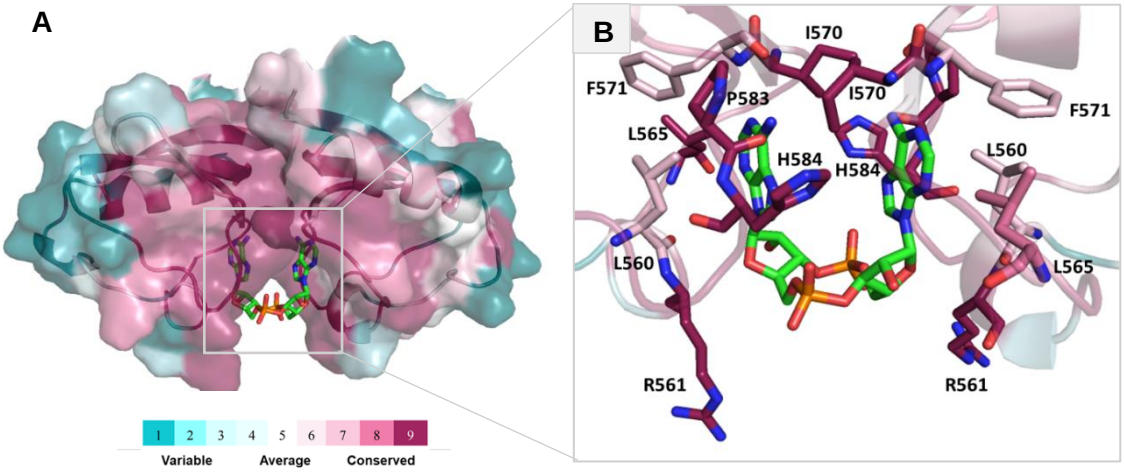

Figure 4.24 - Consurf conservation analysis on the C-terminal subdomain of YjbQ. A) Overview of the conservation score of the C-terminal subdomain. Grey box delimits the binding site of c-di-AMP. **B)** Detailed view of the conservation in the c-di-AMP binding pocket. The structure (drawn as surface) and residues (drawn as sticks) are coloured by its conservation grades, using the nine grade colour-coding bar of Consurf Server. On the conservation scale, grade 1 was defined as the most highly variable amino acid positions (turquoise), and grade 9 was defined as the most highly conserved positions (maroon). Image generated by PyMOL.

The C-terminal domain of *Sa*CpaA shares approximately 60% of amino acid sequence similarity to the C-terminal subdomain of the RCK domain of YjbQ and the two C-terminal subdomains are structurally very similar (**Figure 4.25 B**). In particular, the ligand binding pocket displays the same properties in the two structures, with the adenine bases surrounded by apolar residues (**Figure 4.25 C**) and two water molecules present and coordinating the same atoms (**Figure 4.25 A**,**C**).

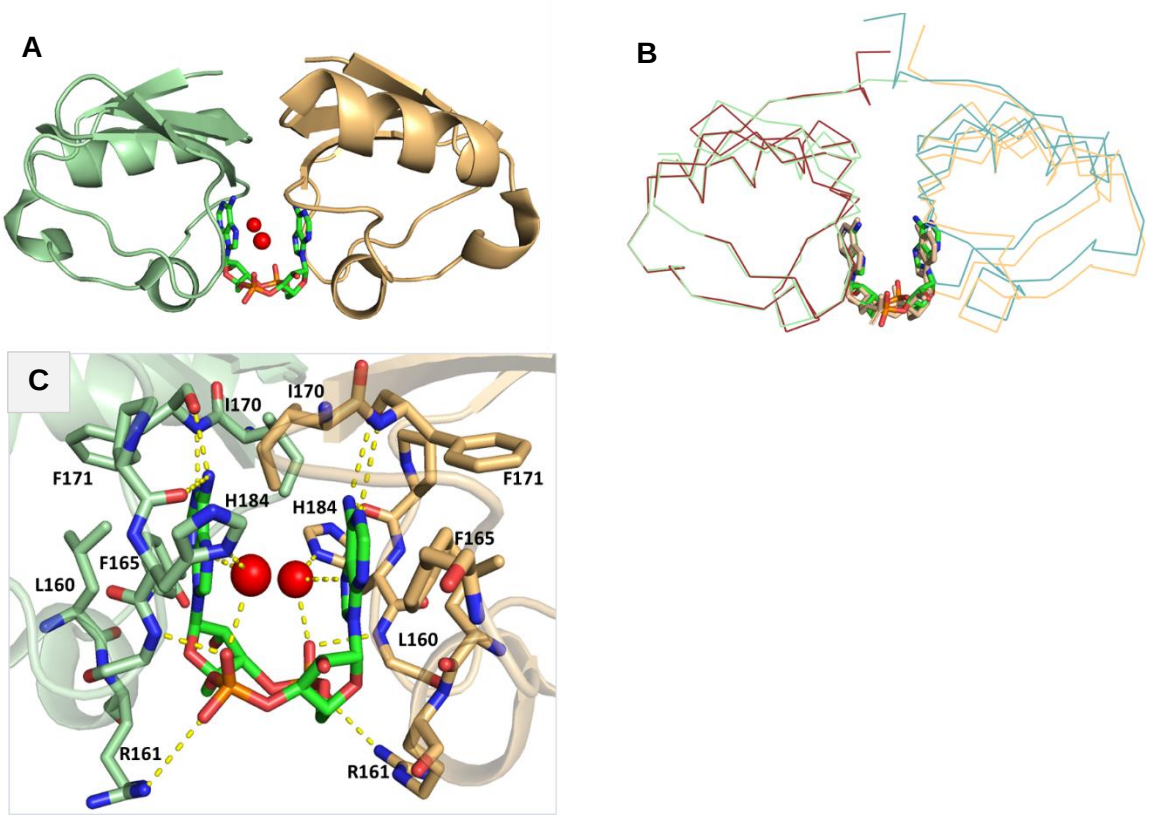

Figure 4.25 - Structural characteristics of the C-terminal subdomain of the RCK domain of CpaA from *Staphylococcus aureus.* A) The C-terminal subdomain (PDB accession code: 5F29) in complex dimer as cartoon, with the protomers coloured in green and orange. c-di-AMP is drawn as sticks with green carbon atoms. Two water molecules are shown as red-coloured spheres. **B**) Superimposition of the C-terminal subdomain of SaCpaA (coloured in green and orange) and YjbQ (coloured in red and blue). **C)** Detailed interactions on the c-di-AMP binding pocket of SaCpaA Images generated by PyMOL.

KtrA from *Staphylococcus aureus*, which is the only available structure of KtrA in complex with c-di-AMP, exhibits a slightly different binding pocket in comparison to YjbQ and CpaA. Despite adopting a similar overall tertiary structure (**Figure 4.26 A**), the binding interaction with c-di-AMP reveals significant differences. As shown in **Figure 4.26 B**, the polar residues participating in the binding are quite different and located in different positions. One major difference is the appearance of an Arginine (R168) in the middle of the pocket. This Arginine interacts with the c-di-AMP molecule, one water molecule and with the Asparagine residue (N174) (**Figure 4.26 B**).

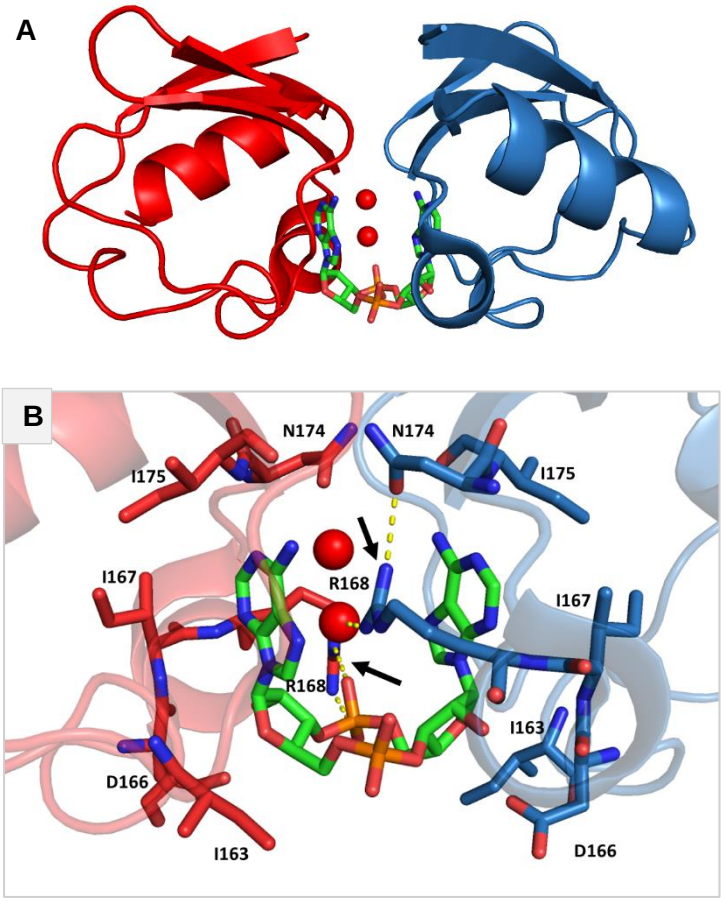

Figure 4.26 - Structural characteristics of the C-terminal subdomain of the RCK domain of KtrA from *Staphylococcus aureus*. A) The C-terminal subdomain (PDB accession code: 4XTT) in complex dimer as cartoon, with the protomers coloured in red and blue. c-di-AMP is bound at the bottom region and drawn as sticks with green carbon atoms. Two water molecules are shown as red-coloured spheres. **B)** Detailed interactions on the c-di-AMP binding pocket. Black arrow points to R168. Images generated by PyMOL.

In short, it was demonstrated that the RCK domain of YjbQ possesses two distinct subdomains: the N-terminal subdomain, with the conserved Rossman fold and the C-terminal subdomain, which comprises the binding site of c-di-AMP. Unlike many prokaryotic K^+-transporters, the RCK domain of YjbQ does not form octamers and does not possess a nucleotide binding site in the N-terminal subdomain. The C-terminal subdomain, which exhibits a high degree of conservation, is very similar to the one present in CpaA from Staphylococcus aureus, especially in the region surrounding c-di-AMP. On the other hand, the presence of c-di-AMP does not greatly change the structure of the RCK domain of YjbQ.

4.6. Cross-linking experiments with YjbQ

At this point, it is clear that the RCK domain of YjbQ forms dimers. However, very little is known about the oligomeric state of full-length YjbQ. Previous studies have demonstrated that amino group cross-linkers are useful tools in the determination of the oligomeric state of membrane proteins, such as KtrB, trimeric glutamate transporters and copper uptake transporters[61,70,71]. In these cases, where proteins exist in higher oligomeric states (dimers in KtrB and trimers in the glutamate and copper transporters), exposure of membranes containing the membrane protein to increasing concentrations of cross-linker resulted in the emergence of the final-state band (dimer or trimer) before the monomer band disappeared. Thereby, the same approach was used with YjbQ, in order to investigate its oligomeric state in the membrane.

Several bifunctional amino-group cross-linkers with different spanning lengths and chemical properties were chosen: 3,3′-dithiobis(sulfosuccinimidylpropionate) (DTSSP, spacer arm 12Å), ethyleneglycol bis(succinimidylsuccinate) (EGS, spacer arm 16Å), dithiobis(succinimidyl propionate) (DSP, spacer arm 12Å) and 1,5-difluoro-2,4-dinitrobenzene (DFDNB, spacer arm 3Å). In the end, only DTSSP and EGS produced visible results, reason why the other two cross-linkers were discarded.

The resulting western blot image (**Figure 4.27**) shows that increasing concentrations of cross-linker result in the decrease of intensity of the band migrating between 50 and 70 kDa, consistent with a YjbQ monomer (expected molecular mass, 67 kDa). Concomitantly, the band that migrates between 130 and 180 kDa (equivalent to the YjbQ dimer) increases.

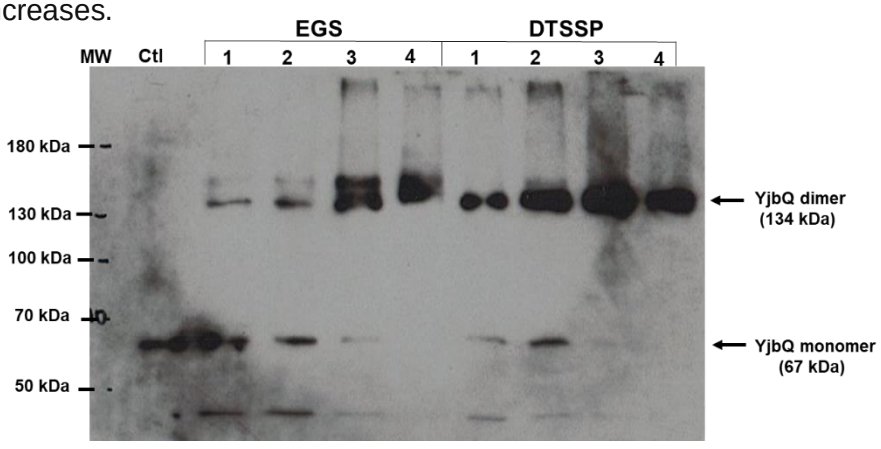

Figure 4.27 - Dimerization of YjbQ molecules. Western blot of E. coli membrane preparations containing His-tagged B. subtilis YjbQ and probed with anti-His tag monoclonal antibodies. The identity of cross-linkers is shown above the lanes. with cross-linker concentration (1 to 4): 31.25 µM, 62.5 µM, 125 µM, and 500 µM, respectively. Molecular mass (MW) markers are shown and Ctl" lane corresponds to protein without cross-linker present.

In light of these results, it is possible to conclude that YjbQ forms dimers in its natural environment, without the presence of c-di-AMP.

4.7. YjbQ's CPA motif and phenotype analysis

The function of YjbQ is still largely unknown. In order to gain some insights into the functional properties of YjbQ, a sequence analysis of the membrane-buried regions was performed. As mentioned before, YjbQ belongs to the large family of cation/proton antiporters (CPAs), which are commonly subdivided in two major groups: CPA1 and CPA2. YjbQ is inserted in the CPA2 subdivision based on its assumed electrogenicity and ion selectivity. In 2018, Masrati et al[55] proposed that all CPAs possess a well-defined sequence motif, the so called CPA motif, that distinguishes CPA1s from CPA2s and appears to determine the characteristics of electrogenicity and ion selectivity. The CPA motif comprises 8 highly conserved residues, which are located at the protein's core near the ion binding site in the N-terminus. However, they reside on three different helices and therefore, do not form a continuous sequential motif. This motif is usually represented as $X_1X_2X_3X_4$ … $[E/-]_5$ - - - X_6D_7 … $[R/K]_8$, where X stands for a limited set of residues that characterize each group, the dashes represent any residue, and the dots represent two segments with average lengths of 23 and 156 residues, respectively. The numbers in subscript correspond to the eight motif residues. Residues 1-through-4 reside on the fourth transmembrane helix, residues 5-through-7 reside on the fifth helix and the last residue is found in the tenth transmembrane helix of the protein core. To identify the residues in YjbQ that form the CPA motif and possibly conclude about its phenotypic characteristics, a model of the membrane-buried regions (residues 1-394) of YjbQ was generated (see Materials and Methods, section **3.12**).

According to the authors, the CPA2 family has distinctive features regarding its CPA motifs. Firstly, CPA2s lack a residue in position 5, which is usually filled by a highly conserved glutamate in CPA1s. In addition, electrogenic CPAs, which usually belong to the CPA2 subfamily, are characterized by an aspartate at position 6 of the CPA motif and a lysine at position 8. K^+-selective antiporters are commonly characterized by CPA motifs populated with small-size residues (serine, threonine, and alanine) in positions 1-throught-4. Interestingly, YjbQ was contemplated in the study, being inserted in a CPA2 clade next to NhaS5, a Na^+/H^+ antiporter from *Synechocystis sp.*.

Through analysis of residues in the YjbQ model and comparing them with residues in YjbQ's sequence with other CPA2 proteins members with characterized CPA motifs (KhtU, SsNhaS5, and E.coli NhaA), it was possible to estimate that estimate the CPA motif for YjbQ is $S_1T_2I_3S_4$ … $[-]_5$ - - - A_6D_7 … K_8 (**Figure 4.28**).

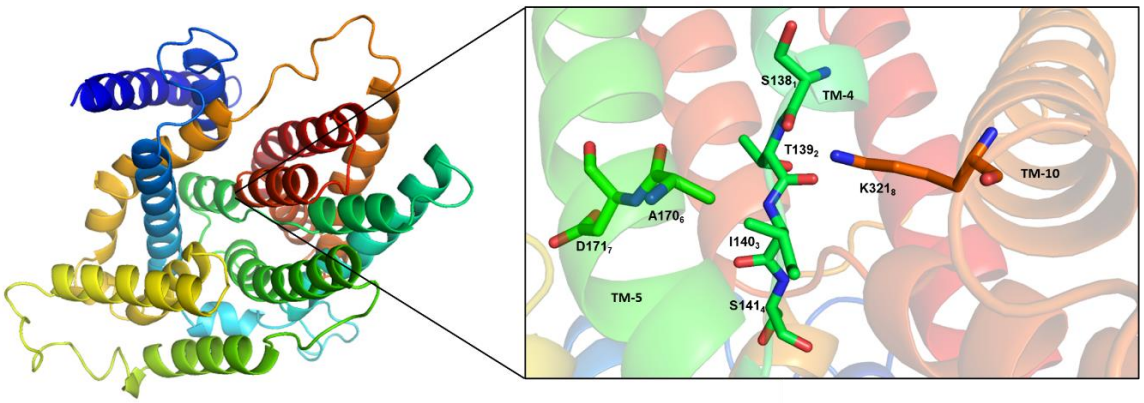

Figure 4.28 - The CPA motif of YjbQ. The highlighted amino acids correspond to the eight constituent residues of the CPA motif, located in three transmembrane helixes in the protein's core. Image generated by PyMOL.

It is that three out of the first four residues of the CPA motif are small-size polar residues, which suggests that YjbQ is K^+-selective. In addition, the highly conserved Aspartate in position 6 is absent in YjbQ, instead being replaced by the non-polar residue Alanine, characteristic of an electroneutral transporter. In the end, YjbQ is characterized as an K^+-selective, electroneutral transporter member of the CPA2 family, however, it is important to stress that these conclusions are based on a model that was generated based on protein structures with which YjbQ shares very little sequence similarity, which reduces the accuracy of the homology model.

4.8. Complementation studies in *E. coli* mutant strains

In order to investigate the function of YjbQ as an K^+/H^+ antiporter, *E. coli* phenotype complementation assays were performed. The first assays used the *E. coli* triple mutant strain TK2420, defective for the Kdp, Trk and Kup K^+-uptake systems and consequently unable to grow in conditions with less than 30 mM of K^+. To validate YjbQ proposed

function, TK2420 cells expressing wild-type YjbQ would have to require more than 30 mM of K^+ to grow, as exporters exacerbate the K^+-dependent phenotype of this strain. This apparent shift in phenotype was previously demonstrated in the K^+ exporter KhtTU[57]. On the other hand, K^+ importers, like KtrAB, are able to grow in concentrations of K^+ smaller than 30 mM, since they complement theTK2420 phenotype[72].

A simple test was first performed to determine the concentration of L-Arabinose, the inducer of pBAD expression systems, for optimal expression of YjbQ. TK2420 cells were transformed with empty pBAD plasmid and pBAD_YjbQ. Two different concentrations were tested: 0.02 and 0.2%. However, when analysing cell growth with 0.02% (**Figure 4.29 A**) and 0.2% of L-Arabinose (**Figure 4.29 B**), it is visible that there is not a clear preference for either of the two amounts tested as the curves exhibit very similar profiles. In both cases, empty vector and YjbQ-expressing cells exhibit the wild-type phenotype of the TK2420 strain, requiring a minimum of 30 mM of K^+ to grow. Despite this, the following assays were performed using 0.2% of L-Arabinose to promote higher protein expression.

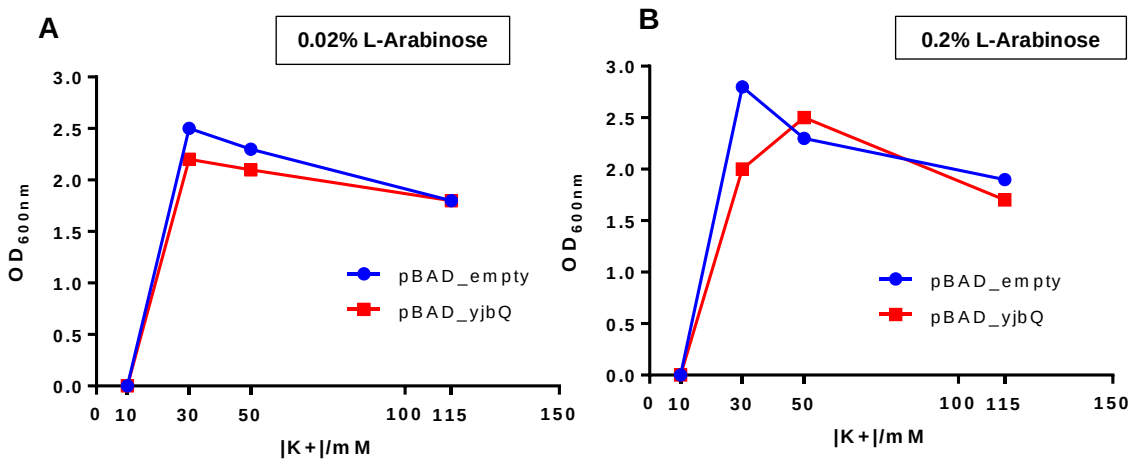

Figure 4.29 - Effects of different concentrations of L-Arabinose on the growth of E. coli TK2420 mutant strain transformed with control plasmid pBADHis b and pBAD_YjbQ. Cell growth was performed on minimal medium supplemented with 10, 30, 50 and 115 mM of K^+. A) Protein expression induced with 0.02% of L-Arabinose. B) Protein expression induced with 0.2% of L-arabinose.

The full assay was performed with three replicas for each condition. In addition, intermediate concentrations of K^+ (20 mM and 40 mM) were added, to assess if there were any differences in cell growth. As before, there is no significant difference in the growth curves and YjbQ-expressing cells continued to display the TK2420 wild-type phenotype (**Figure 4.30**).

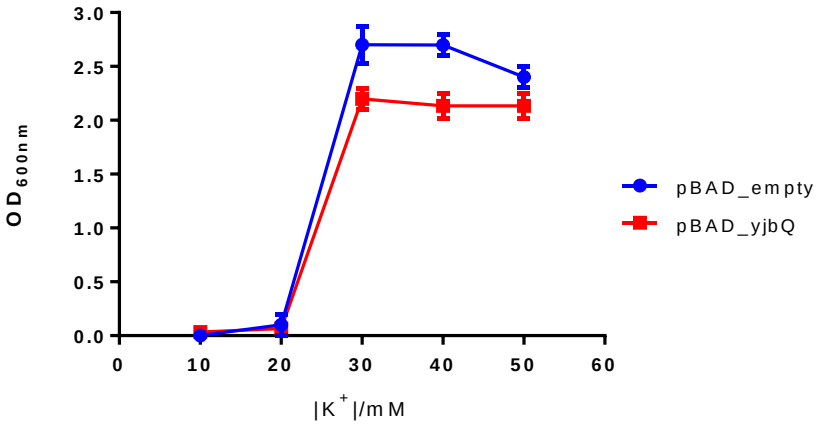

Figure 4.30 - Growth curves of E. coli TK2420 mutant strain transformed with control plasmid pBADHis b and pBAD_YjbQ. Cell growth was performed on minimal medium supplemented with 10, 20, 30, 40 and 50 mM of K+. The results represent the averages of three independent experiments, with error bars representing the standard deviations.

The possibility that like KhtTU, YjbQ lacking the cytoplasmatic regulatory RCK domain is constitutively active was also explored. For this, I repeated the complementation assay with the two mutant constructs of YjbQ that lack the RCK domain. Unfortunately, once again there are no significant differences concerning the studied phenotype relative to empty vector-containing cells (**Figure 4.31**), ruling-out the proposed hypothesis.

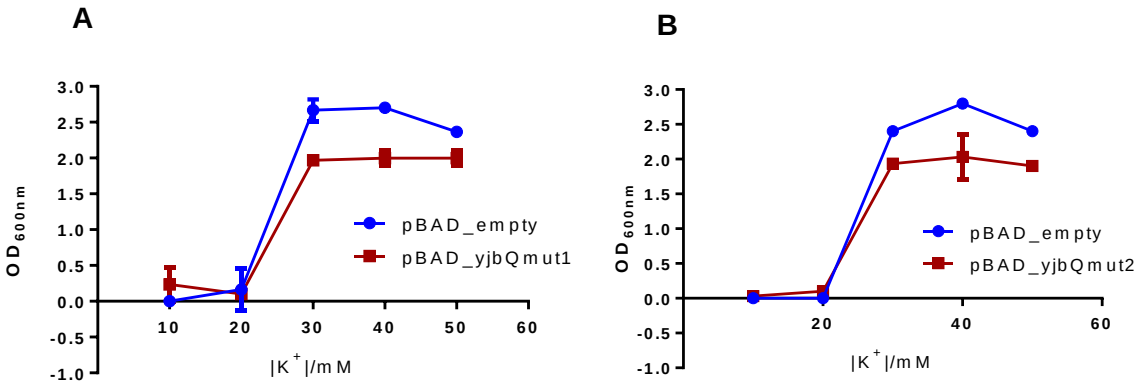

Figure 4.31 - Growth curves of E. coli TK2420 mutant strain transformed with control plasmid pBADHis b and pBAD His b_YjbQΔRCK1 or YjbQΔRCK2. Cell growth was performed on minimal medium supplemented with 10, 20, 30, 40 and 50 mM of K+. The results represent the averages of three independent experiments, with error bars representing the standard deviations.

Not observing a phenotype for YjbQ may result from the lack of c-di-AMP in *E. coli*. With this in mind, the DAC domain from *Listeria monocytogenes* CdaA was cloned into another arabinose-induced vector: pBAD33, that is compatible with $pBAD_{Hisb}$. Consequently, another round of complementation assays was performed, this time with TK2420 cells co-expressing YjbQ and the DAC domain of CdaA. In fact, cells exhibited a slightly different growth pattern in these assays (**Figure 4.32**). TK2420 cells could now grow at 20 mM K^+, when before this was not observed (cf. **Figure 4.31** and **Figure 4.29**). Unfortunately, this change in phenotype was registered for both control and YjbQ and DAC domain co-expressing cells.

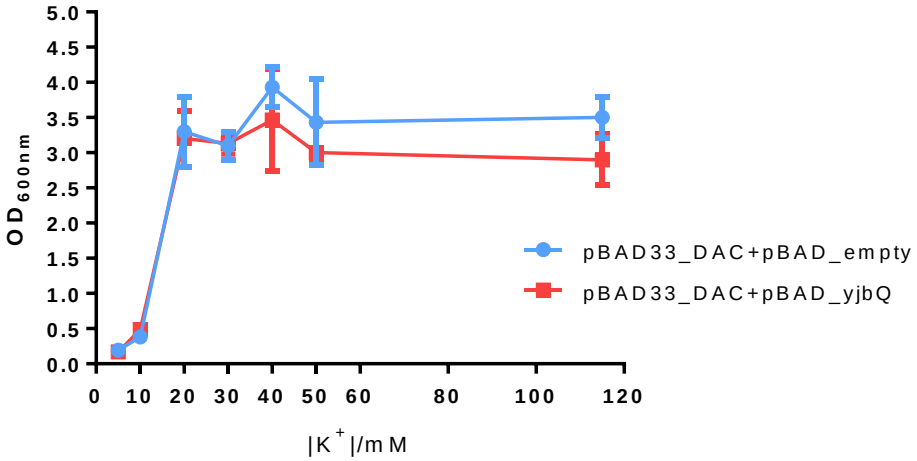

Figure 4.32 - Effects of the co-expression of YjbQ and DAC domain from CdaA on the growth of E. coli TK2420 mutant strain. pBAD33 expressing the DAC domain alone served as a control in this experiment. Cell growth was performed on minimal medium supplemented with 10, 20, 30, 40, 50 and 115 mM of K+. The results represent the averages of three independent experiments, with error bars representing the standard deviations.

One possible reason for not observing a phenotype in this assay is that c-di-AMP is not produced in our system. In order to investigate this possibility, the assay was performed by co-expressing the DAC domain with a transporter of known function and regulation and that is known to respond to c-di-AMP. It has been described that TK2420 expressing wild-type KtrAB or KtrBC grow with K^+ concentrations of 0.3 mM[72] and that the cytoplasmic regulatory subunit KtrC is inhibited by c-di-AMP in vivo[73], while KtrA binds c-di-AMP with 100-fold lower affinity. Consequently, complementation assays with DAC domain co-expressed with KtrAB or KtrBC were performed, expecting that cells co-expressing KtrBC and DAC will not grow in 0.3 mM of K^+ due to c-di-AMP inhibition, while those expressing KtrAB will grow better. Different inoculation OD and time points were tested for measuring final OD.

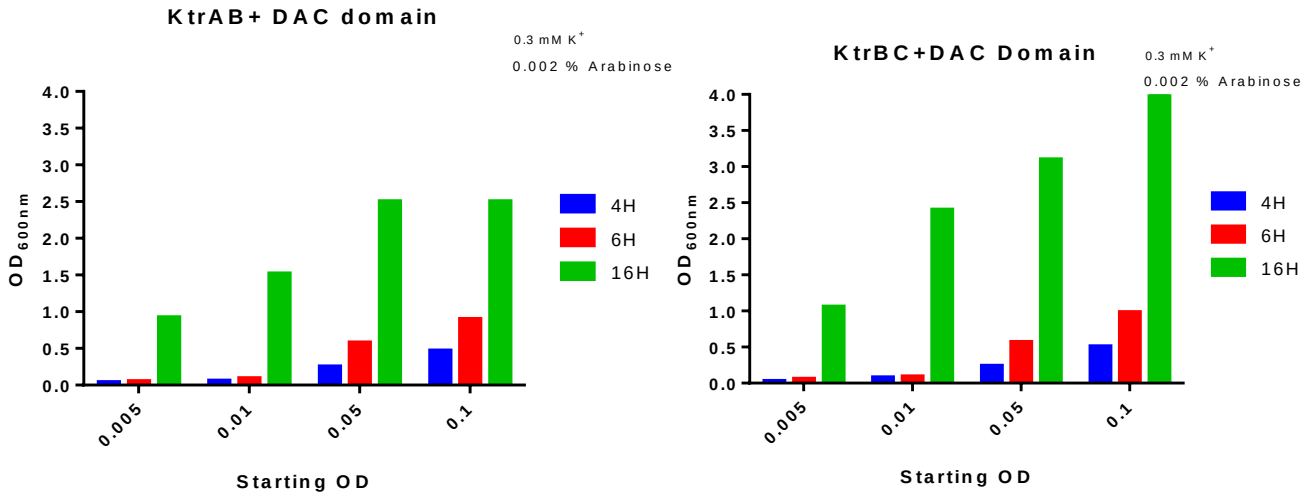

Figure 4.33 - Effect of KtrAB and KtrBC co-expressed with DAC on growth of TK2420 E. coli mutant strain. Cell growth was performed on minimal media supplemented with 0.3 mM of K+ and 0.002% of L-Arabinose. Four different starting ODs were tested: 0.005; 0.01; 0.05 and 0.1. Final ODs were measured after 4, 6 and 16 hours of incubation at 37ºC.

In 0.3 mM of K^+, TK2420 cells co-expressing KtrBC and DAC did not exhibit the predicted phenotype (**Figure 4.33**). There was not a significant growth difference between cells expressing KtrAB and KtrBC. In media supplemented with 1 mM of K^+, there were also no significant differences concerning the studied phenotype (**Figure 4.34**).

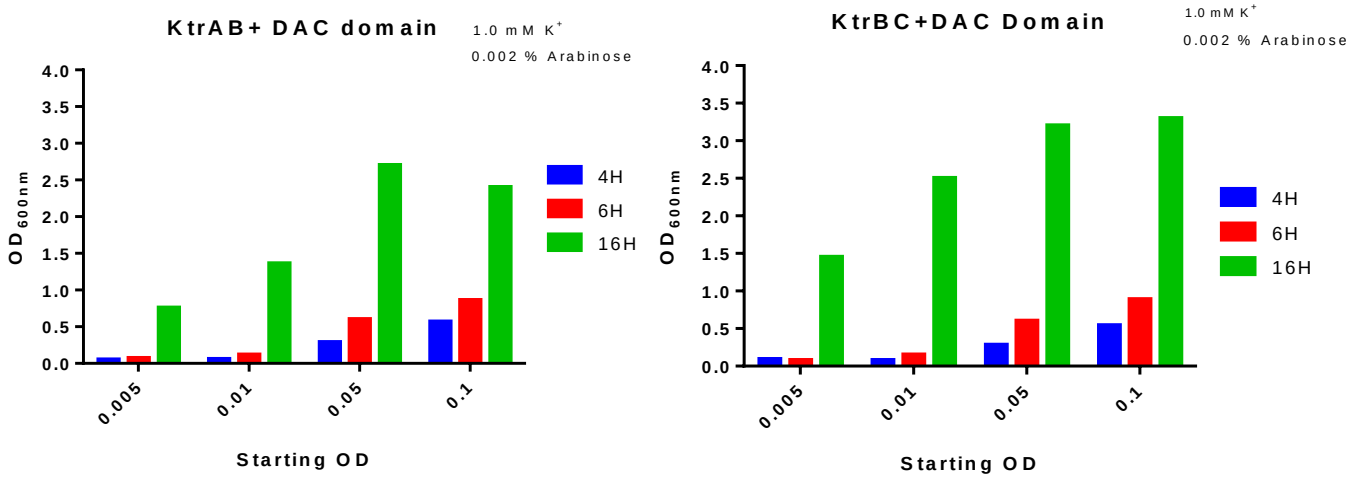

Figure 4.34 - Effect of KtrAB and KtrBC co-expressed with DAC on growth of TK2420 E. coli mutant strain. Cell growth was performed on minimal media supplemented with 1 mM of K+ and 0.002% of L-Arabinose. Four different starting ODs were tested: 0.005; 0.01; 0.05 and 0.1. Final ODs were measured after 4, 6 and 16 hours of incubation at 37ºC.

The assays were also performed with a higher concentration of L-Arabinose, 0.02% instead of 0.002%. However, as before no growth differences between the cells expressing both KtrAB or KtCB were detected (**Figures 4.35**, **4.36**). The increase in L-Arabinose concentration only seemed to increase the final OD of the cell culture, as expected if protein expression increases with inducer.

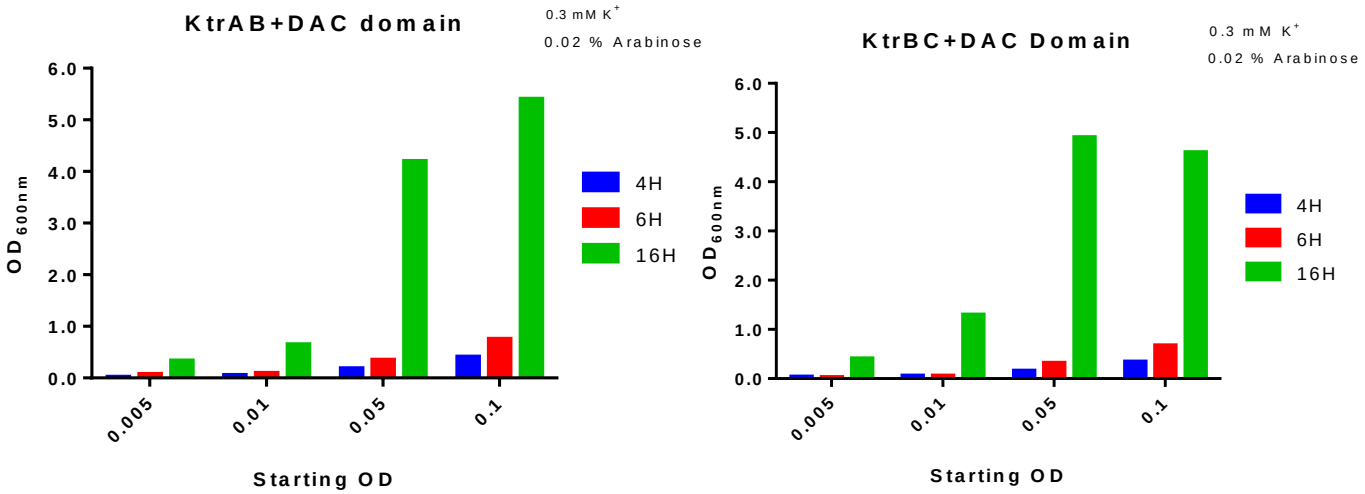

Figure 4.35 - Effect of KtrAB and KtrBC co-expressed with DAC on growth of TK2420 E. coli mutant strain. Cell growth was performed on minimal media supplemented with 0.3 mM of K+ and 0.02% of L-Arabinose. Four different starting ODs were tested: 0.005; 0.01; 0.05 and 0.1. Final ODs were measured after 4, 6 and 16 hours of incubation at 37ºC.

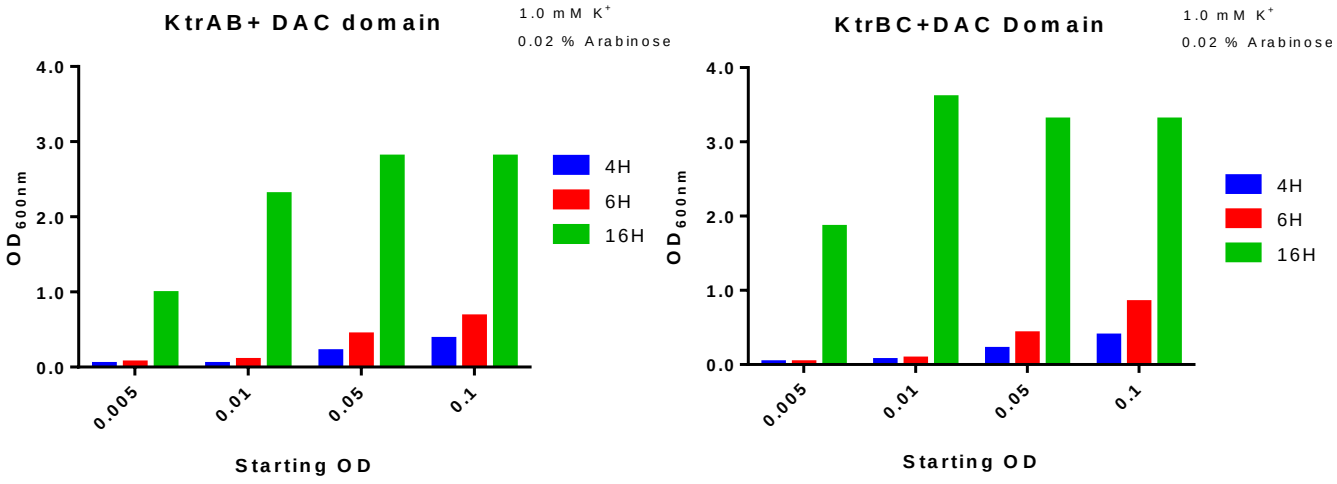

Figure 4.36 - Effect of KtrAB and KtrBC co-expressed with DAC on growth of TK2420 E. coli mutant strain. Cell growth was performed on minimal media supplemented with 0.3 mM of K+ and 0.02% of L-Arabinose. Four different starting ODs were tested: 0.005; 0.01; 0.05 and 0.1. Final ODs were measured after 4, 6 and 16 hours of incubation at 37ºC.

These experiments raise therefore the possibility that c-di-AMP is not produced in enough amount to affect the function of KtrBC or YjbQ. However, there is also the possibility that this protocol does not produce conclusive results because it was performed in a microorganism with distinct properties from the native *B. subtilis*.

Another possible explanation for the inconclusive TK2420 assays is that YjbQ selectively transports Na^+ instead of K^+. This possibility was addressed by performing complementation assays with the Na^+ and Ca^{2+}/H^+ antiporter-deficient E. coli KNabc strain. Previous studies showed that KNabc cells transformed with a characterized Na^+ exporter grew in medium supplemented with concentrations up to 500 mM of Na^+[57], while without the transporter the strain is limited to 50 mM of Na^+. Moreover, KNabc cells transformed with KhtTU, a transporter selective for K^+, demonstrated an inability to grow in media supplemented with more than 50 mM of Na^+.

Thereby, KNabc cells were transformed with the vector expressing YjbQ and its tolerance to Na^+ was assessed. YjbQ expressing cells did not exhibit the phenotype of a Na^+ exporter, as there is little difference in their sensitivity to Na^+, relative to the strain with empty plasmid (**Figure 4.37**).

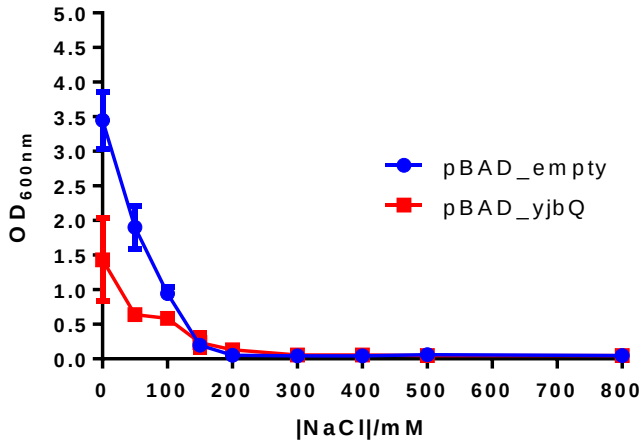

Figure 4.37 - Efects of different concentrations of NaCl on the growth of E. coli strain KNabc transformed with control plasmid pBAD His b and pBAD expressing YjbQ. Minimal media was supplemented with 50, 100, 150, 200, 300, 400, 500 and 800 mM of NaCl. The results represent the averages of three independent experiments, with error bars representing the standard deviations.

In order to follow the same line of thinking used with the TK2420 assays, co-expression of the DAC domain with YjbQ was also performed in KNabc cells. As before, KNabc cells co-expressing YjbQ and DAC domain behaved in a similar fashion to the control (**Figure 4.38**)

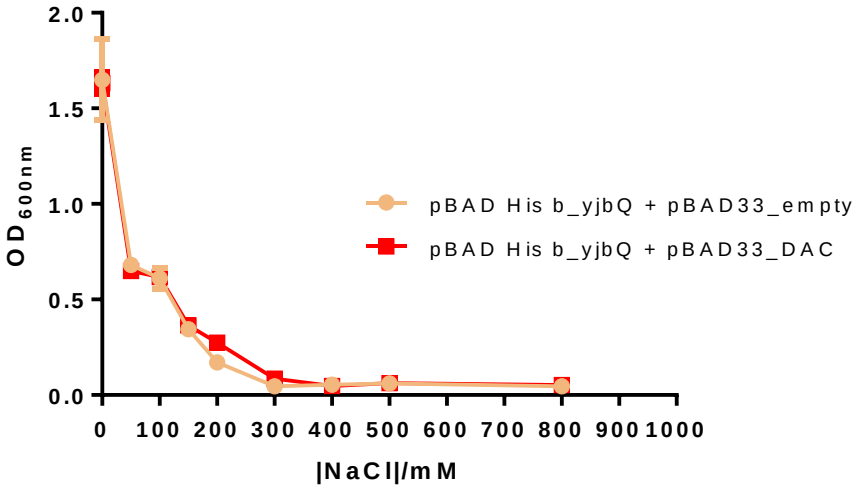

Figure 4.38 - Effects of the co-expression of YjbQ and DAC domain from CdaA on the growth of E. coli KNabc mutant strain. LBK media was supplemented with 50, 100, 150, 200, 300, 400, 500 and 800 mM of NaCl. The results represent the averages of three independent experiments, with error bars representing the standard deviations.

Strikingly, the pattern of effects of YjbQ expression in mutant E. coli strains suggest that YjbQ is not a functional K^+ or Na^+ transporter. However, it is premature to reach this conclusion as YjbQ might be missing an activator or co-factor. Unfortunately, the assays used to unveil c-di-AMP mode of action, exhibited flaws and need to be rethought.

4.9. YjbQ Antiporter Activity Assay

As an alternative to characterize the functional properties of YjbQ an *in vitro* functional assay was setup. This assay, based on a method described by Rosen[74], measures the antiport activity of YjbQ in inside-out (everted) vesicles and it begins with the overexpression of YjbQ in KNabc cells. This step is followed by the preparation of the everted vesicles with a French press, an apparatus used to disrupt the plasma membrane of cells. These vesicles contain the membrane proteins of the cell in a reversed orientation (the lumen of the vesicle corresponds to the extracellular space

while the outside of the vesicle corresponds to the intracellular space). From this point on, the membrane-binding fluorophore 9-amino-6-chloro-2-methoxyacridine (ACMA) is added to the vesicles. This fluorophore answers to changes in proton gradient. Sodium lactate is added to the vesicles to generate a proton gradient with high H^+ concentration in the lumen. Consequently, ACMA fluorescence is quenched. At this point, it is possible to study the activity of YjbQ by generating a cation gradient outside de vesicles (e.g. KCl or NaCl). If YjbQ is an antiporter, it will exchange cations and protons, leading to the dissipation of the proton gradient and dequenching of ACMA fluorescence (**Figure 4.39**). The rate of dequenching can be related to the antiporter activity of the protein.

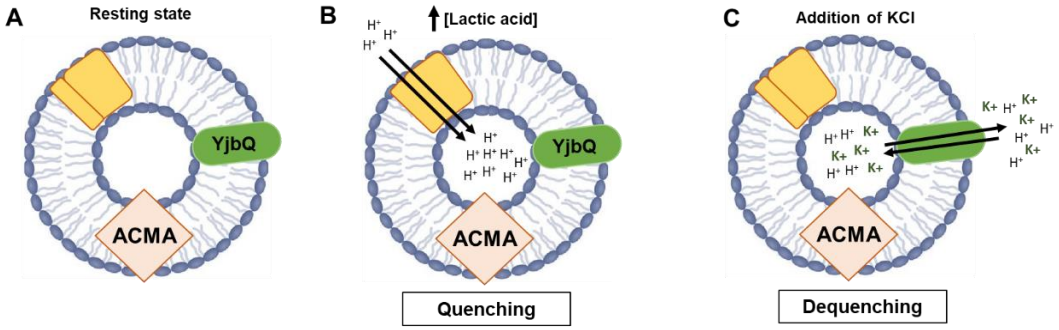

Figure 4.39 - Cartoon representation of the hypothetical activity of YjbQ in the antiporter assay. A) Everted vesicles general composition and initial fluorescence by ACMA (orange square). **B)** Addition of lactic acid energizes the respiratory chain (yellow shapes), pumping H^+ to the inside of the vesicles, generating a proton gradient, quenching ACMA. **C)** Addition of a KCl gradient activates YjbQ (green shape). The exchange of protons and cations dissipates the gradient, dequenching ACMA.

Four simple experiments were performed to evaluate whether YjbQ had the capacity to exchange cations and protons. Two salts were tested to assess YjbQ specificity to potassium: sodium chloride and potassium chloride. In addition, the influence of c-di-AMP on YjbQ's activity was tested.

However, addition of KCl and NaCl resulted in a very low dequenching, which is resembles background leak of H^+ from the vesicles (**Figure 4.40**). Addition of 15 µM of c-di-AMP did not increase fluorescence dequenching.

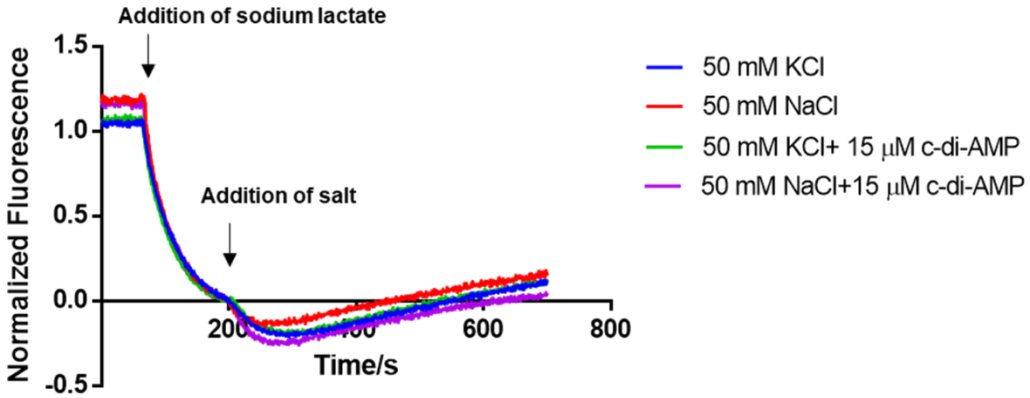

Figure 4.40 - YjbQ's activity in the presence of different monovalent cationic gradients with and without 15 μM of c-di-AMP. Example curves of the time dependent change of ACMA fluorescence when 50 mM KCl or NaCl was added to the sample at pH 7.5 after a steady state ΔpH was obtained by addition of 4 mM sodium lactate.

At this point, several questions were raised to explain this absence of antiport activity. Does YjbQ need a cofactor to activate exchange of cations and protons? Is something interfering with YjbQ's function? An hypothesis was formulated: magnesium ions present in the Vesicle Assay Buffer might be acting as inhibitors of YjbQ. Magnesium ions are the most abundant intracellular divalent cations in living cells and play important roles in a large number of cellular processes. Mg^{2+} has profound effects on water and solute transport in cells and regulates various biochemical reactions acting as a cofactor in transmembrane movements[75]. In the original assay, (**Figure 4.40**; see Materials and Methods, section **3.9**), the Vesicle Assay Buffer contains 5 mM of $MgCl_2$. Therefore, another set of experiments were performed to test the influence of $MgCl_2$ by running the assays in a Vesicle Assay Buffer without any Mg^{2+} ions present (**Figure 4.41**).

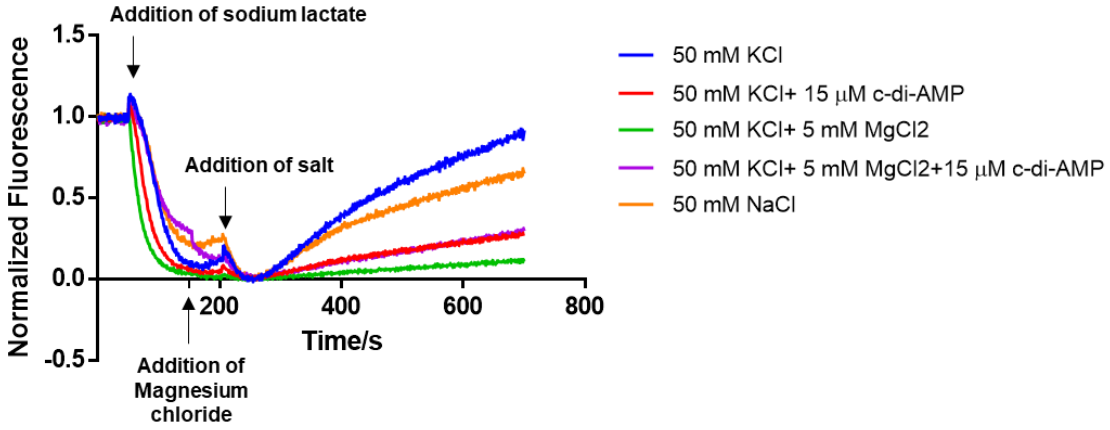

Figure 4.41 - Influence of Mg^{2+} ions in YjbQ's activity in everted vesicles without MgCl2. Example curves of the time dependent change of ACMA fluorescence when 50 mM KCl or NaCl was added to the sample at pH 7.5 after a steady state ΔpH was obtained by addition of 4 mM sodium lactate.

In these conditions, it was possible to detect a difference in the dequenching curves after addition of Na^+ and K^+ with and without $MgCl_2$. Strikingly, c-di-AMP did not accentuate YjbQ's antiporter activity in the absence of Mg^{2+}. Altogether, this assay strongly suggests that Mg^{2+} ions act as inhibitors for YjbQ's activity and that YjbQ might function as cation/proton antiporter.

The assay was repeated but now besides Na^+ and K^+, choline chloride was also tested. Choline is an organic cation that is too large to be translocated across the membrane by an ion transporter. As such, the experimental curve generated after addition of choline chloride works as the basal line for the experiment and serves as comparison for the remaining curves (**Figure 4.42**).

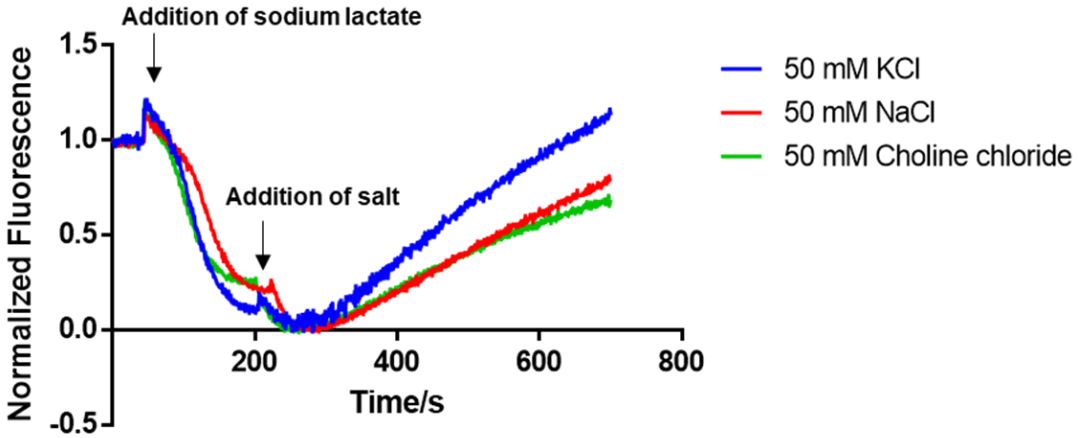

Figure 4.42 - Cation/proton activity of everted vesicles containing YjbQ in different monovalent cation gradients. Example curves of the time dependent change of ACMA fluorescence when 50 mM KCl or NaCl was added to the sample at pH 7.5 after a steady state ΔpH was obtained by addition of 4 mM sodium lactate.

According to the results shown in **Figure 4.42**, there is no difference in dequenching curves with Na^+ or choline but dequenching is slightly accentuated in the presence of K^+. It appears therefore that YjbQ is K+ antiporter despite being very inefficient. Overall, this suggests that YjbQ is selective for potassium and that Mg^{2+} highly influences its ability to exchange cations and protons. When it comes to smaller cations like Na^+, experiments with choline chloride clearly demonstrated YjbQ's inability to transport Na^+ ions. In the end, c-di-AMP effect on YjbQ remains undiscovered, as its addition on everted vesicles did not enhance YjbQ activity in any way. This inability to see c-di-AMP mode of action, together with the crystallography data that show that c-di-AMP does not induce structural modifications on the structure of the RCK domain, strongly suggest that there is a need for a second ligand to bind to YjbQ's RCK domain to produce visible effects.

5. Conclusions

The main objectives of this work were: to establish a protocol for large-scale expression and purification for the RCK domain of YjbQ, to crystallize the RCK domain and determine its three-dimensional structure and finally, to characterize the functional role and the biochemical properties of the RCK domain.

In sum, the protocol for large-scale expression and purification of RCK domain was established. The elution profile from size-exclusion chromatography showed two distinct peaks, suggesting that each one corresponds to a different oligomeric form of the protein. Posterior size-exclusion chromatography experiments revealed that this elution profile is not pH nor concentration dependent. A ligand screening performed by Thermal Shift revealed that c-di-AMP is a ligand for the RCK domain of YjbQ. Once established that c-di-AMP binds to this RCK domain, another size-exclusion chromatography experiment was performed that revealed that c-di-AMP stabilizes one of the conformations of the protein, possibly its dimeric form.

Crystallization screens were performed in the presence and absence of c-di-AMP. Crystals appeared predominately in conditions supplemented with divalent salts. Several datasets were collected and structures with and without of c-di-AMP were determined at a resolution of 1.85 Å and 2.2 Å, respectively. The monomer of the RCK domain of YjbQ comprises three different regions: an N-terminal subdomain with the conserved Rossman fold, a Helix-turn-Helix motif and a C-terminal subdomain connected in a similar fashion to the RCK domain of MthK . Strikingly, the differences between the structures with and without c-di-AMP are small. Despite the small deviations, it appears that c-di-AMP can enter the binding site in the apo-structure without requiring further structural changes.

Complementation studies in *E. coli* mutant strains were performed in order to unravel YjbQ's function. Unfortunately, neither the YjbQ's function as an antiporter nor c-di-AMP's mode of action were clarified with these assays. Antiporter assays with everted vesicles suggest that YjbQ functions as cation/proton antiporter selective to K^+. YjbQ's antiporter activity appeared to be strongly influenced by the presence of Mg^{2+} ions but the role of c-di-AMP in YjbQ's function remained unclear. In addition, it was demonstrated that full-length YjbQ is a dimer in the membrane, without the presence of c-di-AMP.

In the end, the majority of the goals of this work were accomplished, with the exception of the determination of YjbQ's function and c-di-AMP's mode of action, which remained

largely undiscovered. To explain this, two hypotheses were formulated. Either the functional assays performed did not work because protein expression was not ideal, or simply because there was some important factor that is missing from the assays. To evaluate the first hypothesis, it would be of interest to clone the full-length YjbQ in a different expression vector, possibly one with a leaky expression, and repeat the functional assays with this construct. Leaky expression systems allow a phased expression of low amounts of protein and prevents the overloading of the cell with many copies of the protein at the same time. To test the second hypothesis, another round of antiporter assays has to be performed, this time testing other possible co-factors for YjbQ. Possibly, c-di-AMP requires the binding of a second co-factor in order to fulfil its function and produce visible effects on YjbQ.

References

1. Udensi, U. K. & Tchounwou, P. B. Potassium Homeostasis, Oxidative Stress, and Human Disease. *Int. J. Clin. Exp. Physiol.* **4**, 111–122 (2017).

2. Epstein, W. The roles and regulation of potassium in bacteria. *Prog. Nucleic Acid Res. Mol. Biol.* **75**, 293–320 (2003).

3. CRC Handbook of Chemistry and Physics: A Ready-Reference of Chemical and Physical Data, 85th ed Edited by David R. Lide (National Institute of Standards and Technology). CRC Press LLC: Boca Raton, FL. 2004. 2712 pp. $139.99. ISBN 0-8493-0485-7. *J. Am. Chem. Soc.* **127**, 4542 (2005).

4. Rozov, A. *et al.* Importance of potassium ions for ribosome structure and function revealed by long-wavelength X-ray diffraction. *Nat. Commun.* **10**, 1–12 (2019).

5. Rastegar A. Serum Potassium. In: Walker HK, Hall WD, Hurst JW, editors. Clinical Methods: The History, Physical, and Laboratory Examinations. 3rd edition. Boston: Butterworths; 1990. Chapter 195. **2**,

6. Cheng, C.-J., Kuo, E. & Huang, C.-L. Extracellular potassium homeostasis: insights from hypokalemic periodic paralysis. *Semin. Nephrol.* **33**, 237–247 (2013).

7. Cameron, I. L., Fullerton, G. D. & Smith, N. K. Influence of cytomatrix proteins on water and on ions in cells. *Scanning Microsc.* **2**, 275–288 (1988).

8. Gundlach, J. *et al.* Adaptation of Bacillus subtilis to life at extreme potassium limitation. *MBio* **8**, 1–12 (2017).

9. McLaggan, D., Naprstek, J., Buurman, E. T. & Epstein, W. Interdependence of K+ and glutamate accumulation during osmotic adaptation of Escherichia coli. *J. Biol. Chem.* **269**, 1911–1917 (1994).

10. Lo, C.-J., Leake, M. C. & Berry, R. M. Fluorescence measurement of intracellular sodium concentration in single Escherichia coli cells. *Biophys. J.* **90**, 357–365 (2006).

11. Tsuchiya, T. & Takeda, K. Calcium/Proton and Sodium/Proton Antiport Systems in Escherichia coli1. *J. Biochem.* **85**, 943–951 (1979).

12. Hirota, N., Kitada, M. & Imae, Y. Flagellar motors of alkalophilic bacillus are

powered by an electrochemical potential gradient of Na+. *FEBS Lett.* **132**, 278–280 (1981).

13. Wood, J. M. Osmosensing by bacteria: signals and membrane-based sensors. *Microbiol. Mol. Biol. Rev.* **63**, 230–262 (1999).

14. Booth, I. R. & Louis, P. Managing hypoosmotic stress: aquaporins and mechanosensitive channels in Escherichia coli. *Curr. Opin. Microbiol.* **2**, 166–169 (1999).

15. Dinnbier, U., Limpinsel, E., Schmid, R. & Bakker, E. P. Transient accumulation of potassium glutamate and its replacement by trehalose during adaptation of growing cells of Escherichia coli K-12 to elevated sodium chloride concentrations. *Arch. Microbiol.* **150**, 348–357 (1988).

16. Brown, A. D. Microbial water stress. *Bacteriol. Rev.* **40**, 803–846 (1976).

17. Holtmann, G., Bakker, E. P., Uozumi, N. & Bremer, E. KtrAB and KtrCD: two K+ uptake systems in Bacillus subtilis and their role in adaptation to hypertonicity. *J. Bacteriol.* **185**, 1289–1298 (2003).

18. Whatmore, A. M., Chudek, J. A. & Reed, R. H. The effects of osmotic upshock on the intracellular solute pools of Bacillus subtilis. *J. Gen. Microbiol.* **136**, 2527–2535 (1990).

19. Boch, J., Kempf, B. & Bremer, E. Osmoregulation in Bacillus subtilis: synthesis of the osmoprotectant glycine betaine from exogenously provided choline. *J. Bacteriol.* **176**, 5364–5371 (1994).

20. Zaprasis, A. *et al.* Osmoprotection of Bacillus subtilis through import and proteolysis of proline-containing peptides. *Appl. Environ. Microbiol.* **79**, 576–587 (2013).

21. Fisher, M. T. Proline to the rescue. *Proc. Natl. Acad. Sci. U. S. A.* **103**, 13265–13266 (2006).

22. Kappes, R. M., Kempf, B. & Bremer, E. Three transport systems for the osmoprotectant glycine betaine operate in Bacillus subtilis: characterization of OpuD. *J. Bacteriol.* **178**, 5071–5079 (1996).

23. Nyyssola, A., Kerovuo, J., Kaukinen, P., von Weymarn, N. & Reinikainen, T. Extreme halophiles synthesize betaine from glycine by methylation. *J. Biol. Chem.* **275**, 22196–22201 (2000).

24. Hoffmann, T. & Bremer, E. Management of Osmotic Stress by Bacillus Subtilis: Genetics and Physiology. *Stress and Environmental Regulation of Gene Expression and Adaptation in Bacteria* 657–676 (2016).

25. Kappes, R. M. *et al.* Two evolutionarily closely related ABC transporters mediate the uptake of choline for synthesis of the osmoprotectant glycine betaine in Bacillus subtilis. *Mol. Microbiol.* **32**, 203–216 (1999).

26. Boch, J., Kempf, B., Schmid, R. & Bremer, E. Synthesis of the osmoprotectant glycine betaine in Bacillus subtilis: characterization of the gbsAB genes. *J. Bacteriol.* **178**, 5121–5129 (1996).

27. Roosild, T. P., Miller, S., Booth, I. R. & Choe, S. A mechanism of regulating transmembrane potassium flux through a ligand-mediated conformational switch. *Cell* **109**, 781–791 (2002).

28. Albright, R. A., Ibar, J.-L. V., Kim, C. U., Gruner, S. M. & Morais-Cabral, J. H. The RCK domain of the KtrAB K+ transporter: multiple conformations of an octameric ring. *Cell* **126**, 1147–1159 (2006).

29. Roosild, T. P. *et al.* KTN (RCK) domains regulate K+ channels and transporters by controlling the dimer-hinge conformation. *Structure* **17**, 893–903 (2009).

30. Bossemeyer, D. *et al.* K+-transport protein TrkA of Escherichia coli is a peripheral membrane protein that requires other trk gene products for attachment to the cytoplasmic membrane. *J. Biol. Chem.* **264**, 16403–16410 (1989).

31. Jiang, Y., Pico, A., Cadene, M., Chait, B. T. & MacKinnon, R. Structure of the RCK domain from the E. coli K+ channel and demonstration of its presence in the human BK channel. *Neuron* **29**, 593–601 (2001).

32. Hanukoglu, I. Proteopedia: Rossmann fold: A beta-alpha-beta fold at dinucleotide binding sites. *Biochem. Mol. Biol. Educ. a Bimon. Publ. Int. Union Biochem. Mol. Biol.* **43**, 206–209 (2015).

33. Giraldez, T. & Rothberg, B. S. Understanding the conformational motions of RCK gating rings. *J. Gen. Physiol.* **149**, 431–441 (2017).

34. Schlosser, A., Hamann, A., Bossemeyer, D., Schneider, E. & Bakker, E. P. NAD+ binding to the Escherichia coli K+-uptake protein TrkA and sequence similarity between TrkA and domains of a family of dehydrogenases suggest a role for NAD+ in bacterial transport. *Mol. Microbiol.* **9**, 533–543 (1993).

35. Kröning, N. *et al.* ATP binding to the KTN/RCK subunit KtrA from the K+ -uptake system KtrAB of Vibrio alginolyticus: its role in the formation of the KtrAB complex and its requirement in vivo. *J. Biol. Chem.* **282**, 14018–14027 (2007).

36. Yuan, P., Leonetti, M. D., Pico, A. R., Hsiung, Y. & MacKinnon, R. Structure of the human BK channel Ca2+-activation apparatus at 3.0 A resolution. *Science* **329**, 182–186 (2010).

37. Diskowski, M. *et al.* Helical jackknives control the gates of the double-pore K+ uptake system KtrAB. *Elife* **6**, e24303 (2017).

38. Healy, J. *et al.* Understanding the structural requirements for activators of the Kef bacterial potassium efflux system. *Biochemistry* **53**, 1982–1992 (2014).

39. Pliotas, C. *et al.* Adenosine Monophosphate Binding Stabilizes the KTN Domain of the Shewanella denitrificans Kef Potassium Efflux System. *Biochemistry* **56**, 4219–4234 (2017).

40. Fahey, R. C., Brown, W. C., Adams, W. B. & Worsham, M. B. Occurrence of glutathione in bacteria. *J. Bacteriol.* **133**, 1126–1129 (1978).

41. Newton, G. L. *et al.* Bacillithiol is an antioxidant thiol produced in Bacilli. *Nat. Chem. Biol.* **5**, 625–627 (2009).

42. Prindle, A. *et al.* Ion channels enable electrical communication in bacterial communities. *Nature* **527**, 59–63 (2015).

43. Fujisawa, M., Ito, M. & Krulwich, T. A. Three two-component transporters with channel-like properties have monovalent cation/proton antiport activity. *Proc. Natl. Acad. Sci. U. S. A.* **104**, 13289–13294 (2007).

44. Gundlach, J. *et al.* Sustained sensing in potassium homeostasis: Cyclic di-AMP controls potassium uptake by KimA at the levels of expression and activity. *J. Biol. Chem.* **294**, 9605–9614 (2019).

45. Hengge, R., Gründling, A., Jenal, U., Ryan, R. & Yildiz, F. Bacterial Signal Transduction by Cyclic Di-GMP and Other Nucleotide Second Messengers. *J. Bacteriol.* **198**, 15–26 (2016).

46. Commichau, F. M., Gibhardt, J., Halbedel, S., Gundlach, J. & Stülke, J. A Delicate Connection: c-di-AMP Affects Cell Integrity by Controlling Osmolyte Transport. *Trends Microbiol.* **26**, 175–185 (2018).

47. Fahmi, T., Port, G. C. & Cho, K. H. c-di-AMP: An Essential Molecule in the

Signaling Pathways that Regulate the Viability and Virulence of Gram-Positive Bacteria. *Genes (Basel).* **8**, 197 (2017).

48. Corrigan, R. M. & Gründling, A. Cyclic di-AMP: another second messenger enters the fray. *Nat. Rev. Microbiol.* **11**, 513–524 (2013).

49. Corrigan, R. M. *et al.* Systematic identification of conserved bacterial c-di-AMP receptor proteins. *Proc. Natl. Acad. Sci. U. S. A.* **110**, 9084–9089 (2013).

50. Oppenheimer-Shaanan, Y., Wexselblatt, E., Katzhendler, J., Yavin, E. & Ben-Yehuda, S. c-di-AMP reports DNA integrity during sporulation in Bacillus subtilis. *EMBO Rep.* **12**, 594–601 (2011).

51. Luo, Y. & Helmann, J. D. Analysis of the role of Bacillus subtilis σ(M) in β-lactam resistance reveals an essential role for c-di-AMP in peptidoglycan homeostasis. *Mol. Microbiol.* **83**, 623–639 (2012).

52. Gundlach, J. *et al.* Identification, characterization, and structure analysis of the cyclic di-AMP-binding PII-like signal transduction protein DarA. *J. Biol. Chem.* **290**, 3069–3080 (2015).

53. Rocha, R., Teixeira-Duarte, C. M., Jorge, J. M. P. & Morais-Cabral, J. H. Characterization of the molecular properties of KtrC, a second RCK domain that regulates a Ktr channel in Bacillus subtilis. *J. Struct. Biol.* **205**, 34–43 (2019).

54. Gundlach, J. *et al.* Sustained sensing in potassium homeostasis: Cyclic di-AMP controls potassium uptake by KimA at the levels of expression and activity. *J. Biol. Chem.* **294**, 9605–9614 (2019).

55. Masrati, G. *et al.* Broad phylogenetic analysis of cation/proton antiporters reveals transport determinants. *Nat. Commun.* **9**, 4205 (2018).

56. West, I. C. & Mitchell, P. Proton/sodium ion antiport in Escherichia coli. *Biochem. J.* **144**, 87–90 (1974).

57. Fujisawa, M., Wada, Y. & Ito, M. Modulation of the K+ efflux activity of Bacillus subtilis YhaU by YhaT and the C-terminal region of YhaS. *FEMS Microbiol. Lett.* **231**, 211–217 (2004).

58. Mäder, U., Schmeisky, A. G., Flórez, L. A. & Stülke, J. SubtiWiki--a comprehensive community resource for the model organism Bacillus subtilis. *Nucleic Acids Res.* **40**, D1278-87 (2012).

59. Chin, K.-H. *et al.* Structural Insights into the Distinct Binding Mode of Cyclic Di-

AMP with SaCpaA_RCK. *Biochemistry* **54**, 4936–4951 (2015).

60. Agilent. QuikChange ® II Site-Directed Mutagenesis Kit User Manual. **200518**, 1–19 (2010).

61. Albright, R. A., Joh, K. & Morais-Cabral, J. H. Probing the structure of the dimeric KtrB membrane protein. *J. Biol. Chem.* **282**, 35046–35055 (2007).

62. Celniker, G. *et al.* ConSurf: Using Evolutionary Data to Raise Testable Hypotheses about Protein Function. *Isr. J. Chem.* **53**, 199–206 (2013).

63. Ashkenazy, H., Erez, E., Martz, E., Pupko, T. & Ben-Tal, N. ConSurf 2010: calculating evolutionary conservation in sequence and structure of proteins and nucleic acids. *Nucleic Acids Res.* **38**, W529–W533 (2010).

64. Ashkenazy, H. *et al.* ConSurf 2016: an improved methodology to estimate and visualize evolutionary conservation in macromolecules. *Nucleic Acids Res.* **44**, W344–W350 (2016).

65. Consortium, T. U. UniProt: a worldwide hub of protein knowledge. *Nucleic Acids Res.* **47**, D506–D515 (2018).

66. Schwede, T., Kopp, J., Guex, N. & Peitsch, M. C. SWISS-MODEL: An automated protein homology-modeling server. *Nucleic Acids Res.* **31**, 3381–3385 (2003).

67. Grøftehauge, M. K., Hajizadeh, N. R., Swann, M. J. & Pohl, E. Protein-ligand interactions investigated by thermal shift assays (TSA) and dual polarization interferometry (DPI). *Acta Crystallogr. D. Biol. Crystallogr.* **71**, 36–44 (2015).

68. Dong, J., Shi, N., Berke, I., Chen, L. & Jiang, Y. Structures of the MthK RCK domain and the effect of Ca2+ on gating ring stability. *J. Biol. Chem.* **280**, 41716–41724 (2005).

69. Bellamacina, C. R. The nicotinamide dinucleotide binding motif: a comparison of nucleotide binding proteins. *FASEB J.* **10**, 1257–1269 (1996).

70. Yernool, D., Boudker, O., Folta-Stogniew, E. & Gouaux, E. Trimeric subunit stoichiometry of the glutamate transporters from Bacillus caldotenax and Bacillus stearothermophilus. *Biochemistry* **42**, 12981–12988 (2003).

71. Aller, S. G., Eng, E. T., De Feo, C. J. & Unger, V. M. Eukaryotic CTR copper uptake transporters require two faces of the third transmembrane domain for helix packing, oligomerization, and function. *J. Biol. Chem.* **279**, 53435–53441

(2004).

72. Vieira-Pires, R. S., Szollosi, A. & Morais-Cabral, J. H. The structure of the KtrAB potassium transporter. *Nature* **496**, 323–328 (2013).

73. Gundlach, J. *et al.* Control of potassium homeostasis is an essential function of the second messenger cyclic di-AMP in Bacillus subtilis. *Sci. Signal.* **10**, eaal3011 (2017).

74. Brey, R. N., Beck, J. C. & Rosen, B. P. Cation/proton antiport systems in Escherichia coli. *Biochem. Biophys. Res. Commun.* **83**, 1588–1594 (1978).

75. Groisman, E. A. *et al.* Bacterial Mg2+ homeostasis, transport, and virulence. *Annu. Rev. Genet.* **47**, 625–646 (2013).

Appendix

YjbQ Crystallography Handmade Screens Composition

Screens of the RCK domain of YjbQ supplemented with 1 mM of c-di-AMP

Composition of the 96 well handmade screens around condition D11 (1260 mM Ammonium sulphate; 100 mM Tris base/HCl pH 8.5; 200 mM Lithium sulphate), C1 (30% (v/v) PEG 400; 100 mM Tris base/ HCl pH 8.5; 200 mM Magnesium chloride) and E3 (20% (w/v) PEG8000, 100 mM Tris-HCl pH 8.5; 200 mM Magnesium chloride) from Wizard I&II commercial kit. This screen was divided in three quadrants, each one supplement with a different salt. The top-left quadrant was supplemented with 200 mM of Lithium sulphate and the top-right and bottom quadrants were supplemented with 200 mM of Magnesium chloride.

Table 7.1- Composition of handmade screens around condition D11, C1 and E3 from Wizard I&II commercial kit. Top quadrants are coloured in different shades of grey and bottom quadrant is coloured in white.

	[Ammonium sulphate] / M					**%(v/v) PEG400**							
	1	**2**	**3**	**4**	**5**	**6**	**7**	**8**	**9**	**10**	**11**	**12**	
A	1.10	1.15	1.20	1.26	1.30	24	26	28	30	32	34	36	100 mM Tris/HCl pH **7.0**
B	1.10	1.15	1.20	1.26	1.30	24	26	28	30	32	34	36	100 mM Tris/HCl pH **7.5**
C	1.10	1.15	1.20	1.26	1.30	24	26	28	30	32	34	36	100 mM Tris/HCl pH **8.0**
D	1.10	1.15	1.20	1.26	1.30	24	26	28	30	32	34	36	100 mM Tris/HCl pH **8.5**
E	10	12	14	16	18	20	22	24	26	28	30	32	100 mM MES pH **6.5**
F	10	12	14	16	18	20	22	24	26	28	30	32	100 mM Tris/HCl pH **7.0**
G	10	12	14	16	18	20	22	24	26	28	30	32	100 mM Tris/HCl pH **7.5**
H	10	12	14	16	18	20	22	24	26	28	30	32	100 mM Tris/HCl pH **8.5**
	% (w/v) PEG8000												

Composition of the 96 well handmade screens around condition B5 (30% (w/v) PEG 8000;100 mM Sodium acetate/ Acetic acid pH 4.5; 200 mM Lithium sulphate) and E7 (30% (w/v) PEG 3000; 100 mM Tris base/ HCl pH 7.0; 200 mM Sodium chloride) from Wizard I&II commercial kit. The screen was divided into four quadrants. The top-left quadrant was supplemented with 200 mM of Lithium sulphate, the top-right quadrant was

supplemented with 100 mM of Lithium sulphate, bottom-right with 100 mM of Sodium chloride and bottom-left quadrant with 200 mM of Sodium chloride.

Table 7.2- Composition of handmade screens around condition B5 and E7 from Wizard I&II commercial kit. Top and bottom-left quadrants are coloured in different shades of grey and bottom-right quadrant is coloured in white.

	% (w/v) PEG8000						% (w/v) PEG8000						
	1	**2**	**3**	**4**	**5**	**6**	**7**	**8**	**9**	**10**	**11**	**12**	
A	20	25	30	35	40	45	20	25	30	35	40	45	100 mM Sodium acetate pH **4.5**
B	20	25	30	35	40	45	20	25	30	35	40	45	100 mM Sodium acetate pH **5.0**
C	20	25	30	35	40	45	20	25	30	35	40	45	100 mM Sodium acetate pH **5.5**
D	20	25	30	35	40	45	20	25	30	35	40	45	100 mM Tris/HCl pH **7.0**
E	20	25	30	35	40	45	20	25	30	35	40	45	100 mM Tris/HCl pH **7.5**
F	20	25	30	35	40	45	20	25	30	35	40	45	100 mM Tris/HCl pH **7.0**
G	20	25	30	35	40	45	20	25	30	35	40	45	100 mM Tris/HCl pH **7.5**
H	20	25	30	35	40	45	20	25	30	35	40	45	100 mM Tris/HCl pH **8.5**
	% (w/v) PEG3000						% (w/v) PEG3000						

The remaining assays correspond to re-optimizations of the previous screens. The first re-optimization screen was divided into four quadrants. The top-left quadrant was supplemented with 100 mM of Magnesium chloride, the top-right quadrant was supplemented with 200 mM of Magnesium chloride, bottom-right with 300 mM of Sodium chloride and bottom-left quadrant with 150 mM of Sodium chloride.

Table 7.3- Composition of the first re-optimization screen. Top and bottom-left quadrants are coloured in different shades of grey and bottom-right quadrant is coloured in white.

	% (w/v) PEG8000						%(w/v) PEG8000						
	1	**2**	**3**	**4**	**5**	**6**	**7**	**8**	**9**	**10**	**11**	**12**	
A	20	22	24	26	28	30	20	22	24	26	28	30	100 mM MES pH **6.5**
B	20	22	24	26	28	30	20	22	24	26	28	30	100 mM Tris/HCl pH **7.0**
C	20	22	24	26	28	30	20	22	24	26	28	30	100 mM Tris/HCl pH **7.5**
D	20	22	24	26	28	30	20	22	24	26	28	30	100 mM Tris/HCl pH **8.0**
E	20	22	24	26	28	30	20	22	24	26	28	30	100 mM MES pH **6.5**
F	20	22	24	26	28	30	20	22	24	26	28	30	100 mM Tris/HCl pH **7.0**
G	20	22	24	26	28	30	20	22	24	26	28	30	100 mM Tris/HCl pH **7.5**
H	20	22	24	26	28	30	20	22	24	26	28	30	100 mM Tris/HCl pH **8.0**
	% (w/v) PEG8000						% (w/v) PEG8000						

The second re-optimization screen was divided into two quadrants. The top quadrant was supplemented with 200 mM of Magnesium chloride, and bottom quadrant with 300 mM of Magnesium chloride.

Table 7.4- Composition of the second re-optimization screen. Top and bottom quadrants are coloured in grey and white, respectively.

	% (w/v) PEG3000												
	1	**2**	**3**	**4**	**5**	**6**	**7**	**8**	**9**	**10**	**11**	**12**	
A	20	22	24	26	28	30	32	34	36	38	40	42	100 mM MES pH **6.5**
B	20	22	24	26	28	30	32	34	36	38	40	42	100 mM Tris/HCl pH **7.0**
C	20	22	24	26	28	30	32	34	36	38	40	42	100 mM Tris/HCl pH **7.5**
D	20	22	24	26	28	30	32	34	36	38	40	42	100 mM Tris/HCl pH **8.0**
E	20	22	24	26	28	30	32	34	36	38	40	42	100 mM MES pH **6.5**
F	20	22	24	26	28	30	32	34	36	38	40	42	100 mM Tris/HCl pH **7.0**
G	20	22	24	26	28	30	32	34	36	38	40	42	100 mM Tris/HCl pH **7.5**
H	20	22	24	26	28	30	32	34	36	38	40	42	100 mM Tris/HCl pH **8.0**
	% (w/v) PEG3000												